TKK Dissertations 181
Espoo 2009

NONEQUILIBRIUM AND TRANSPORT IN PROXIMITY OF SUPERCONDUCTORS

Doctoral Dissertation

Pauli Virtanen

Helsinki University of Technology
Low Temperature Laboratory

Helsinki University of Technology
Faculty of Information and Natural Sciences

TKK Dissertations 181
Espoo 2009

NONEQUILIBRIUM AND TRANSPORT IN PROXIMITY OF SUPERCONDUCTORS

Doctoral Dissertation

Pauli Virtanen

Dissertation for the degree of Doctor of Science in Technology to be presented with due permission of the Faculty of Information and Natural Sciences for public examination and debate in Auditorium K216 at Helsinki University of Technology (Espoo, Finland) on the 22nd of October, 2009, at 12 noon.

Helsinki University of Technology
Low Temperature Laboratory

Teknillinen korkeakoulu
Kylmälaboratorio

Helsinki University of Technology
Faculty of Information and Natural Sciences

Teknillinen korkeakoulu
Informaatio- ja luonnontieteiden tiedekunta

Distribution:
Helsinki University of Technology
Low Temperature Laboratory
P.O. Box 5100
FI - 02015 TKK
FINLAND
URL: http://ltl.tkk.fi/
Tel. +358-9-451 5619
Fax +358-9-451 2969
E-mail: pauli.virtanen@ltl.tkk.fi

ISBN 978-952-248-085-9
ISBN 978-952-248-086-6 (PDF)
ISSN 1795-2239
ISSN 1795-4584 (PDF)
URL: http://lib.tkk.fi/Diss/2009/isbn9789522480866/

TKK-DISS-2644

Picaset Oy
Helsinki 2009

ABSTRACT OF DOCTORAL DISSERTATION	HELSINKI UNIVERSITY OF TECHNOLOGY P. O. BOX 1000, FI-02015 TKK http://www.tkk.fi

Author Pauli Virtanen

Name of the dissertation

Nonequilibrium and transport in proximity of superconductors

Manuscript submitted June 8, 2009	Manuscript revised September 17, 2009
Date of the defence October 22, 2009	
☐ Monograph	☑ Article dissertation (summary + original articles)
Faculty	Faculty of Information and Natural Sciences
Department	Low Temperature Laboratory
Field of research	Theoretical condensed matter physics
Opponent(s)	Prof. Carlo W. J. Beenakker
Supervisor	Prof. Martti Puska
Instructor	Doc. Tero T. Heikkilä

Abstract

Mesoscopic physics studies systems that are larger than atoms but small enough to exhibit quantum coherent effects. Thanks to improved fabrication techniques, study of superconductivity and its effect on contacted materials in tailored micrometer-scale mesoscopic structures has become possible in the recent decades. Electron transport, non-equilibrium response, thermoelectricity, and fluctuations in such devices have attained significant interest. Thermoelectric effects in particular are one of the least understood aspects of superconductivity. Quantitative understanding of the observations in the mesoscopic regime has turned out to require quantum-mechanical models. Devices based on mesoscopic superconductivity have also technological applications, in addition to being of primary scientific interest.

This thesis discusses theoretical studies on thermoelectric and out-of-equilibrium effects in superconducting proximity structures. Green function methods are applied for computing the thermoelectric and nonequilibrium response of mesoscopic structures to external driving. The results explain several features observed in experiments, and clarify one origin of thermoelectricity in the studied systems.

Electrical fluctuations in mesoscopic structures are also discussed, and a device for characterizing the statistics and spectrum of the fluctuations is proposed. This mesoscopic on-chip detector is based on a superconducting Josephson junction in the Coulomb blockade regime. It is expected to bypass problems in conventional measurements of higher-order statistics of noise. That the detector can be manufactured close to the measured mesoscopic noise source could also enable studies of quantum properties in the higher-order statistics of the fluctuations.

Keywords mesoscopic physics, superconducting proximity effect	
ISBN (printed) 978-952-248-085-9	ISSN (printed) 1795-2239
ISBN (pdf) 978-952-248-086-6	ISSN (pdf) 1795-4584
Language English	Number of pages 90 + app. 108
Publisher Low Temperature Laboratory, Helsinki University of Technology	
Print distribution Low Temperature Laboratory, Helsinki University of Technology	
☑ The dissertation can be read at http://lib.tkk.fi/Diss/2009/isbn9789522480866/	

VÄITÖSKIRJAN TIIVISTELMÄ	TEKNILLINEN KORKEAKOULU PL 1000, 02015 TKK http://www.tkk.fi

Tekijä Pauli Virtanen

Väitöskirjan nimi

Epätasapaino- ja kuljetusilmiöt suprajohteiden lähellä

Käsikirjoituksen päivämäärä 8.6.2009	Korjatun käsikirjoituksen päivämäärä 17.9.2009
Väitöstilaisuuden ajankohta 22.10.2009	
☐ Monografia	☑ Yhdistelmäväitöskirja (yhteenveto + erillisartikkelit)

Tiedekunta	Informaatio- ja luonnontieteiden tiedekunta
Laitos	Kylmälaboratorio
Tutkimusala	teoreettinen materiaalifysiikka
Vastaväittäjä(t)	prof. Carlo W. J. Beenakker
Työn valvoja	prof. Martti Puska
Työn ohjaaja	dos. Tero T. Heikkilä

Tiivistelmä

Mesoskooppisen fysiikan tutkimusaiheisiin kuuluvat atomitasoa suuremmat mutta silti kvanttimekaanisesti koherentit rakenteet. Modernin valmistustekniikan myötä mesoskooppisten mikrometrien kokoluokan rakenteiden räätälöinti on mahdollistanut suprajohtavuuden ja sen läheisilmiön yksityiskohtaisen tutkimuksen. Kuljetus-, epätasapaino- ja lämpösähköilmiöt sekä fluktuaatiot näissä rakenteissa ovat saaneet paljon huomiota. Kuitenkin lämpösähköilmiöt ovat suprajohtavuuden ilmiöistä edelleen huonosti tunnettuja. Mesoskooppisten ilmiöiden mallintaminen vaatii yleensä kvanttimekaanista lähestymistapaa. Suprajohtavilla mikrorakenteilla on myös teknologisia sovelluksia niiden tieteellisen kiinnostavuuden lisäksi.

Tämä väitöskirja käsittelee lämpösähkö- ja epätasapainoilmiöiden teoriaa suprajohteiden läheisilmiön tutkimukseen soveltuvissa mikrorakenteissa. Näiden lämpösähköinen ja epätasapainovaste lasketaan Greenin funktio -menetelmillä. Tulokset selittävät useita kokeellisia havaintoja, ja selventävät kuvaa lämpösähköilmiöistä suprajohteiden läheisyydessä.

Väitöskirja käsittelee myös sähköisiä fluktuaatioita mikrorakenteissa, ja ehdottaa näiden fluktuaatioiden statistiikan ja spektrin tutkimiseen soveltuvaa laitetta. Tämä mesoskooppinen rakenne perustuu Coulombin saartoalueella olevaan suprajohtavaan Josephson-liitokseen ja odotettavasti kykenee ohittamaan eräitä tavalliseen kohinamittaukseen liittyviä ongelmia. Koska laite voidaan valmistaa mesoskooppisen kohinalähteen läheisyyteen, sillä voi mahdollisesti havaita myös fluktuaatioiden statistiikan kvanttimekaanisia piirteitä.

Asiasanat mesoskooppinen fysiikka, suprajohteen läheisilmiö

ISBN (painettu) 978-952-248-085-9	ISSN (painettu) 1795-2239
ISBN (pdf) 978-952-248-086-6	ISSN (pdf) 1795-4584
Kieli englanti	Sivumäärä 90 + liit. 108

Julkaisija Kylmälaboratorio, Teknillinen korkeakoulu

Painetun väitöskirjan jakelu Kylmälaboratorio, Teknillinen korkeakoulu

☑ Luettavissa verkossa osoitteessa http://lib.tkk.fi/Diss/2009/isbn9789522480866/

Preface

This thesis would not exist as it is without the help and support from a number of people.

First, I would like to thank my instructor Tero Heikkilä for advice and encouragement in the theory and practice of science, given over the years. I also thank Mikko Paalanen for the opportunity to pursue research at the Low Temperature Laboratory, one of the leading scientific facilities in Finland. Martti Puska is thanked for acting as a supervisor of this thesis on the behalf of the Department of Applied Physics.

My thanks to Norman Birge, Mike Crosser, Göran Johansson, Matthias Meschke, Victor Petrashov, Igor Sosnin, Frank Wilhelm, and Jing Zou, for fruitful collaboration on the work presented in this thesis. The input from the experimental side of physics has had a large impact on my work. I also thank Sebastian Bergeret, Carlos Cuevas, Matthias Eschrig, Joonas Peltonen, Markku Stenberg, and Fan Wu for useful discussions and collaboration on other topics. I'm indebted to Pertti Hakonen, and also to Jukka Pekola, for insightful discussions and interaction on experimental projects conducted at LTL.

The present and past members of our nano-theory group, Matti Laakso, Teemu Ojanen, Janne Viljas, and Juha Voutilainen, have been an enjoyable lot to work with. Erkki Thuneberg and Nikolai Kopnin are thanked for discussions and the occasional sage advice. I'd also like to thank all the people at LTL for maintaining an excellent atmosphere, and inspired exchange of ideas in and out of office. A few names should be mentioned: Rob de Graaf, Heikki Junes, Risto Hänninen, Tommy Holmqvist, Andrey Timofeev, Sarah MacLeod, Juha Muhonen, Joonas Peltonen, David Gunnarsson, Lorenz Lechner, Mika Sillanpää, Rob Blaauwgeers, Pieter Vorselman, Anssi Salmela.

My friends in Finland have my gratitude for many joyful occasions and for company in general. Lastly, I wish to thank Varpu, Aija and Olli for their support during all these years.

Helsinki, September 2009

Pauli Virtanen

Contents

List of Publications

This thesis consists of an overview and of the following publications which are referred to in the text by their Roman numerals.

I P. Virtanen, and T.T. Heikkilä, *Thermopower induced by a supercurrent in superconductor-normal-metal structures*, Physical Review Letters, **92**, 177004 (2004).

II P. Virtanen, and T.T. Heikkilä, *Thermopower in Andreev interferometers*, Journal of Low Temperature Physics, **136**, 401 (2004).

III M.S. Crosser, P. Virtanen, T.T. Heikkilä, and N.O. Birge, *Supercurrent-induced temperature gradient across a nonequilibrium SNS Josephson junction*, Physical Review Letters, **96**, 167004 (2006).

IV J. Zou, I. Sosnin, P. Virtanen, M. Meschke, V.T. Petrashov, T.T. Heikkilä, *Influence of supercurrents on low-temperature thermopower in mesoscopic N/S structures*, Journal of Low Temperature Physics, **146**, 193 (2007).

V P. Virtanen, and T.T. Heikkilä, *Peltier effects in Andreev interferometers*, Physical Review B, **75**, 104517 (2007).

VI P. Virtanen, and T.T. Heikkilä, *Thermoelectric effects in superconducting proximity structures*, Applied Physics A, **89**, 625 (2007).

VII P. Virtanen, J. Zou, I. Sosnin, V.T. Petrashov, and T.T. Heikkilä, *Phase states of multiterminal mesoscopic normal-metal-superconductor structures*, Physical Review Letters, **99**, 217003 (2007).

VIII M.S. Crosser, J. Huang, F. Pierre, P. Virtanen, T.T. Heikkilä, F.K. Wilhelm, and N.O. Birge, *Nonequilibrium transport in mesoscopic multi-terminal SNS Josephson junctions*, Physical Review B, **77**, 014528 (2008).

IX T. T. Heikkilä, P. Virtanen, G. Johansson, and F.K. Wilhelm, *Measuring non-Gaussian fluctuations through incoherent Cooper-pair current*, Physical Review Letters, **93**, 247005 (2004).

X P. Virtanen and T. T. Heikkilä, *Circuit theory for noise in incoherent normal-superconductor structures*, New Journal of Physics, **8**, 50 (2006).

Author's contribution

The work reported in this Thesis was carried out by me, during 2003-2009 in the Low Temperature Laboratory of Helsinki University of Technology, Finland. I contributed a significant parts of the theoretical results and several main ideas in publications **I**, **II**, **V**, **VI**, **VII**, **IX**, and **X**, and did all numerical computations required by these articles. Manuscripts for **V** and **X** are written entirely by me, and I also wrote large parts of the text in the other publications mentioned above. I performed the numerical computations in **III** that concerned theoretical predictions, and part of those in **IV**. I also wrote parts of both manuscripts. In publication **VIII**, I contributed the theoretical results concerning the effect of the magnetic field, and gave advice for other parts of the manuscript.

List of Symbols

A	Surface area
$\boldsymbol{A}$	Vector potential
A_k	Cross-sectional area of wire k
$\boldsymbol{B}$	Magnetic field
C	Capacitance
χ	Local complex phase in θ-parameterization (section 2), or, counting field (section 3)
D	Diffusion constant
d	Length
Δ	Superconducting order parameter
E	Energy
e	Unit charge (taken positive)
E_C	Charging energy
E_f	Fermi energy
E_J	Josephson energy
E_T	Thouless energy, $E_T = \hbar D/L^2$
f	Electron distribution function
F, $F^\dagger$	Anomalous Green functions / coherence functions
f_L	Longitudinal mode of the electron distribution function
f_T	Transverse mode of the electron distribution function
g	Gyromagnetic ratio for electron, $g \approx 2$, or, superconducting interaction constant
γ, $\tilde{\gamma}$	Coherence factors in Riccati parametrization
γ_{sf}	Spin-flip scattering rate
$\check{G}$	4×4 nonequilibrium Green function, in Keldysh $\otimes$ Nambu space
$\hat{G}^{R/A/K}$	2×2 nonequilibrium Green function, in Nambu space
$\hbar$	Planck constant divided by 2π
I	Charge current
I_c	Critical current
$\check{I}$	Matrix current
I_n	Normal current (as opposed to supercurrent)
I_Q	Heat current
I_S	Supercurrent
$\boldsymbol{j}_c$	Observable charge current density
$\boldsymbol{j}_E$	Energy current density
$\boldsymbol{j}_L(E)$	Longitudinal mode spectral current
$\boldsymbol{j}_Q$	Observable heat current density
$\boldsymbol{j}_S$	Spectral supercurrent density
$\boldsymbol{j}_T(E)$	Transverse mode spectral current
k_B	Boltzmann constant

k_f	Fermi wave vector
l, L	Length
λ	Superconducting coupling constant
λ_f	Fermi wavelength
L_{ij}	Transport coefficient in the Onsager-type scheme between terminals i and j
$\tilde{L}^{ij}_{T/L,T/L}(E)$	Response coefficient in an energy-dependent Onsager-type scheme, between terminals i and j and modes T or L
m, m_e	(Free-)Electron mass
μ	Chemical potential
μ_B	Bohr magneton
μ_S	Potential of Cooper pairs
$\hat{\boldsymbol{n}}$	Outward normal unit vector
N_f	Density of states per unit volume at Fermi surface, in normal state
ω	Frequency (angular)
ω_m	Matsubara frequency
C_1, C_2, ...	Cumulants
p_f	Fermi momentum
$\mathfrak{P}$	Path in a circuit
Φ	Magnetic flux
ϕ	Superconducting phase, or scalar potential
Φ_0	Magnetic flux quantum
φ	Superconducting phase difference
Π	Peltier coefficient
q	Charge
$\boldsymbol{R}$	Spatial coordinate vector
R	Resistance
ρ	Charge density
ρ_0	Charge density in normal state
R_N	Resistance in normal state
S	Thermopower (in section 2), or, noise (in section 3)
σ_N	Normal-state conductivity
$\check{\Sigma}$	Self-energy
$\check{\sigma}$	Quasiclassical self-energy
σ_k	Normal-state conductivity of wire k
T	Temperature
t	Time or thickness
τ_1, σ_1	Spin matrix $\begin{pmatrix} 0 & 1 \\ 1 & 0 \end{pmatrix}$
τ_2, σ_2	Spin matrix $\begin{pmatrix} 0 & -i \\ i & 0 \end{pmatrix}$
τ_3, σ_3	Spin matrix $\begin{pmatrix} 1 & 0 \\ 0 & -1 \end{pmatrix}$

$\tau_\uparrow$	Spin matrix $\begin{pmatrix} 0 & 1 \\ 0 & 0 \end{pmatrix}$
$\tau_\downarrow$	Spin matrix $\begin{pmatrix} 0 & 0 \\ 1 & 0 \end{pmatrix}$
θ	Pairing amplitude (in θ-parametrization)
T_n	Transmission eigenvalue
U	Potential
V	Potential or voltage
v_f	Fermi velocity
v_S	Superfluid velocity
w	Width
ξ	Superconducting coherence length, or, energy (corresponding to a momentum)
ξ_0	Superconducting coherence length at zero temperature
ξ_T	Superconducting coherence length at temperature T
ξ_f	Fermi energy (when comparing to momentum)

1 Introduction

Superconductivity is one of the striking discoveries of the last century: a macroscopic state of matter that has unambiguous exotic properties which can be fully explained only with quantum mechanics. Research in superconductivity has consequently blossomed and sprouted many offshoots, both in the applied and pure sciences.

One of the active research fields today where superconductivity has found a natural place is that of mesoscopic or nanophysics; physics concerned with structures larger than atoms ($l \gtrsim 1$ Å) but typically smaller than the macroscopic length scales the human eye can easily see ($l \lesssim 50\,\mu$m). These structures are large enough to be tailored to a given purpose, but small enough so that many microscopic and quantum effects are expressed in them. Understanding of the properties of superconductivity in this regime has both fueled theoretical interest and technological hopes, such as those of understanding limits of quantum coherence and building a workable quantum computer in solid state [1–3], and it has also contributed novel devices, such as sensitive radiation detectors that are today very relevant for astronomy [4–6].

An important facet of superconductivity can be found in contacts between superconductors and non-superconducting materials: superconducting properties tend to leak short distances across such interfaces. Although this proximity effect was discovered and studied early [7], significant new aspects of it were revealed when an improved control and understanding of the mesoscopic structures useful for its study were achieved in the 1980-90s [8, 9]. Recently, studies also extended to novel nanomaterials, such as carbon nanotubes and graphene. [10–12] New data renewed interest in theoretical studies of the proximity effect: for example its effect on transport and other nonequilibrium properties of materials has been recently studied, as have its behavior in more involved mesoscopic structures and prospective technological applications. This thesis is a part of this ongoing work: a major section of the text is devoted to describing the role the proximity effect has in thermoelectric transport phenomena, which are one of the less understood aspects of the proximity effect. We also discuss modelling transport in proximity circuits and certain signatures of the proximity effect in devices driven more strongly out of thermal equilibrium.

A second topic of mesoscopic physics relevant for this thesis is the study of electrical noise. As in the macroscopic world, noise can be a nuisance also in mesoscopic systems, where it for example tends to destroy the delicate quantum coherence. However, nonequilibrium noise from mesoscopic conductors carries a fingerprint of the transport processes giving rise to it. [13] This has motivated a large body of theoretical work studying the electrical fluctuations and especially their statistics in detail. However, measuring the predicted effects has turned out to be challenging. The latter part of this thesis details one of the mesoscopic devices suggested for accessing statistics of the fluctuations. It is also interesting to note that when quantum coherence is taken into account, the problem of understanding the noise becomes intimately related to the problem of quantum measurement [14]. Mesoscopic detec-

tors that are themselves quantum coherent could shed experimental light on this subtle issue.

Organization of this Thesis

The first part of this thesis concerns the superconducting proximity effect. Section 2 introduces it and gives general background information. Section 2.1 is a bird's-eye view on the nonequilibrium Green function technique that can be used to study it. Sections 2.2 and 2.3 give some background and a few new results on the proximity effect in and out of equilibrium.

Several main results of this thesis concerning thermoelectric effects in proximity structures are discussed in Section 2.4. Results on other proximity-related effects further away from equilibrium are discussed in Section 2.5.

The second part of this thesis, Section 3, discusses the noise in mesoscopic structures. This part contains a brief introduction to the mesoscopic noise and counting statistics, and some results on the semiclassical noise theory is explained in 3.1. The last part, Section 3.2, details a suggested measurement scheme for the spectrum of a part of the counting statistics.

The thesis concludes with a summary of what was done and a discussion of some open problems and future prospects in Section 4. This is followed by appendixes that supplement technical detail for the main text.

2 Superconducting proximity effect

When a non-superconducting ("normal") material is in contact to a superconductor, it can exhibit signs of superconductivity in its properties: the superconductivity appears to leak slightly. This is called the *superconducting proximity effect*. [7] In this section, some history and a physical picture concerning this phenomenon is explained. Section 2.1 gives an overview on the theory with which it can be studied quantitatively, and sections starting from 2.2 concentrate on the main topics of this thesis.

Study of the proximity effect dates back to the 1950-1960s [7, 15, 16], when it was examined in thin metal layers, manufactured on substrate or on another metal. A characteristic example of these structures can be found in [17], a 11...200 nm silver (normal, "N") film below 50 nm of lead (superconductor, "S"). The other dimensions of the films were macroscopic. Exploration of the proximity effect concentrated on variants of this type of structures and for example point contacts, both in equilibrium and out of equilibrium. To name a few examples, effects of bias voltage [18], microwave irradiation [19], and magnetic field [20] were studied in S-N-S stacks before 1980s. Later, the field experienced a boost in the beginning of 1990s when more complicated mesoscopic hybrid structures could be manufactured, and the proximity effect could be studied in more detail. [8, 9] The subsequent work in the mesoscopic proximity effect has not been restricted only to metal structures: its fingerprints have been observed in 2D electron gases in semiconductors [21], and unconventional effects have been predicted and seen in ferromagnets [22] and in novel nanomaterials such as carbon nanotubes [10, 11] and graphene [12].

To understand where the proximity effect comes from, some facts on superconductivity need to be mentioned. Superconductivity is characterized by two major microscopic features: existence of a condensate of Cooper pairs and a gap $|\Delta|$ in the density of states. [23] These have significant consequences on for example their transport properties: the Cooper pair condensate can carry charge current without resistance and generation of heat. However, Cooper pairs do not carry heat current, and since no excitations (see Fig. 2.1) can occur at energies below $|\Delta|$, at low temperatures $T \ll |\Delta|$ the conduction of heat is inhibited. The two microscopic features are also responsible for the proximity effect.

The mechanism occurring at N-S interfaces that gives rise to the proximity effect is the Andreev reflection. [23, 24] (See Fig. 2.2.) An electron excitation cannot directly penetrate a superconductor at energies below the superconducting gap, since there are no single-particle states available. However, it can form a Cooper pair with another electron, and the pair can propagate inside the superconductor. The second electron leaves behind a hole-like excitation, which is correlated with the original electron. Momentum and energy E is conserved in the pairing: electron has momentum $p \simeq p_f + p_f E/E_f$ and hole momentum $p' \simeq p_f - p_f E/E_f$. This implies that the Cooper pair has a total momentum $|\boldsymbol{P}| \ll p_f$, much smaller than the

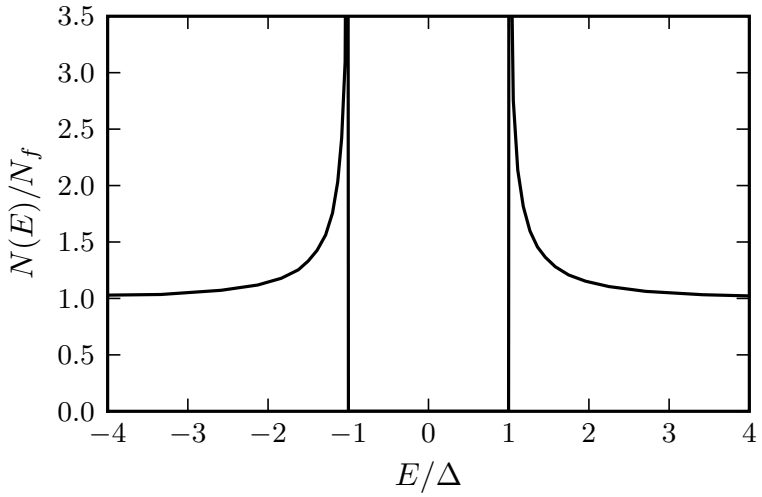

Figure 2.1: Density of states in a superconductor. There is an energy gap of size $2|\Delta|$ centered at the Fermi energy E_f, in which there are no single-particle states available. In all known materials $|\Delta| \ll E_f$, so that at energies away from E_f, the DOS approaches the normal-state value N_f.

Fermi momentum p_f of the electron. Moreover, since holes have an opposite group velocity $\boldsymbol{v} = \nabla_{\boldsymbol{p}} E(\boldsymbol{p})$ as compared to electrons, the hole travels almost exactly to the opposite direction, away from the interface. This coherent exchange of electrons to holes (and vice versa) at superconducting interfaces causes superconductivity-like correlations to appear in the vicinity of superconductors.

In the language of quantum mechanics, the coherence implied by the Andreev reflection can be quantified by the correlation function [7, 25]

$$F^\dagger(\boldsymbol{R}, t_2; \boldsymbol{R}, t_1) \sim \left\langle \psi^\dagger(\boldsymbol{R}) U(t_2, t_1) \psi^\dagger(\boldsymbol{R}) U(t_1, t_2) \right\rangle , \tag{2.1}$$

which is large near and inside superconductors, and zero deep inside non-superconducting materials. In the above expression, the rightmost $\psi^\dagger$ creates the electron excitation at point $\boldsymbol{R}$, the time evolution $U(t_2, t_1)$ moves time forward by $t_2 - t_1$, and the leftmost $\psi^\dagger$ probes for a hole excitation at the starting point at the later time t_2. An overview how this type of correlation functions can be calculated from basic principles is given in subsequent sections.

How far from the superconductor does the proximity effect reach? A rough dimensional analysis can be made: [9] consider again the Andreev reflection in Fig. 2.2. The difference $\Delta p = 2Ep_f/E_f$ between electron and hole momenta implies that the two will lose phase coherence at distances l for which $\Delta\phi = l\Delta p/\hbar \gtrsim \pi$. In clean metals, at distance d from the interface, typical l is $l = d$, and for dirty metals where the electron is scattered from many impurities, this is instead given by the diffusion

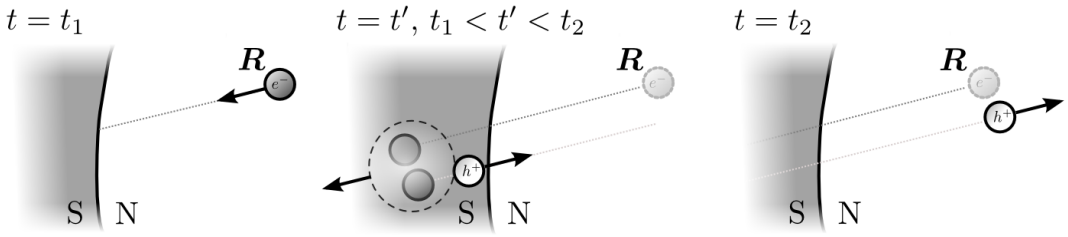

Figure 2.2: Andreev reflection at a superconductor–normal-metal interface. Electron e^- starting at point $\boldsymbol{R}$ at time t_1 hits the interface at time t'. It can enter the superconductor only by pairing with another electron and forming a Cooper pair. The pairing creates a hole excitation h^+, which propagates in the opposite direction, and finally back to $\boldsymbol{R}$. This coherent process creates electron-hole correlations near the interface.

length $l \sim vd^2/2D$, where D is the diffusion constant. This means that the proximity effect has a certain characteristic coherence length scale: $\xi \sim \hbar v/E$ in clean metals and $\xi \sim \sqrt{\hbar D/E}$ when the impurity concentration is large. At equilibrium, relevant excitation energies E are given by the temperature T. For typical metal parameters, the corresponding length is then $\xi_T \sim 0.1 \ldots 1\,\mu$m at the temperatures below 1 K where for example aluminum is still superconducting. Hence, the proximity effect manifests on length scales that are well inside the domain of mesoscopic physics.

Andreev reflection also offers a way for Cooper pairs to pass through non-superconducting metals: [26, 27] the hole reflected back from one interface can enter a second superconducting interface, be reflected back as an electron, and this process can repeat. Electrons bound in this way between two interfaces coherently transfer charge $2e$ per cycle, without dissipation: supercurrent can flow through such an S-N-S link. By similar reasoning as in the above argument, the characteristic energy scale for these Andreev bound states is given by the transport energy $E_T = \hbar v/d$ or $E_T = \hbar D/d^2$. However, it is limited from above by the magnitude of the superconducting energy gap Δ, giving the energy range in which Andreev reflection is possible.

The physical picture of Andreev reflection explains several features of the proximity effect. In the following section, an overview on the theory of inhomogeneous superconductivity that explains it rigorously is given. Below it, in Section 2.2.2 this theory is applied for finding a convenient expression for supercurrents in mesoscopic structures (cf. **VII**). Analysis of the effect of magnetic field in **VIII** is discussed in 2.2.3, and the tools used for describing thermoelectricity in **V** and **VI** are discussed in Section 2.3.2. Results concerning the thermoelectric proximity-Seebeck effect in **I**, **II**, and **IV** are reported in Section 2.4. Properties of its time-reversed counterpart, the proximity-Peltier effect discussed in **V** is then explained in Section 2.4.2. The last section 2.5 concentrates on two out-of-equilibrium effects: analysis of the distribution function modification in **III**, and discussion of stability of phase config-

urations under nonequilibrium in **VII**.

2.1 Quasiclassical theory: Boltzmann equations for superconductivity

The quasiclassical theory is a Green's function technique with certain simplifications that are valid for metals. Superconductivity fits naturally in this framework; the correlation function (2.1) is a part of the total the Green function. When dealing with nonequilibrium problems, the final quasiclassical equations split naturally into two parts: one describing the superconducting correlations (eg. the F function), and one describing the kinetics of excitations. The final kinetic equation often resembles an extension of the Boltzmann equation. [28, 29] Consequently, quasiclassics can be seen as the appropriate extension of the semiclassical method to superconductors.

This section contains no new results, and similar discussions can be found in textbooks [30–33] and reviews [29, 34]. The main motivation for this brief review is to start from first principles and proceed in a linear fashion up to the point where the publications **I**, **II**, **III**, **IV**, **VI**, and **VIII** begin, to indicate where the subsequent parts of this thesis and the published articles fit in a wider theoretical context. Below, we introduce the basis of the quasiclassical theory of inhomogeneous nonequilibrium superconductivity, the corresponding notation, the parameterizations used in practical calculations, and finally theoretical additions needed in mesoscopic structures.

2.1.1 Nonequilibrium Green's functions

Describing many-body quantum systems runs immediately into two problems: First, the full quantum-mechanical description of a N-particle system is given by its density matrix, $\rho(\boldsymbol{R}_1, \ldots, \boldsymbol{R}_N; \boldsymbol{R}'_1, \ldots, \boldsymbol{R}'_N)$. However, for large N (eg. number of electrons in a block of metal), it is in general impossible to handle this quantity because of the large number of dimensions. Second, while it is possible to write down the expression for ρ that describes a system in equilibrium, there is no single well-defined ρ that describes a system that is out of equilibrium. Indeed, a system of particles can be driven out of equilibrium in many different ways, and the challenge is in describing the time evolution of such systems in a tractable fashion.

The above problems in many-body physics call for coarse-graining: describing the system using a simpler quantity, which obeys laws that can be derived from those governing ρ. The nonequilibrium Green function methods are one systematic way to do this. They usually follow a formulation similar to that of Keldysh. [29, 35]

The nonequilibrium theory in electron systems is usually formulated in terms of correlation functions: the Green functions $G(1, 1') = -i \operatorname{Tr}\{T_c[S_c \psi(1)\psi^\dagger(1')]\rho\}$ with $1 = (\boldsymbol{r}_1, \sigma_1, \tau_1)$ specifying the location, spin and contour-time arguments of the

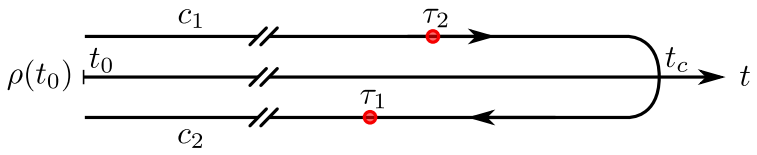

Figure 2.3: Keldysh contour, consisting of forward (c_1) and backward (c_2) branches, on which the Green function $G(\tau_1, \tau_2)$ is defined. The event at τ_1 occurs after τ_2 on the contour, but at an earlier time. Contour ordering $T_c[\psi(\tau_1)\psi(\tau_2)]$ places the operator with the last τ first, contributing a factor of -1 for each transposition.

electron creation and annihilation operators. Meaning of T_c, S_c, and the contour is explained below. The main point is that the two-point function G depends only on two coordinates and can describe the state of the system in a coarse-grained fashion: many physical observables, such as particle or current densities, can be written in terms of Green functions, and so many problems are essentially solved after the Green function is found. However, the Keldysh technique is not restricted to the above one-point Green functions; other quantities describing correlations in more detail can be defined and handled (see eg. [36]).

The main idea leading to equations of motion in the Keldysh approach is very natural: The expectation value of a quantum operator evolving under Hamiltonian $H(t) = H_0 + V_S(t)$ can in the interaction picture be written as $\langle A(t)\rangle = \mathrm{Tr}\{\bar{T}[\exp(-i\int_t^{t_0} \mathrm{d}t'\, V(t'))]A(t)T[\exp(-i\int_{t_0}^{t} \mathrm{d}t'\, V(t'))]\rho(t_0)\}$, using (anti)time ordering operators $(\bar{})T$. [1] This can be compactly rewritten using a contour ordering (see Fig. 2.3): $\langle A(t)\rangle = \left\langle T_c[\exp(-i\int_c \mathrm{d}\tau'\, V(\tau'))A(\tau)]\right\rangle = \langle T_c[S_c A(\tau)]\rangle$. Note that the end-point t_c of the contour can be chosen arbitrarily provided $t < t_c$; $\langle A(t)\rangle$ does not depend on $V(t')$ for $t' > t$. That there is only one time-ordering operator is useful for applying methods from the standard toolbox of diagrammatic perturbation theory. [29]

Assuming that $\rho(t_0)$ is the equilibrium state of H_0, $\langle \ldots \rangle = \mathrm{Tr}\{e^{-\beta H_0}(\ldots)\}/\,\mathrm{Tr}\{e^{-\beta H_0}\}$, the standard perturbation expansion applies,

$$\left\langle T_c[S_c\psi(1')\psi^\dagger(1'')]\right\rangle = \sum_{k=0}^{\infty} \frac{(-i)^k}{k!} \int_c \mathrm{d}1 \ldots \mathrm{d}k \left\langle T_c[V(1)\ldots V(k)\psi(1')\psi^\dagger(1'')]\right\rangle . \quad (2.2)$$

Now, provided H_0 is quadratic in ψ, one can apply the Wick theorem to decompose the time-ordered products $\left\langle T_c[\psi^{(\dagger)}\ldots\psi^{(\dagger)}]\right\rangle_0$ into expressions involving only G. The terms obtained from the (formal) perturbation expansion can be reordered and

[1] Most of this thesis is written in dimensionless units, $\hbar = k_B = e = 1$. Units are restored to emphasize important final results only.

collected into a self-energy Σ in a Dyson equation

$$[G_0^{-1}(1,3) - \Sigma(2,3)]G(3,2) = \delta(1-2)\,, \tag{2.3}$$

where $G_0^{-1}(1,3) = \delta(1-3)[i\partial_{t_3} - H_0(3)]$ and $H_0(3)$ is the operator on $(\boldsymbol{r}_3, \sigma_3, \tau_3)$ representing the Hamiltonian H_0; for example for free electrons $H_0(3) = -\frac{\hbar^2}{2m}(\nabla_{\boldsymbol{r}_3} - i\boldsymbol{A})^2$ where $\boldsymbol{A}$ is the vector potential and m the electron mass. As usual, integration and summation over repeated indices is implied in the notation above. The self-energy Σ can be written as a functional of G, and it effectively plays the role of a mean field where the electrons move in. In the context of solid state, it can represent interactions such as scattering of electrons from phonons, impurities, or other electrons. [32]

Alternatively to the perturbation expansion, one can also derive the Dyson equation by finding the equation of motion [33, 37] for the contour time dependence of the Green function G. The equation will in general contain multi-point Green functions, eg. $G(12;34)$, which do not reduce to two-point functions. In this framework, the self-energies can be understood as approximations for the expressions containing these terms, often motivated by the perturbation expansion (2.2).

The above framework, Green functions and their Dyson equations on the Keldysh contour, has proved successful in studies of nonequilibrium superconductivity. How superconductivity can be taken into account is explained in the next section.

2.1.2 Superconductivity

The physical cause for conventional superconductivity is an attractive interaction between electrons, mediated by phonons. There are several ways to model this: simple point-like electron-electron interaction $V = g\int \mathrm{d}^3\boldsymbol{r}\, \psi^\dagger(\boldsymbol{r})\psi^\dagger(\boldsymbol{r})\psi(\boldsymbol{r})\psi(\boldsymbol{r})$ with $g < 0$ [25, 38–40], local interaction mediated by bosons $V = g\int \mathrm{d}^3\boldsymbol{r}\, \psi^\dagger(\boldsymbol{r})\psi(\boldsymbol{r})\varphi(\boldsymbol{r})$ plus some model for the boson field [30], or other alternatives. An important point is that the ground state of this type of models is the superconducting state (at zero temperature), even for arbitrarily weakly attractive interaction. [38–40] The exact form of a weak interaction turns out to be unimportant for understanding many of the phenomena associated with superconductivity.

Superconducting state is characterized by finite electron-hole correlations, as noted by Bardeen, Cooper and Schrieffer: [38–40] correlators such as $\langle\psi_\downarrow\psi_\uparrow\rangle$ and $\left\langle\psi_\uparrow^\dagger\psi_\downarrow^\dagger\right\rangle$ are finite, unlike in the normal state. This property of the superconducting ground state must be taken into account when approximating the multi-point function $G(12;34)$, or in the perturbation expansion (2.2). For this purpose, one can define anomalous Green's functions, [25, 41] $F(1,1') = -i\langle T_c[S_c\psi(1)\psi(1')]\rangle$ and $F^\dagger(1,1') = -i\left\langle T_c[S_c\psi^\dagger(1)\psi^\dagger(1')]\right\rangle$. Including them and approximating the interaction term (eg. via the perturbation expansion) leads to a set of Dyson equations — the Gor'kov

equations [25]

$$[G_0^{-1} - \Sigma]G - \Sigma_F F^\dagger = \delta\,, \qquad [G_0^{-1} - \Sigma]F - \Sigma_F \bar{G} = 0\,, \tag{2.4}$$

$$-[G_0^{-1*} - \bar{\Sigma}]F^\dagger + \Sigma_{F^\dagger} G = 0\,, \qquad [G_0^{-1*} - \bar{\Sigma}]\bar{G} + \Sigma_{F^\dagger} F = \delta\,, \tag{2.5}$$

which determine G, F, $F^\dagger$, and $\bar{G}(12) = G(21)$, once the self-energies Σ are given. Here, $\delta(1,2) = \delta(\boldsymbol{r}_1 - \boldsymbol{r}_2)\delta(\tau_1 - \tau_2)\delta_{\sigma_1,\sigma_2}$. The above equations describe not only superconductivity, but also the superconducting proximity effect: the interaction g can depend on the position $\boldsymbol{r}$, being zero inside normal metals and finite inside superconductors.

The self-energy terms in the Gor'kov equation depend on the model of the interaction. What is done in the conventional weak-coupling approximation is that the parts of Σ and $\bar{\Sigma}$ related to the interaction (g) are usually absorbed into G_0, and subsequently neglected: they mostly adjust some parameters such as the chemical potential of the normal-state electron system and bring no qualitative new behavior. Also, inserting eg. the point interaction, one can relate the self-energies Σ_F and $\Sigma_{F^\dagger}$ back to F and $F^\dagger$. For example, the equations of motion give in the simplest approximation [25, 30]

$$\Sigma_F(1,2) = gF(1,2)\delta(\tau_1 - \tau_2)\delta(\boldsymbol{r}_1 - \boldsymbol{r}_2)\,, \tag{2.6}$$

$$\Sigma_{F^\dagger}(1,2) = gF^\dagger(1,2)\delta(\tau_1 - \tau_2)\delta(\boldsymbol{r}_1 - \boldsymbol{r}_2)\,. \tag{2.7}$$

For a more detailed phonon model, similar results are found in the weak-coupling limit, see for example [29, 30].

Using the "off-diagonal" part of the self-energy, one can define the superconducting pair potential Δ, sometimes also known as the order parameter,

$$\Delta_{\sigma_1,\sigma_2}(\boldsymbol{r}_1, \tau_1) \equiv |g|F(\boldsymbol{r}_1, \sigma_1, \tau_1; \boldsymbol{r}_1, \sigma_2, \tau_1)\,, \tag{2.8}$$

which is finite inside a superconductor, but vanishes in the normal state. Its presence also causes an energy gap of size $|\Delta|$ to open in the density of states as indicated in Fig. 2.1.

The above concepts, the "anomalous" functions F and $F^\dagger$ and the order parameter Δ, are fundamental in descriptions of superconductivity. However, for eg. numerical calculations it is necessary to step back from the abstract Keldysh contour and specify the structure of G and F in more detail. This is discussed next.

2.1.3 Matrix structure

Keeping track of the anomalous functions is made easier by replacing the Green function with a 2×2 matrix, $\hat{G}(1,2) = -i\hat{\tau}_3 \left\langle T_c[\hat{\psi}(1)\hat{\psi}(2)^\dagger] \right\rangle$, ie.,

$$[\hat{G}(1,2)]_{k_1,k_2} = -i(\hat{\tau}_3)_{k_1,k_1} \left\langle T_c[S_c \psi^{k_1}(1)\psi^{k_2}(2)^\dagger] \right\rangle \tag{2.9}$$

using the Nambu spinor $\hat{\psi}$: $\psi^1(1) = \psi_{\sigma_1}(\boldsymbol{r}_1, \tau_1)$, $\psi^2(1) = \psi^\dagger_{\bar{\sigma}_1}(\boldsymbol{r}_1, \tau_1)$. [41] One can express $\langle\psi\psi\rangle$, $\langle\psi\psi^\dagger\rangle$, $\langle\psi^\dagger\psi\rangle$, and $\langle\psi^\dagger\psi^\dagger\rangle$ in terms of elements of $\hat{G}$. The notational simplification requires defining a similar 2×2 matrix structure for V and for Σ, but it preserves the structure of the theory. For example, the Gor'kov equation reads

$$[\hat{G}_0^{-1} - \hat{\Sigma}]\hat{G} = \hat{1}\delta\,, \tag{2.10}$$

where a product between the functions also involves a matrix product in the Nambu space.

Another layer of matrix structure is useful if one wants to map the Green's functions $G(\tau, \tau')$ defined on the contour to functions of time, $G(t, t')$. For each t, t' there are four possible ways to place the corresponding τ and τ' on the contour. By choosing the mapping carefully, one can guarantee an isomorphism between contour-ordered functions and 2×2 matrix functions ($\check{}$),

$$\begin{aligned} &A(1,2) \mapsto \check{A}(\boldsymbol{r}_1, \sigma_1, t_1, \boldsymbol{r}_2, \sigma_2, t_2)\,, \quad B(1,2) \mapsto \check{B}(\boldsymbol{r}_1, \sigma_1, t_1, \boldsymbol{r}_2, \sigma_2, t_2)\,, \\ &A(1,3)B(3,2) \mapsto \sum_{\sigma_3}\int \mathrm{d}\boldsymbol{r}_3\,\mathrm{d}t_3\,\check{A}(\boldsymbol{r}_1, \sigma_1, t_1, \boldsymbol{r}_3, \sigma_3, t_3)\check{B}(\boldsymbol{r}_3, \sigma_3, t_3, \boldsymbol{r}_2, \sigma_2, t_2)\,, \end{aligned} \tag{2.11}$$

and again retain the structure of the theory. There are multiple equivalent ways for choosing this mapping. [42] One convenient choice often used in problems of nonequilibrium superconductivity is [29]

$$\check{G} = \begin{pmatrix} \hat{G}^R & \hat{G}^K \\ 0 & \hat{G}^A \end{pmatrix}\,, \tag{2.12}$$

$$[\hat{G}^R(1,2)]_{k_1,k_2} = \hat{G}_{c_1,c_1} - \hat{G}_{c_1,c_2} = -i(\hat{\tau}_3)_{k_1,k_1}\theta(t_1 - t_2)\left\langle\{\psi^{k_1}(1), \psi^{k_1\dagger}(2)\}\right\rangle\,, \tag{2.13}$$

$$[\hat{G}^A(1,2)]_{k_1,k_2} = \hat{G}_{c_1,c_1} - \hat{G}_{c_2,c_1} = +i(\hat{\tau}_3)_{k_1,k_1}\theta(t_2 - t_1)\left\langle\{\psi^{k_1}(1), \psi^{k_2\dagger}(2)\}\right\rangle\,, \tag{2.14}$$

$$[\hat{G}^K(1,2)]_{k_1,k_2} = \hat{G}_{c_2,c_1} + \hat{G}_{c_1,c_2} = -i(\hat{\tau}_3)_{k_1,k_1}\left\langle[\psi^{k_1}(1), \psi^{k_2\dagger}(2)]\right\rangle\,, \tag{2.15}$$

where the G_{c_1,c_2} notation indicates a contour function, with τ_1 and τ_2 fixed on either the upper (c_1) or lower (c_2) branches of the Keldysh contour. The above representation is what is used below. It turns out that the Retarded (R) and Advanced (A) Green functions mainly describe the available electron states, whereas the Keldysh (K) function has to do with their population.

For example, equation (2.6) can be written in the above form as

$$\begin{aligned} &\Sigma_F^R(t_1,t_2) = gF_{c_1,c_1}(t_1,t_2)\delta(t_1-t_2)\delta(\boldsymbol{r}_1-\boldsymbol{r}_2) = \frac{g}{2}F^K(t_1,t_2)\delta(t_1-t_2)\delta(\boldsymbol{r}_1-\boldsymbol{r}_2)\,, \\ &\Sigma_F^A(t_1,t_2) = gF_{c_1,c_1}(t_1,t_2)\delta(t_1-t_2)\delta(\boldsymbol{r}_1-\boldsymbol{r}_2) = \Sigma_F^R(t_1,t_2)\,, \\ &\Sigma_F^K(t_1,t_2) = 0\,, \end{aligned} \tag{2.16}$$

since $F_{c_1,c_1}(t,t) = F_{c_1,c_2}(t,t) = F_{c_2,c_1}(t,t)$. The corresponding self-consistency rela-

tion for Δ then reads

$$\Delta(\boldsymbol{r},t) = \frac{|g|}{2}F^K(\boldsymbol{r},t;\boldsymbol{r},t) = \frac{|g|}{2}\int_{-E_c}^{E_c}\frac{\mathrm{d}E}{2\pi}F^K(\boldsymbol{r},\boldsymbol{r},E,t) \tag{2.17}$$

in terms of the Fourier transform of $F^K \sim 1/E$ in the time difference. Note the BCS cutoff energy E_c inserted by hand here: it is necessary to regularize a logarithmic divergence in the point interaction approximation. The physical origin of the cutoff is that real interactions caused by phonons cannot operate at very short time scales where there are no corresponding modes in the atom lattice. Consequently, the cutoff E_c is of the order of the Debye frequency ω_D, as a calculation with a better interaction model shows. [30]

The above formulation contains still the spin indices in $1 = (\sigma_1, \boldsymbol{r}_1, t_1)$. The work in this thesis concentrates on conventional spin-singlet superconductors, in which the spin structure of the elements of $\check{G}$ is fixed: $F, F^\dagger \propto -i\sigma_2$ and $G, \bar{G} \propto 1$. For this case, one can consider the quantities as scalars in the spin space, and spin appears only as a prefactor of 2 in observables. Note that the Nambu spinors (2.9) were defined with this simplification in mind.

Combining the above levels of matrix structure allows the theory of nonequilibrium superconductivity to be formulated in terms of 4×4 matrices,

$$\check{G} = \begin{pmatrix} G^R & F^R & G^K & F^K \\ -F^{\dagger R} & \bar{G}^R & F^{\dagger K} & \bar{G}^K \\ 0 & 0 & G^A & F^A \\ 0 & 0 & -F^{\dagger A} & \bar{G}^A \end{pmatrix}, \tag{2.18}$$

in the Keldysh ($\check{}$) $\otimes$ Nambu ($\hat{}$) spaces. However, the equation of motion (2.10) contains some non-essential information and can be simplified, as discussed next.

2.1.4 Quasiclassical approximation

The quasiclassical theory is the geometrical optics of quantum transport. Its approximations aim to simplify the $|\boldsymbol{r}_1 - \boldsymbol{r}_2|$ dependence of the electron Green function, by averaging out the oscillations occurring on the scale of the Fermi wavelength λ_f of conduction electrons. [24, 43] In the Fourier-transformed Wigner representation, this is equivalent to describing the behavior of a sharp peak on the Fermi surface $k^{-1} = \lambda_f$ in momentum space. [44–46] Similarly to geometrical optics, quasiclassical theory does not describe phenomena that occur on length scales smaller than the wavelength. Nevertheless, since λ_f is for many metals of the order of atomic length scales, quasiclassical methods are a powerful tool for describing many phenomena, conventional inhomogeneous superconductivity among them.

The usual way [44–46] of deriving the necessary approximations is to first transform

to a Wigner representation, where

$$\check{G}(\boldsymbol{R},\boldsymbol{p}) = \int \mathrm{d}\boldsymbol{r}\, e^{-i\boldsymbol{p}\cdot\boldsymbol{r}} \check{G}(\boldsymbol{R}+\frac{\boldsymbol{r}}{2},\boldsymbol{R}-\frac{\boldsymbol{r}}{2})\,, \tag{2.19}$$

$$(\check{A}\otimes\check{B})(\boldsymbol{r}_1,\boldsymbol{r}_2) \mapsto e^{\frac{i}{2}(\nabla_{\boldsymbol{p}_1}\cdot\nabla_{\boldsymbol{R}_2}-\nabla_{\boldsymbol{p}_2}\cdot\nabla_{\boldsymbol{R}_1})}\check{A}(\boldsymbol{R}_1,\boldsymbol{p}_1)\check{B}(\boldsymbol{R}_2,\boldsymbol{p}_2)\big|_{\boldsymbol{R}_1=\boldsymbol{R}_2=\boldsymbol{R},\boldsymbol{p}_1=\boldsymbol{p}_2=\boldsymbol{p}}\,, \tag{2.20}$$

with $\otimes$ denoting spatial and time convolution (see Appendix B), then expand the exponent of differential operators in the left-right subtracted Dyson equation, $[G_0^{-1}-\Sigma,G]_\otimes = 0$ to first order in gradients, and finally integrate over $\xi = \boldsymbol{p}^2/(2m)$ neglecting the $|\boldsymbol{p}|$-dependence of the self-energy. This is permissible due to the peak of G and smoothness of Σ at the Fermi surface. Subsequently,[2]

$$\check{G} \mapsto \check{g}(\boldsymbol{R},\hat{\boldsymbol{p}},t,t') = \frac{i}{\pi}\int \mathrm{d}\xi\, \check{G}(\boldsymbol{R},\hat{\boldsymbol{p}}p(\xi),t,t')\,, \tag{2.21}$$

and calculations can after that be made using quasiclassical Green's functions $\check{g}$ only. This approximation however neglects some physics, which is discussed in more detail Section 2.4.

The quasiclassical Dyson equation is the Eilenberger equation, [45] which also applies in nonequilibrium, [48, 49]

$$\boldsymbol{v}_f\cdot\hat{\nabla}\circ\check{g} + [-i\epsilon\hat{\tau}_3 + \phi + \check{\sigma} + \check{\Delta},\check{g}]_\circ = 0\,. \tag{2.22}$$

Above, $\circ$ denotes time convolution, and $\hat{\nabla}\circ B = \nabla_{\boldsymbol{R}}B - i[\boldsymbol{A}\hat{\tau}_3,B]_\circ$ is the gauge-invariant gradient involving the vector potential $\boldsymbol{A}(t,t') = \delta(t-t')\boldsymbol{A}(t)$. In addition, $\phi(t,t') = \phi(t)\delta(t-t')$ is the scalar potential, $\check{\sigma}$ the self-energy at the Fermi surface, and $\epsilon(t,t') = i\delta(t-t')\partial_{t'}$. The velocity $\boldsymbol{v}_f(\hat{\boldsymbol{p}})$ is perpendicular to the Fermi surface, and $|\boldsymbol{v}_f| = k_f/m$. The superconducting pair potential $\check{\Delta} = \hat{\tau}_\uparrow\Delta - \hat{\tau}_\downarrow\Delta^*$ is off-diagonal in the Nambu space and diagonal in Keldysh, as indicated in Eq. (2.16). The above already strongly resembles a transport equation, and in fact Boltzmann-like transport equations can be derived from it.

However, because of the left-right subtraction, (2.22) does not fully determine the Green's function: since the equation is homogeneous, $L\{\check{g}\} = 0$, and the coefficient operator is linear and distributive, $L\{\check{a}\circ\check{b}\} = L\{\check{a}\}\circ\check{b} + \check{a}\circ L\{\check{b}\}$, for a solution $\check{g}$, any $\check{g}\circ\check{g}\circ\ldots\circ\check{g}$ is also a solution. The missing information can be represented by a normalization condition $\check{g}\circ\check{g} = \check{1}\delta$. [32, 43, 45, 46] It is useful to note that the Eilenberger equation does not contain spatial convolutions, and the equation can be solved by integrating along trajectories in the velocity directions $\boldsymbol{v}_f$ (see eg. [50]).

The direction-of-momentum dependence in the Eilenberger equation can be ne-

[2] The integral actually needs to be cut off at some large ξ_c or otherwise regularized [45] to render it convergent. Moreover, usually one also assumes that the Green function and the self-energies are already renormalized, ie., strong interactions are absorbed in quantities such as the quasiparticle mass and electron-phonon coupling constants. In this sense, the quasiclassical theory can be understood as an extension of Landau's Fermi liquid theory, see e.g. [47].

glected in some cases. One important case is the dirty limit; it is valid for metals with a large enough concentration of impurities that scatter electrons and randomize their trajectories. This transforms the Eilenberger equation to a diffusion equation for the momentum-averaged (ie. s-wave) Green function $G = \langle g \rangle_{\hat{\boldsymbol{p}}}$, [3]

$$D\hat{\nabla} \circ \left(\check{G} \circ \hat{\nabla} \circ \check{G} \right) = \left[-i\epsilon\, \hat{\tau}_3 + \check{1}\phi + \check{\sigma}_{\mathrm{in}} + \check{\Delta}, \check{G} \right]_\circ . \tag{2.23}$$

First derivation of an equation resembling this was given by Usadel. [51] Here, $D = \frac{1}{3} v_f l^2$ is the 3D diffusion constant corresponding to the elastic scattering length l, and $\check{\sigma}_{\mathrm{in}}$ a momentum-averaged self-energy from which impurity scattering has been subtracted. This equation is solved below for several static nonequilibrium situations. Note that for these problems, the scalar potential ϕ disappears from the above equation, and self-consistency of the electric field can be consequently neglected.

After the Green functions are known, one can obtain the observable charge and current densities directly from them [30, 47]

$$\rho(\boldsymbol{R}, t) - \rho_0 = -2N_f e^2 \phi(\boldsymbol{R}, t) - eN_f \frac{\pi}{2} \operatorname{Tr} \check{G}^K(\boldsymbol{R}, t, t)\,, \tag{2.24a}$$

$$\boldsymbol{j}(\boldsymbol{R}, t) = \frac{\pi \sigma_N}{e} \operatorname{Tr}[(\check{G} \circ \hat{\nabla} \circ \check{G})^K(t, t)\hat{\tau}_3]\,, \tag{2.24b}$$

where σ_N is the normal-state conductance, ρ_0 the normal-state charge density, and N_f the density of states per unit volume at the Fermi surface. Note that the expression for the change $\rho - \rho_0$ in the charge density splits in the quasiclassical approximation into two parts: the first $\propto \phi$ is a normal-state high-energy contribution, and the latter the low-energy contribution $\mu_n \propto \check{G}^K$ that is affected by superconductivity. [30]

In addition to the above, one has the self-consistency equation for the gap parameter Δ, which in terms of the quasiclassical function reads [30]

$$\Delta(\boldsymbol{R}, t) = \frac{\pi}{2} \lambda f^K(\boldsymbol{R}, t, t)\,, \tag{2.25}$$

where the superconducting coupling constant is $\lambda = |g| N_f$. One should note that the pair potential Δ is related to the potential $\mu_s(\boldsymbol{R}, t) = (2e/\hbar)\partial_t \arg \Delta(\boldsymbol{R}, t)$ of the Cooper pairs. In nonequilibrium situations, this can differ from the electric potential $e\phi$.

When one combines the Eilenberger (or Usadel) equation with the Maxwell equations and self-consistency condition, the set of equations is closed. Moreover, it is tractable in many practical situations.

[3] The left-hand side of the equation is often written as $[\underline{\partial}, \check{G} \circ \underline{\partial} \circ \check{G}]_\circ$ with long gradient $\underline{\partial} = \nabla - iA\hat{\tau}_3$. This is equivalent to the above form, since $\hat{\nabla} \circ (\check{G} \circ \hat{\nabla} \circ \check{G}) = [\underline{\partial}, \check{G} \circ [\underline{\partial}, \check{G}]_\circ]_\circ = [\underline{\partial}, \check{G} \circ \underline{\partial} \circ \check{G}]_\circ - [\underline{\partial}, \check{G} \circ \check{G} \circ \underline{\partial}]_\circ = [\underline{\partial}, \check{G} \circ \underline{\partial} \circ \check{G}]_\circ - [\underline{\partial}, \underline{\partial}]_\circ = [\underline{\partial}, \check{G} \circ \underline{\partial} \circ \check{G}]_\circ$.

2.1.5 Parameterization

Solving the above equations for the Green's function becomes easier if one can eliminate the normalization condition $\check{g} \circ \check{g} = \check{1}\delta$. One convenient way to do this for the Retarded block is the Riccati parameterization [52–54]

$$\hat{g}^R = \begin{pmatrix} N & 0 \\ 0 & \tilde{N} \end{pmatrix} \circ \begin{pmatrix} 1-\gamma\circ\tilde{\gamma} & 2\gamma \\ 2\tilde{\gamma} & -1+\tilde{\gamma}\circ\gamma \end{pmatrix}, \qquad \begin{matrix} N = (1+\gamma\circ\tilde{\gamma})^{-1}, \\ \tilde{N} = (1+\tilde{\gamma}\circ\gamma)^{-1}, \end{matrix} \tag{2.26}$$

where the inverses $(\ldots)^{-1}$ are defined in the sense $C^{-1} \circ C = \delta$. The advanced function is, by definition, related to the retarded via $\hat{g}^A = -\hat{\tau}_3(\hat{g}^R)^\dagger\hat{\tau}_3$, where the hermitian conjugate exchanges the Green function arguments, $1 \leftrightarrow 2$, and transposes and complex conjugates the matrix structure. The Keldysh function can be parameterized similarly by

$$\hat{g}^K = \begin{pmatrix} N & 0 \\ 0 & \tilde{N} \end{pmatrix} \circ \begin{pmatrix} x-\gamma\circ\tilde{x}\circ\gamma^\dagger & -x\circ\tilde{\gamma}^\dagger-\gamma\circ\tilde{x} \\ \tilde{x}\circ\gamma^\dagger+\tilde{\gamma}\circ x & \tilde{x}-\tilde{\gamma}\circ x\circ\tilde{\gamma}^\dagger \end{pmatrix} \circ \begin{pmatrix} N^\dagger & 0 \\ 0 & \tilde{N}^\dagger \end{pmatrix}, \tag{2.27}$$

or, using a distribution function h [55, 56]

$$\hat{g}^K = \hat{g}^R \circ \begin{pmatrix} h & 0 \\ 0 & \tilde{h} \end{pmatrix} - \begin{pmatrix} h & 0 \\ 0 & \tilde{h} \end{pmatrix} \circ \hat{g}^A . \tag{2.28}$$

The above parameterizations are valid also for time-dependent problems where the products and inverses are noncommutative.

For time-independent problems, the distribution functions h and $\tilde{h}$ can be related to the more commonly used electron distribution function by

$$h(E) = 1 - 2f(\mu_S + E), \qquad \tilde{h}(E) = 2f(\mu_S - E) - 1 . \tag{2.29}$$

In the normal state, the distribution function f coincides with the semiclassical distribution function of the Boltzmann theory, [28] which is proportional to the particle density in a given energy interval, $N \propto f(E)\delta E$. Moreover, the Eilenberger equation (2.22) is in this approximation equivalent to the semiclassical Boltzmann equation. [29]

For time-independent problems, the θ-parameterization is also often used:

$$\hat{g}^R = \begin{pmatrix} \cosh\theta & e^{i\chi}\sinh\theta \\ -e^{-i\chi}\sinh\theta & -\cosh\theta \end{pmatrix} . \tag{2.30}$$

It is slightly easier to handle analytically than (2.26). However, the Riccati parameterization is in practice more useful for numerical work due to several reasons: first, $|\gamma| \leq 1$ whereas θ is unbounded. Second, it turns out that χ can undergo rapid spatial changes where θ is small, and even discontinuous ones where $\theta = 0$. Third, hyperbolic functions have $2\pi i$ periodicity which can lead to spurious solutions. These issues can be seen for example in **I** and **II**, where they limit the numerically acces-

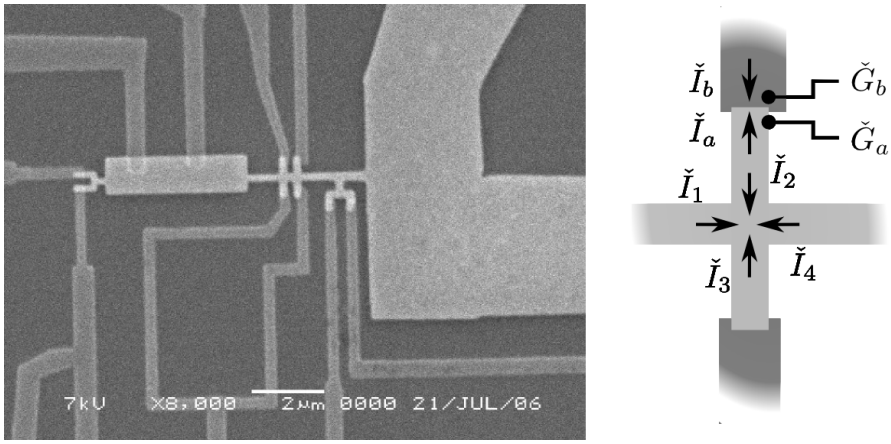

Figure 2.4: Left: A scanning electron microscope image of the mesoscopic metal structure studied in **IV**. Superconductor (aluminum) appears dark gray, the normal metal (silver) light gray; both are deposited on a wafer of silicon that can be seen as the dark background. Right: Schematic description of matrix currents $\check{I}$ in a part of the structure.

sible range of phase differences to $\varphi \lesssim 0.8\pi$. The Riccati parameterization does not exhibit such problems, and was used in the later publications.

2.1.6 Restricted geometries

When proximity effect is studied in mesoscopic circuits, such as that shown in Fig. 2.4, two facts need to be accounted for. First, the equations need boundary conditions since the structure is not of infinite size. Second, the quasiclassical equations need to be considered only within the metallic parts of the structure that may be thin, which may allow for simplifications.

Boundaries between different materials or vacuum interfaces cannot be handled with the quasiclassical equations, since the rapid changes in structure can there occur on length scales small compared to λ_f. The quasiclassical equations need to be supplemented with boundary conditions that give a coarse-grained description of the interface in terms of the quasiclassical functions. Such boundary conditions have been developed by various authors, both for the Eilenberger equation [54, 57] and for the Usadel equation. [58, 59] A general boundary condition for the Usadel equation corresponding to an interface can be written as [59]

$$\check{I}_a = -\check{I}_b = \sum_n \frac{2T_n[\check{G}_a, \check{G}_b]}{4 - T_n(\{\check{G}_a, \check{G}_b\} - 2)}\,, \tag{2.31}$$

where the subscripts refer to the right part of Fig. 2.4. The scalars $T_n \in [0, 1]$ are transmission eigenvalues of transmission channels n describing the properties of

the interface, and $\check{I}$ are matrix currents. [59, 60] In those parts of the structure where the Usadel equation applies, the matrix current density is $\check{j} = \check{G}\hat{\nabla}\check{G}$, which connects Eq. (2.31) to the Usadel equation. The above boundary conditions written in terms of the parameterizations introduced in the previous chapter can be found for example in Refs. [6, 34, 54, 61].

If the considered geometry consists of cylinders of metal ("wires") whose cross-sections A are small compared to their length, one can average the equations across the cross-section. A similar approximation can be made in the presence of translation invariance (e.g. in the wide S-N-S thin film stacks). Typically, this quasi-1D approximation is equivalent with dropping transverse gradients from the equations. At connections where two or more such wires meet ("nodes"), one then needs an additional condition, which turns out to be the conservation of matrix currents [59, 60]

$$\check{G} \text{ is continuous}\,, \qquad \sum_k \check{I}_k = 0\,, \qquad \check{I}_k = A_k\sigma_k(\check{G}\partial_x\check{G})_k\,, \tag{2.32}$$

where k indexes the wires connecting to the node, and the gradients point toward the node, see Fig. 2.4. The above equations are Kirchoff-type conditions for the matrix current $\check{I}$. [59, 60]

When one is interested in only the properties of the proximity effect, the nearby superconductors can often be approximated to remain unperturbed by the contacted normal metal parts, ie., "rigid". [62] This can be justified in the limit where the size of the NS contact is vanishingly small, as compared to the superconducting coherence length, $\xi_0 = \sqrt{\hbar D/2|\Delta|}$ in dirty metals, and the approximation can produce qualitatively correct results even away from this limit. However, at large energies $E > |\Delta|$, excitations in the superconductor may relax slowly in nonequilibrium situations, and this may need to be taken into account. [62]

This completes the overview on the basic theoretical concepts in the background of **I**, **II**, **III**, **IV**, **VI**, and **VIII**. The following sections take a closer look on topics discussed in these articles.

2.2 Equilibrium

In this Section, some aspects of the thermal equilibrium state are discussed, as relevant for the published articles. First, the quasiclassical equations at equilibrium are discussed and general features of supercurrents in superconductor–normal metal structures are remarked on. Second, the approximation scheme derived for and used in **VII** for calculating supercurrents in multiterminal structures is explained. Finally, effects caused by magnetic field in the interferometers studied in **I**, **II**, **III**, **IV**, and its effect on the supercurrent measured in **VIII** are addressed.

At thermal equilibrium, the quasiclassical equations are radically simplified. The first simplification permissible at equilibrium is that all $\circ$ products reduce to ordinary

matrix or scalar products, since at equilibrium no quantity depends on time T in the (E, T) representation (see Appendix B). Second, a detailed-balance relation (see eg. [29, 37]) implies that $\check{G}^K = (\check{G}^R - \check{G}^A)(1 - 2f_0)$, signifying that the population of electrons is given by the equilibrium Fermi function $f_0(E) = [1 + e^{(E-\mu)/T}]^{-1}$ depending on the chemical potential μ and the temperature T. What remains to be solved is only the retarded Green function, which is in the diffusive limit determined from the equations [53, 54]

$$D(\nabla - 2i\boldsymbol{A})^2\gamma - \frac{2\tilde{\gamma}[(\nabla - 2i\boldsymbol{A})\gamma]^2}{1+\gamma\tilde{\gamma}} = -2iE\gamma + i\Delta^*\gamma^2 + i\Delta\,, \tag{2.33a}$$

$$D(\nabla + 2i\boldsymbol{A})^2\tilde{\gamma} - \frac{2\gamma[(\nabla + 2i\boldsymbol{A})\tilde{\gamma}]^2}{1+\gamma\tilde{\gamma}} = -2iE\tilde{\gamma} + i\Delta\tilde{\gamma}^2 + i\Delta^*\,, \tag{2.33b}$$

in the Riccati parameterization, or in the θ-parameterization,

$$D\nabla^2\theta = -2iE\sinh\theta + \frac{v_S^2}{2D}\sinh(2\theta) + 2i|\Delta|\cos(\phi-\chi)\cosh(\theta)\,, \tag{2.34a}$$

$$\nabla\cdot(-v_S\sinh^2\theta) = -2i|\Delta|\sin(\phi-\chi)\sinh(\theta)\,, \qquad v_S \equiv D(\nabla\chi - 2e\boldsymbol{A})\,, \tag{2.34b}$$

where $\Delta = |\Delta|e^{i\phi}$. In both of the above it is assumed that the inelastic self-energy Σ can be neglected. It can be seen in both equations that in the absence of pairing ($g = 0$, $\Delta = 0$), the proximity effect has a length scale $l_E = \sqrt{D/2|E|}$ of decay, which was also the conclusion obtained from the physical arguments in Section 2.

Due to the equilibrium form of $\check{G}^K$, the inverse Fourier transforms required for obtaining the observables (2.24) also eventually lead to energy integrals of the form

$$\int_{-\infty}^{\infty} \mathrm{d}E\, g(E)\tanh\left(\frac{E}{2T}\right) = 2i\pi T \sum_{\omega_n = 2\pi T(n+1/2)>0} g^M(i\omega_n) \tag{2.35}$$

where $\tanh = 1 - 2f_0$ is related to the Fermi function, and function g is analytic on the upper half-plane. As indicated above, the result can be expressed in terms of residues of tanh, and an appropriately analytically continued function g^M, evaluated at the Matsubara frequencies ω_n [63]. This also directly shows why $\xi_T = \sqrt{D/(2\pi T)}$ is the decay scale of proximity effect at equilibrium: physical quantities depend on the Green functions only at energies $E = i\omega_n$, and the smallest of these frequencies is $\omega_0 = \pi T$.

2.2.1 Supercurrent

One of the important consequences of the proximity effect is that it allows current to flow from one superconductor through a short (L/ξ_T not too large) normal metal junction to a second superconductor, without dissipation. This is the DC Josephson effect in proximity structures. The supercurrent I_S is not driven by a potential difference (which cannot exist at equilibrium), but a difference $\varphi = \phi_2 - \phi_1$ in the phases of the superconducting order parameters Δ_1, Δ_2 at the two sides of the

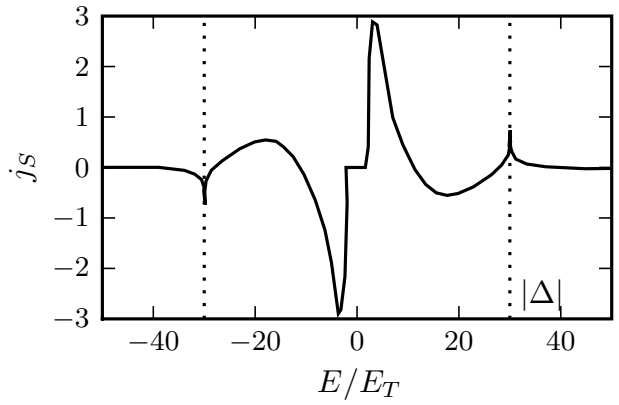

Figure 2.5: Current-weighed density of Andreev bound states (ie. spectral supercurrent) in an S-N-S junction, for a fixed phase difference $\varphi = \pi/2$ and energy gap $|\Delta| = 30E_T$.

junction. In general, the current-phase relation $I_S(\varphi)$ can be complicated, but for many types of junctions it resembles the Josephson result $I_S(\varphi) = \sin(\varphi)I_c$. [62, 64]

The supercurrent in S-N-S structures is carried by Andreev bound states. [26, 27] Within the Usadel equation framework, they can be characterized with the quantity (see [61, 65])

$$j_S = \frac{1}{4}\,\mathrm{Im}[\hat{G}^R\nabla\hat{G}^R\hat{\tau}_3 - \hat{G}^A\nabla\hat{G}^A\hat{\tau}_3] = \mathrm{Im}[-\upsilon_S \sinh^2(\theta)/D]\,, \tag{2.36}$$

which is essentially their density per energy interval, weighed by the current each interval contributes. [34, 66] This quantity is called the "spectral supercurrent density" below, as the total supercurrent is

$$I_S = \frac{-A\sigma_N}{2e}\int_{-\infty}^{\infty} \mathrm{d}E\, j_S(E)\tanh\left(\frac{E}{2T}\right)\,, \tag{2.37}$$

ie., a weighed average of j_S. A method for approximating j_s is also discussed in the next section and in Appendix A.2. As seen in Fig. 2.5, j_S has structure on the energy scale of the Thouless energy E_T corresponding to the distance L between the superconductors and the diffusion constant D:

$$E_T = \begin{array}{c} 13.2\,\mu\mathrm{eV} \\ 153\,\mathrm{mK}\times k_B \end{array} \times \frac{(D/200\ \mathrm{cm^2/s})}{(L/1\,\mu\mathrm{m})^2}\,, \tag{2.38}$$

which is also a characteristic energy scale for many quantities in such structures.

Table 2.1: Factors forming $I_{\mathfrak{P}}$. Here, R is the resistance for a tunnel contact (R is assumed large), $\theta_0 = \operatorname{artanh}(|\Delta|/E)$, $\gamma_0 = \tanh(\theta_0/2)$, and $N = 1/(1-\gamma_0^2)$. For a diffusive wire, L is the length, $A\sigma$ the area-conductance product, and $k = \sqrt{-2iE}$,

(p,q)	p	q	$a(E)$	$b(E)$
tunnel junction	terminal	node	$R^{-1}N\gamma_0$	$R^{-1}(2N-1)$
tunnel junction	node	node	R^{-1}	R^{-1}
diffusive wire	terminal	node	$4A\sigma k e^{-kL}\tanh(\frac{\theta_0}{4})$	$A\sigma k$
diffusive wire	node	node	$A\sigma k\,\operatorname{csch}(kL)$	$A\sigma k\coth(kL)$

Table 2.2: Factors forming $I_{\mathfrak{P}}$, at high temperature. It is assumed that $\Delta \gg T$ and $\sqrt{2\pi T} \gg L$, and that every current path goes through at least a single diffusive wire segment: then $I_{\mathfrak{P}} \approx 4(2\pi T)^{3/2}\prod_{(p,q)\in\mathfrak{P}} a'_{p,q}/\prod_{r\in\mathfrak{P}}\sum_{(r,s)\in\mathfrak{P}} b'_{r,s}$.

(p,q)	p	q	a'	b'
tunnel junction	terminal	node	$(2R\sqrt{2\pi T})^{-1}$	0
tunnel junction	node	node	$(R\sqrt{2\pi T})^{-1}$	$(R\sqrt{2\pi T})^{-1}$
diffusive wire	terminal	node	$4A\sigma\tan(\pi/8)e^{-L\sqrt{2\pi T}}$	$A\sigma$
diffusive wire	node	node	$2A\sigma e^{-L\sqrt{2\pi T}}$	$A\sigma$

2.2.2 Multiterminal supercurrent

Often, one is interested in supercurrents flowing in multiterminal circuits: they are experimentally accessible and can be used to characterize parts of the circuit. In interpreting the experiments in **III**, **IV**, **VII**, **VIII** it was also important to know what the quasiclassical theory predicts for these structures.

In practice, it is often possible to solve Usadel equations (2.33) numerically for a given structure. However, this is not always necessary, since it is possible to devise various approximations that give accurate analytical results in closed form. Finding these results is of course not a new problem, as S-N-S proximity structures have been studied for tens of years. However, the best-known results typically consider only quasi-1D structures or are restricted to small junctions $L < \xi$, [62, 67] or are computed separately for each special case. A generally applicable approximation that I derived for article **VII** is discussed below, and the details can be found in Appendix A.1. It is expected to be asymptotically exact in the limit of high temperatures, $T \gg E_T$. The result is based on linearizing the Usadel equation in the structure: this is a commonly used approximation procedure in the literature, but to my knowledge the result below has not been discussed earlier.

First, one divides the proximity structure to nodes, terminals and connectors, in the spirit of circuit theory. [60] Connectors can here be quasi-1D diffusive wires or tunnel junctions, and a node is a small portion of metal in the circuit, to which

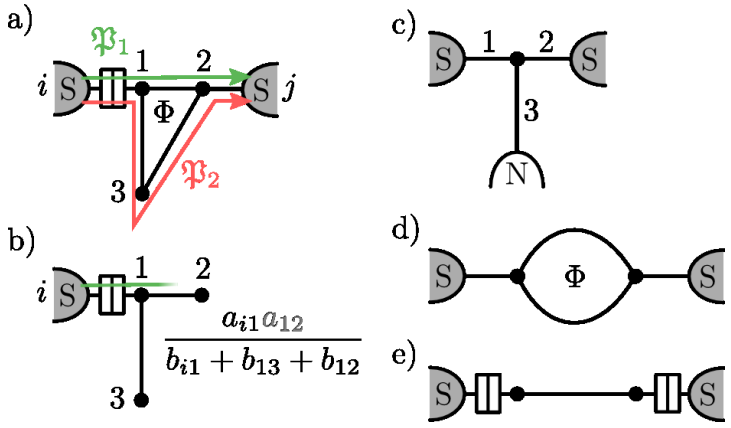

Figure 2.6: Schematic representations of proximity circuits. Nodes are marked with black dots, diffusive wires with black lines between nodes, and tunnel junctions with boxes. (a) Example with two current paths $\mathfrak{P}_1 = [(i,1),(1,2),(2,j)]$ and $\mathfrak{P}_2 = [(i,1),(1,3),(3,2),(2,j)]$ marked. (b) Factor coming from the first step in $\mathfrak{P}_1$. (c) T-shaped circuit, with two superconducting terminals. Structures of this type were studied also in **III** and **VIII**. (d) Loop, with threading magnetic flux Φ, studied also in [68–71]. (e) SINIS structure, consisting of two tunnel barriers and a diffusive wire.

several connectors are joined. Some examples are shown in Fig. 2.6. The main result is that the supercurrent between two terminals (see Fig. 2.6a) can then be expressed as

$$I_{ij} = \sum_{\mathfrak{P}} I_{\mathfrak{P}} \sin(\phi_i - \phi_j - 2\int_{\mathfrak{P}} \mathrm{d}\boldsymbol{l}\cdot\boldsymbol{A})\,, \tag{2.39}$$

$$I_{\mathfrak{P}} = 2\,\mathrm{Re}\int_{-\infty}^{\infty} \mathrm{d}E\,\tanh\left(\frac{E}{2T}\right)\frac{\prod_{(p,q)\in\mathfrak{P}} a_{pq}(E)}{\prod_{r\in\mathfrak{P}}\sum_{(r,s)\in\mathfrak{P}} b_{rs}(E)} \tag{2.40}$$

where the sum over $\mathfrak{P}$ runs over all paths that connect j to i and do not visit other terminals. The notation $(p,q)\in\mathfrak{P}$ refers to a connector between nodes p and q belonging to the path, and $r\in\mathfrak{P}$ a node in the path. $I_{\mathfrak{P}}$ is the critical current along the path, written in terms of the factors $a(E)$ and $b(E)$ listed in Table 2.1, and the second factor is the sine of the gauge-invariant phase difference between the two terminals, as measured along the path.

Expression (2.40) is illustrated in Figs. 2.6ab, where two current paths are marked. These are not the only possibilities — there is an infinite number of paths winding around the loop arbitrarily many times — however the leading order contribution comes only from $\mathfrak{P}_1$ and $\mathfrak{P}_2$. The contribution $I_{\mathfrak{P}_1}$ is

$$I_{\mathfrak{P}_1} = 2\,\mathrm{Re}\int_{-\infty}^{\infty} \mathrm{d}E\,\tanh\left(\frac{E}{2T}\right)\frac{a_{i1}a_{12}a_{2j}}{(b_{i1}+b_{13}+b_{12})(b_{12}+b_{23}+b_{2j})}\,, \tag{2.41}$$

the first factor of which is illustrated in Fig. 2.6b. Note that the result is affected by the branching of the circuit, which was also observed in the numerical computations of Ref. [66]. In general, the current I_{Y} is not equivalent to the current in a structure formed by joining the connectors on the path in series.

One can also find the high-temperature limit for supercurrents by evaluating the integral (2.40) using only the smallest Matsubara frequency. The corresponding factors $a' = a(i\pi T)/\sqrt{2\pi T}$ and $b' = b(i\pi T)/\sqrt{2\pi T}$ are listed in Table 2.2. Using them, we can estimate the high-temperature supercurrents flowing in structures in Figs. 2.6cde at a glance:

$$\text{c)} \quad I \approx \sin(\varphi) \times 4(2\pi T)^{3/2} \tan(\pi/8)^2 e^{-L\sqrt{2\pi T}} \times 16 A_1 A_2/(A_1 + A_2 + A_3)\,, \quad (2.42)$$

$$\text{d)} \quad I \approx [\sin\varphi + \sin(\varphi + 2\pi\Phi/\Phi_0)] \times 4(2\pi T)^{3/2} \tan(\pi/8)^2 e^{-L\sqrt{2\pi T}} \times 32A/9\,, \quad (2.43)$$

$$\text{e)} \quad I \approx \sin(\varphi) \times 2(R_B^2 A\sigma)^{-1} \sqrt{2\pi T} e^{-L\sqrt{2\pi T}}\,. \quad (2.44)$$

Note that here and in the tables, we set $D = 1$, so that all energies and temperatures are in units of the Thouless energy $E_T = \hbar D/L^2$ corresponding to a unit length. Because of the decaying factor $e^{-L\sqrt{2\pi T}}$, only the shortest paths are taken into account here. The comparison to numerically computed results in Fig. 2.7 shows that the approximation is reasonably accurate. Moreover, result (2.44) coincides with that presented eg. in Ref. [72].

The above result for the supercurrent, and the accompanying results for the spectral supercurrent j_S (see Appendix A.2) were useful for the calculations in **VII**. Moreover, the fact that they allow obtaining reasonably accurate results in a very simple way may be useful in designing experiments.

2.2.3 Magnetic field

A magnetic field applied to superconducting (or proximity) structures has two effects: first, analogously to Eq. (2.39), electrons accumulate magnetic phase as they travel. That the phase depends on the path traversed leads to interference, which manifests in several different ways, some of which are discussed below. [15, 23, 62, 73] A secondary effect is a Zeeman splitting $\delta E = g\mu_B B$ of energy levels of electrons with different spins in magnetic field B, which was predicted in Refs. [74, 75] to result in a change of sign in the current-phase relation, a π-state.

Accumulation of the magnetic phase can be used to create phase biased structures, in which the phase difference between two superconducting terminals is kept fixed (as opposed to the current I being kept fixed). One example of this is the SQUID-type loop in Fig. 2.8, where the phase difference φ between points A and B can be tuned with the magnetic flux Φ. This type of structures ("Andreev interferometers") have been used extensively in experiments studying properties of the proximity effect, for example in [76–78].

Presence of a magnetic field also disrupts superconducting coherence, as electrons

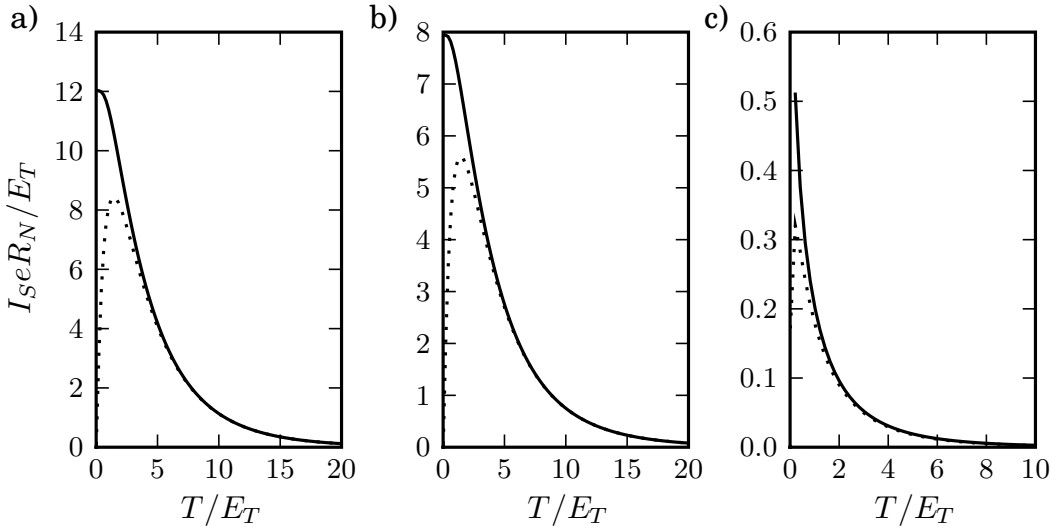

Figure 2.7: Currents obtained from Eq. (2.39), compared to numerical solutions of the Usadel equation. R_N is the normal-state resistance of the whole structure, and $E_T = \hbar D/L^2$ the Thouless energy corresponding to the distance between the superconductors. (a) Numerics (solid) and Eq. (2.42) (dotted), for $A_1 = 2$, $A_2 = 1$, $A_3 = 1/2$ and $L_1 = L_2 = 1/2$, $L_3 = 5$, in relative units. (b) Numerics (solid) and Eq. (2.43) (dotted), with $\varphi = \pi/2$, $2\pi\Phi/\Phi_0 = \pi/4$. (c) Numerics (solid) and Eq. (2.44) (dotted), with $\varphi = \pi/2$ and $R_B/R = 5$.

or holes arriving at the same point obtain path-dependent phases. In the diffusive limit, this can be modeled using the Usadel equation (2.33). There, the magnetic field enters through the vector potential $\boldsymbol{A}$. If one considers the equation in a thin metal cylinder, which the experimental thin films approximatively are, a simpler equation can be obtained by averaging over the cross-sectional area, $\theta \mapsto \langle\theta\rangle_\perp$, $\chi \mapsto \langle\chi\rangle_\perp$. [15, 70, 79, 80] This reduces the $\boldsymbol{A}$-dependent terms to a single "spin-flip" dephasing rate $\gamma_{\rm sf} \propto \boldsymbol{A}^2$ in a 1D equation that is simpler to solve:

$$\partial_x^2\theta = -2iE\sinh\theta + \frac{1}{2}\left\langle(\nabla\chi - 2\boldsymbol{A})^2\right\rangle_\perp \sinh 2\theta \tag{2.45}$$

$$= -2iE\sinh\theta + \frac{1}{2}[(\partial_x\chi)^2 + \gamma_{\rm sf}]\sinh 2\theta \tag{2.46}$$

In the averaging, one must account for the terms $\nabla_\perp\chi$ generated from the variation of the phase of the Green function across the cross-section, which may be of the same order of magnitude as the transverse part $\boldsymbol{A}_\perp$, depending on the gauge chosen. For certain orientations of the field this is straightforward (see eg. [79]), but in general the more careful treatment presented in **VIII** is necessary. There is a special gauge in which the variation is minimal: the London gauge, [15] in which $\nabla_\perp\cdot\boldsymbol{A} = \hat{\boldsymbol{n}}\cdot\boldsymbol{A}_\perp = 0$, where $\hat{\boldsymbol{n}}$ is the outward normal of the cylinder. In this gauge, $\gamma_{\rm sf} = \langle\boldsymbol{A}^2_{\rm London}\rangle_\perp$, and

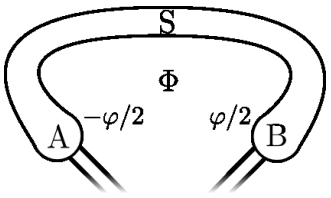

Figure 2.8: Phase-biasing a proximity structure with a superconducting loop. The flux Φ fixes a phase difference $\varphi = 2\pi\Phi/\Phi_0$, where $\Phi_0 = h/2e$ is the flux quantum.

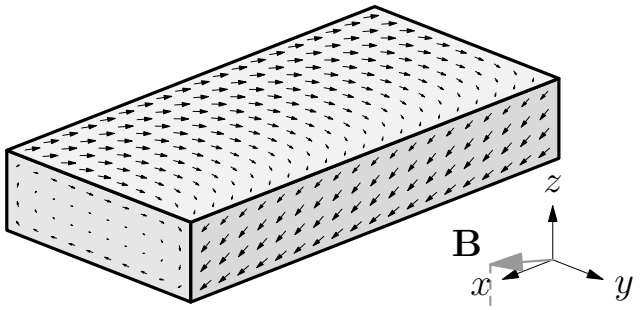

Figure 2.9: Supercurrent flow in a proximity cylinder, induced by a nearly parallel magnetic field. Computed by a variational method, in the way explained in **VIII**.

the transverse part of the supercurrent density $\boldsymbol{j}_s$ is for thin wires proportional to $\boldsymbol{A}$, similarly as in the London theory [23]. Example of such a supercurrent flow pattern in a proximity structure is shown in Fig. 2.9.

The Zeeman splitting was under study in one of the experiments reported in **VIII**, the aim being to observe the π-state, ie., a change in sign of the current-phase relation $I(\phi)$ as a function of the applied field B. However, only decay of the critical current was observed with increasing applied field, similarly as in the thin-film experiments in Ref. [20]. I made an analysis in **VIII** based on the Usadel equation that shows the decay is well explained by the destructive interference caused by the magnetic field, and the experimental results can be understood quantitatively based on Eq. (2.46).

A result which may at first sight be surprising, and was apparently neglected in Refs. [74, 75], is that for a wire of dimensions $L \times w \times t$, $t \sim w$, $L \gg w, t$, the suppression of the supercurrent caused by a magnetic field incident on the area $t \times w$ is proportional to $\gamma_{\rm sf}/E_T \sim (\Phi'/\Phi_0)^2$, with the magnetic flux $\Phi' \sim BLt$ corresponding to an area $L \times t$. The physical reason for this is that in a transport experiment, the electrons carrying the supercurrent have to traverse the length L. If their motion is diffusive, it can be estimated [81] that the standard deviation in the flux enclosed by their trajectories is proportional to $L \times t$. Hence, the result is larger by a factor of $L/t \gg 1$ than the magnetic flux entering the structure.

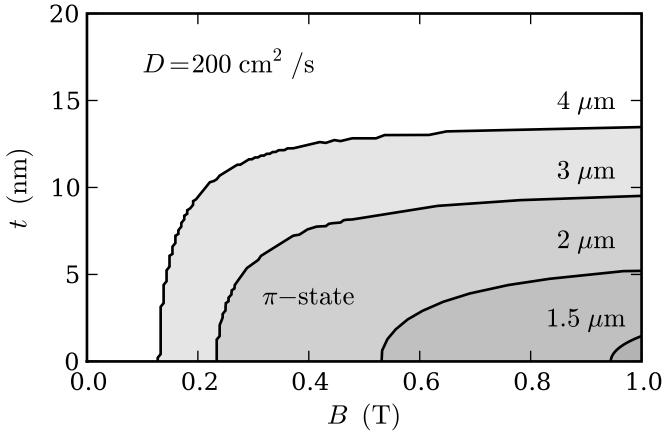

Figure 2.10: Phase diagram for the π-state in a $50\,\mathrm{nm} \times t \times L$ wire, based on the approximate Eq. (2.47). Lengths $L = 1.5 \ldots 4\,\mu$m are shown.

Consequently, the cross-over to a π-state would only be expected in metal films considerably thinner than those achieved in **VIII**, requiring thickness $t \lesssim g\mu_B L/eD \sim 0.001 \ldots 0.003L$. One way to find this condition is from a similar approximate solution for the supercurrent as in [65, 74, 82] and in the previous section, but taking both the Zeeman splitting and dephasing caused by the field into account,

$$I_c \approx 64\pi \frac{k_B T}{eR_N} \operatorname{Re} abe^a \,,\ \epsilon \equiv \pi k_B T + ih \,,\ h = \frac{1}{2} g\mu_B B \,, \tag{2.47}$$

$$a \equiv \sqrt{\frac{2\epsilon}{E_T} + 2\left(\frac{B}{B_0}\right)^2} \,,\ b \equiv \tan^2\left(\frac{1}{4}\arctan\frac{|\Delta|}{\epsilon}\right) \,,\ B_0 \equiv \sqrt{\frac{6(w^2+t^2)}{w^2 t^2}}\frac{\hbar}{eL} \,.$$

From this result, one can estimate the critical thickness t, above which $I_c > 0$ for all B. A phase diagram is shown in Fig. 2.10. The π state might however be observable in graphene or in a 2DEG, although in these structures one should take the electronic structure and the ballistic nature of the conduction into account.

Of the above three effects caused by the magnetic field, mostly the phase biasing is needed below. It is an important tool in experimental studies of the proximity effect, as it allows studying dependence of quantities on the local phase of the pairing amplitude F.

2.3 Stationary nonequilibrium

The proximity effect changes several of the nonequilibrium properties of metals, affecting for example conductance and other linear-response coefficients. The fact that it also allows for supercurrent to flow inside normal metals without dissipation leads

to nonlocal effects: current flowing in a given point depends not only on the electric field in the vicinity of the point, but also on the configuration of superconducting phase differences in the whole structure.

In stationary nonequilibrium problems, the time convolutions $\circ$ to reduce to ordinary (matrix) products similarly as in equilibrium. The difference to equilibrium problems is that the Keldysh component $\check{G}^K$ of the Green function is nontrivial, as the electron distribution function no longer necessarily remains a Fermi function. The changes in it, however, couple back to the Retarded function $\check{G}^R$ only via self-consistency relations.

One implication of stationarity is that the order parameter of superconductors must be constant in time, implying that the chemical potential of Cooper pairs is zero, $\mu_S = (2e/\hbar)\partial_t \arg\Delta(t) = 0$. This is another factor contributing to nonlocal effects: when superconducting terminals float, a counter-flowing supercurrent not only can but must cancel the normal current, for the situation to remain stationary. This leads to a specific type of nonlocal nonequilibrium effects, explored for example in [83], **VII**, and **VIII**.

Below, we first discuss the kinetic equations for the electron distribution function, which follow from the equation for $\hat{G}^K$. Then, we define the thermoelectric linear-response coefficients, and concentrate on the thermoelectric effects in proximity structures, giving an overview on the results in **I**, **II**, **IV**, **V**, and **VI**. Finally, we discuss the two effects in **III** and **VII** that appear when a proximity structure is driven far from equilibrium into nonlinear response.

2.3.1 Kinetic equations and observables

In stationary nonequilibrium problems, the Keldysh part of the Usadel equation reduces to Boltzmann-like kinetic equations for the electron distribution function f (2.29). In problems concerning superconductivity, it is convenient to first express the distribution function in terms of its "longitudinal" and "transverse" parts [55, 56]

$$f_L(E) = f(\mu_S - E) - f(\mu_S + E)\,, \quad f_T(E) = 1 - f(\mu_S - E) - f(\mu_S + E)\,, \tag{2.48}$$

$$\hat{h} = f_L\hat{1} + f_T\hat{\tau}_3\,, \tag{2.49}$$

which also allow considering only positive energies. In terms of these functions, the kinetic equations read (cf. [34, 84], **VI**)

$$D\nabla\cdot\boldsymbol{j}_L = 0, \qquad \boldsymbol{j}_L \equiv \mathcal{D}_L\nabla f_L - \mathcal{T}\nabla f_T + j_S f_T\,, \tag{2.50a}$$

$$D\nabla\cdot\boldsymbol{j}_T = (\nabla\cdot j_S)f_L + 2|\Delta|\mathcal{R}f_T, \qquad \boldsymbol{j}_T \equiv \mathcal{D}_T\nabla f_T + \mathcal{T}\nabla f_L + j_S f_L\,, \tag{2.50b}$$

in the absence of inelastic relaxation. In normal metals, where $\nabla\cdot j_S = 0$ and $\Delta = 0$, they are in this approximation conservation equations for the two spectral currents $\boldsymbol{j}_L$ and $\boldsymbol{j}_T$. If inelastic relaxation is present, collision integrals $I_L = \mathrm{Tr}[\check{\sigma}_{\mathrm{in}}, \check{G}]^K$ and $I_T = \mathrm{Tr}\,\hat{\tau}_3[\check{\sigma}_{\mathrm{in}}, \check{G}]^K$ appear on the RHS of the kinetic equations (2.50).

The coefficients in the kinetic equations consist of the modified (dimensionless) diffusion coefficients $\mathcal{D}_L$ and $\mathcal{D}_T$, the cross-coupling coefficient $\mathcal{T}$, the spectral supercurrent j_S, and a charge recombination coefficient $\mathcal{R}$. These can be expressed in terms of the retarded Green function:

$$\mathcal{D}_L = |N|^2(|\gamma|^2 - 1)(|\tilde{\gamma}|^2 - 1) = \frac{1}{2}(1 + |\cosh\theta|^2 - |\sinh\theta|^2 \cosh(2\,\mathrm{Im}[\chi])), \quad (2.51a)$$

$$\mathcal{D}_T = |N|^2(|\gamma|^2 + 1)(|\tilde{\gamma}|^2 + 1) = \frac{1}{2}(1 + |\cosh\theta|^2 + |\sinh\theta|^2 \cosh(2\,\mathrm{Im}[\chi])), \quad (2.51b)$$

$$\mathcal{T} = |N|^2(|\tilde{\gamma}|^2 - |\gamma|^2) = \frac{1}{2}|\sinh\theta|^2 \sinh(2\,\mathrm{Im}[\chi])), \quad (2.51c)$$

$$j_S = \mathrm{Re}\, 2N^2[\gamma(\nabla + 2i\boldsymbol{A})\tilde{\gamma} - \tilde{\gamma}(\nabla - 2i\boldsymbol{A})\gamma] = \mathrm{Im}[-\sinh^2(\theta)(\nabla\chi - 2i\boldsymbol{A})], \quad (2.51d)$$

$$\mathcal{R} = 2|N|^2\,\mathrm{Re}[(1 + |\tilde{\gamma}|^2)e^{-i\phi}\gamma - (1 + |\gamma|^2)e^{i\phi}\tilde{\gamma}] = \mathrm{Im}\,[-\cos(\phi - \chi)\sinh(\theta)]\ , \quad (2.51e)$$

where $N = (1 + \gamma\tilde{\gamma})^{-1}$, the superconducting order parameter is $\Delta = |\Delta|e^{i\phi}$, and $\boldsymbol{A}$ is the vector potential. Curiously, $\mathcal{T}$ has usually been neglected, [34] except in the recent literature. It has an important role in thermoelectric effects, as noted in **I**.

The spectral currents are related to the charge and energy current densities by

$$\boldsymbol{j}_c = -\frac{\sigma_N}{2e}\int_{-\infty}^{\infty} \mathrm{d}E\, \boldsymbol{j}_T\,, \quad \boldsymbol{j}_E = \frac{\sigma_N}{2e^2}\int_{-\infty}^{\infty} \mathrm{d}E\, E\, \boldsymbol{j}_L\,, \quad (2.52)$$

both proportional to the normal-state conductance σ_N. Charge current $\boldsymbol{j}_c$ is always a conserved quantity, and in the absence of inelastic relaxation also $\boldsymbol{j}_E$ is conserved. [4]

The observable heat current density (see eg. [6, 85])

$$\boldsymbol{j}_Q = \boldsymbol{j}_E - \mu\boldsymbol{j}_c/(-e) \quad (2.53)$$

is a separate quantity from the energy current density. Indeed, the energy current $\boldsymbol{j}_E$ is not a gauge invariant quantity and so cannot be an observable: shifting the zero point of energy changes the value of $\boldsymbol{j}_E$. The expression (2.53) comes essentially from thermodynamics: change in entropy in some small volume close to equilibrium is

$$T\,\mathrm{d}S = \mathrm{d}U - \mu\,\mathrm{d}N \equiv \mathrm{d}Q\,, \quad (2.54)$$

in terms of the change in the entropy S, internal energy U, and number of particles N. This heat current is well-defined only near equilibrium, where the chemical potential μ of the quasiparticles is unambiguous. Consequently, in mesoscopic structures whose internal state can be far from equilibrium, one usually studies only heat currents entering or leaving the terminals. These always stay, by assumption, at equilibrium.

[4] Conservation of $\boldsymbol{j}_E$ is imminent from Eq. (2.50), and the conservation of $\boldsymbol{j}_c$ follows from the self-consistency equation (2.25) for Δ.

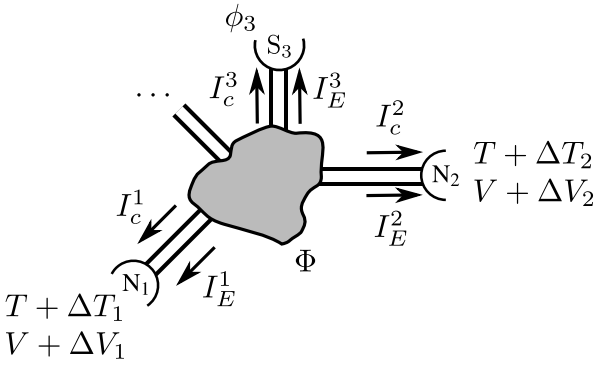

Figure 2.11: Schematic multiterminal circuit where the proximity effect is studied in linear-response; center of the circuit is some unspecified mesoscopic proximity structure. Tunable and measurable parameters are the parameters at the terminals, in addition the magnetic flux Φ.

The above equations form the basis of the discussion in the rest of this thesis. We examine especially the thermoelectric effects implied by the above equations, and several far-from equilibrium effects.

2.3.2 Linear response

Consider now the schematic experimental setup in Fig. 2.11: it consists of several terminals connected together by a proximity circuit. What can be tuned and measured are the quantities at the terminals. These consist of the potentials V_j, temperatures T_j, superconducting phases ϕ_j, and the charge and energy currents I_c^j and I_E^j entering the terminals.

The linear-response relation between the nonequilibrium quantities can be written in the form of an Onsager scheme,

$$\begin{pmatrix} I_c^i - I_{S,\mathrm{eq}}^i \\ I_E^i \end{pmatrix} = \sum_{j \in \mathrm{terminals}} \begin{pmatrix} L_{11}^{ij} & L_{12}^{ij} \\ L_{21}^{ij} & L_{22}^{ij} \end{pmatrix} \begin{pmatrix} \Delta V_j \\ \Delta T_j / \bar{T} \end{pmatrix} , \tag{2.55}$$

in terms of the thermoelectric matrix $L_{\alpha\beta}^{ij}$. Note that the supercurrent is an equilibrium quantity and not proportional to the biases, and that in linear response, the energy current and heat current are equal if the equilibrium chemical potential is chosen as $\mu = 0$. The elements of L characterize the transport in the circuit, and are modified by the superconducting proximity effect. Since the proximity effect is sensitive to the superconducting phase differences, observing the modulation in the L coefficients can confirm its presence.

Modulation in the conductance L_{11} was the first coefficient measured experimentally in mesoscopic multiterminal circuits. [21, 70, 76–78, 86, 87] It also received

significant theoretical interest, [68, 88–90] and is discussed in detail in review articles such as Ref. [8]. Similarly, effect of the proximity of superconductors on the thermal conductance has also been studied in detail. [91–94]

Of the thermoelectric coefficients, L_{12} has been measured in the presence of the proximity effect, see [95–101] and **IV**, and several theoretical studies have been published: [102–105] and **I**, **II**, **VI**. The remaining coefficient L_{21} was discussed in Refs. [106] and **V**. An overview on thermoelectricity associated with the proximity effect is given in the following sections.

2.3.3 Spectral thermoelectric matrix

As discussed in **V** and **VI**, one can note that when inelastic scattering can be neglected in non-superconducting materials ($\Delta = 0$, $\sigma_{\text{in}} = 0$), the kinetic equations (2.50) are linear in the distribution function, and do not mix different energies E.[5] For this situation, Eq. (2.55) applies separately at each energy, and one can write down a similar relation between the distribution functions f^i_β at the terminals and the spectral currents:

$$\boldsymbol{\jmath}^i_T(E) = \sum_{\beta j} \tilde{L}^{ij}_{T\beta}(E) f^j_\beta(E)\,, \tag{2.56a}$$

$$\boldsymbol{\jmath}^i_L(E) = \sum_{\beta j} \tilde{L}^{ij}_{L\beta}(E) f^j_\beta(E)\,. \tag{2.56b}$$

Here, $\beta \in T, L$, and the numbers i and j index the terminals. Related spectral conductances have been used for studying conductance L_{11} eg. in [70, 90, 107] prior to **V**. The linear-response coefficients L can be computed directly from the energy dependent $\tilde{L}(E)$:

$$L^{ij}_{11} = \frac{1}{2k_BT} \int \mathrm{d}E\, \tilde{L}^{ij}_{TT}(E) \operatorname{sech}^2\left(\frac{E}{2k_BT}\right)\,, \tag{2.57a}$$

$$L^{ij}_{21} = \frac{-1}{2k_BT} \int \mathrm{d}E\, E\, \tilde{L}^{ij}_{LT}(E) \operatorname{sech}^2\left(\frac{E}{2k_BT}\right)\,, \tag{2.57b}$$

$$L^{ij}_{12} = \frac{-1}{2k_BT} \int \mathrm{d}E\, E\, \tilde{L}^{ij}_{TL}(E) \operatorname{sech}^2\left(\frac{E}{2k_BT}\right)\,, \tag{2.57c}$$

$$L^{ij}_{22} = \frac{1}{2k_BT} \int \mathrm{d}E\, E^2\, \tilde{L}^{ij}_{LL}(E) \operatorname{sech}^2\left(\frac{E}{2k_BT}\right)\,. \tag{2.57d}$$

Note that above the supercurrent is absorbed in the definition of $\tilde{L}$.

The matrix describing the structure of **V** is shown in Fig. 2.12. One can see several effects in it: low energy suppression of thermal conductivity [93] ie. $\tilde{L}_{LL}$ are

[5] If the superconducting terminals are massive, one can often assume that Δ depends only weakly on what occurs in the proximity region. [62] If this is not the case, then the interactions in the superconducting terminals can couple back to the proximity region via Δ.

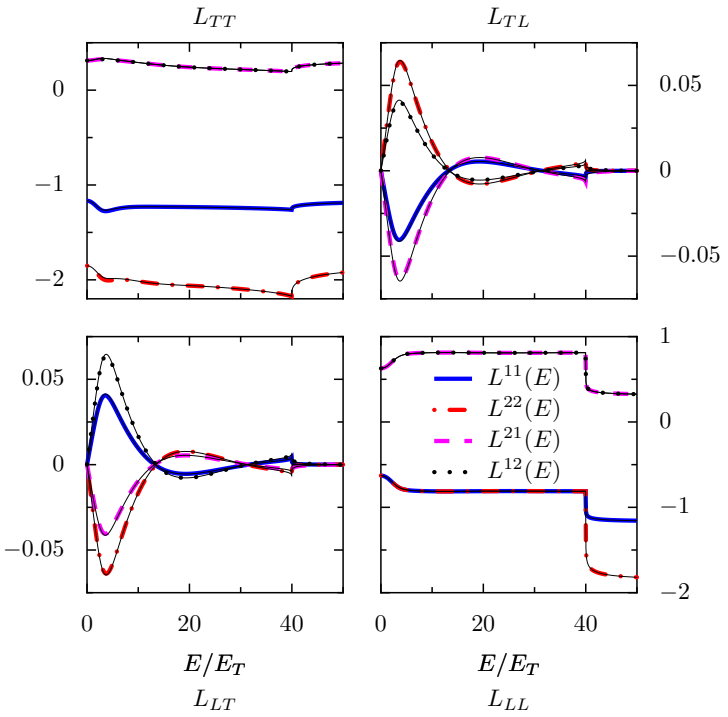

Figure 2.12: Example of a spectral thermoelectric matrix elements (2.56) between the normal terminals of Fig. 2.13. The energy gap of the superconductors is $|\Delta| = 40E_T$, and the phase difference between the superconducting terminals is $\varphi = \pi/2$. Colored/gray lines are computed numerically for the structure of **V**, and thin solid lines indicate the semi-analytic approximations derived in **II**.

reduced for $E = 0$, and the opening of heat transport to superconductors at above-gap energies $|E| > |\Delta|$. The thermoelectric elements $\tilde{L}_{TL}$ resemble the spectral supercurrent in Fig. 2.5 — although there is no low-energy minigap in the structure of Fig. 2.13 because of the connected normal-metal terminals. The correspondence is discussed in more detail in Section 2.4.1 below. There are clear symmetries between the off-diagonal thermoelectric coefficients $\tilde{L}_{TL}$ and $\tilde{L}_{LT}$. These are explained in Section 2.4.2.

Representation (2.56) turned out to be useful for practical numerical computations, needed for example in **V** and **VII**. The response coefficients $\tilde{L}(E)$ depend only on the transport coefficients (2.51) which are equilibrium quantities, and not on the nonequilibrium biases. Consequently, they contain all information required to describe the behavior of the circuit not only in linear response, but also far from equilibrium.

2.3.4 Numerical computations

To find the results in the publications reported in this thesis concerning the proximity effect, I have developed a numerical solver [6] that is able to handle an arbitrary network of normal and superconducting quasi-1D wires in contact to normal and superconducting terminals. The basic approach is to use a relaxation method [108–111], ie., discretizing the Usadel equations (2.33), (2.50), and (2.32) on a domain forming a quasi-1D circuit and solving the resulting algebraic equation system with Newton's method. Using this code, one can for example compute the spectral coefficients (2.51), the matrix $\tilde{L}$ (2.56), the nonequilibrium distribution f, and heat and charge currents that flow in response to applied temperature or potential biases.

2.4 Thermoelectricity

In the normal state of metals, there are several causes for thermoelectric effects. One of the most important and well-understood ones is the electron–hole asymmetry, an asymmetry of density of states (or mean free path, etc.) around the Fermi surface ($\xi \sim p^2/2m = \xi_f$). A Sommerfeld expansion shows that the e-h asymmetry results to the normal-state thermoelectric coefficient, [28, 112]

$$\boldsymbol{j}_c = L_{12}^N \nabla T/T\,, \qquad L_{12}^N = -\frac{\pi^2 k_B^2 T^2}{3e}\left.\frac{\mathrm{d}\sigma(\xi)}{\mathrm{d}\xi}\right|_{\xi=E_f}\,, \tag{2.58}$$

where $\sigma(\xi)$ is an energy-dependent conductivity. This is the classical "Mott law" prediction for the thermoelectric coefficients. Aside from bulk metals, similar asymmetry effects manifest in quantum point contacts and other structures where, roughly speaking, the conductance or transmission probability is energy dependent [113]. The normal-state thermoelectric coefficient is typically rather small for clean metals, $L_{12}^N/TL_{11} \lesssim 10\,\mathrm{nV/K}$, at the cryogenic temperatures below 1 K.

The study of thermoelectric effects in superconductors has a long history. It starts with the observation that they do not exist; [114, 115] indeed, superconductors can be used as absolute reference materials in measurements of the thermoelectric coefficients L_{12} precisely because their $L_{12} \approx 0$ [28]. The explanation (see [115, 116]) for the absence of thermoelectric effects in bulk superconductors is that any thermoelectric currents induced by temperature gradients are cancelled by supercurrent $\boldsymbol{j}_{c,\mathrm{thermoemf}} + \boldsymbol{j}_{c,\mathrm{sc}} = 0$. This cancellation is not necessarily complete, for example near the edges of superconductors or in multiply connected structures, which leaves room for various secondary thermoelectric effects. [115]

A review on thermoelectrics of superconductors can be found in [116]. Some of the effects arise from incomplete cancellation of the underlying normal state thermoelectric effect (2.58) [117, 118], some from electrostatic effects, [116, 119] and others

[6] Full source code, usage instructions and examples are available via internet in the address `http://ltl.tkk.fi/~theory/usadel1/`.

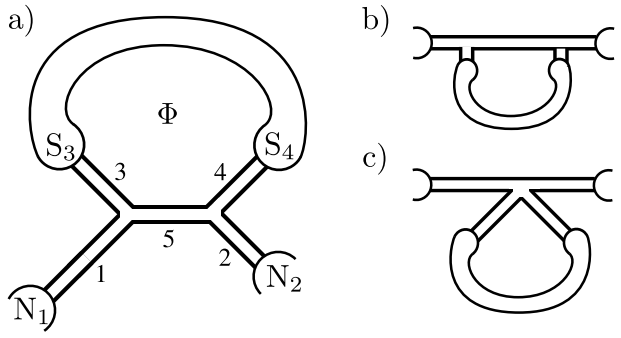

Figure 2.13: Andreev interferometers. a) General schematic for structures studied in **I**. b) Model for the "parallelogram" of [97]. c) The "house" geometry of [97].

are related to charge imbalance in superconductors. [120–123] It should be noted that some of the experiments related to the first type are still controversial, and cannot be claimed to be very well understood. [119, 124, 125]

More recently, several experiments probing for thermoelectric effects in superconducting proximity structures were made, [95–101] and **IV**, which motivated several subsequent theoretical studies [102–105, 126–128], including **I**, **II**, **V**. The studied structures in these works were essentially Andreev interferometers, schematically illustrated in Fig. (2.13), and fairly similar to the structures used for studying the proximity modification of conductance. In these structures, one can tune the superconducting phase differences and flow of the supercurrent, in addition to maintaining temperature gradients and measuring voltage differences. This is sufficient for probing the thermoelectric coefficient L_{12} and how the proximity effect changes it.

The main observations in the experiments [95–101] and **IV** are that

(i) the thermoelectric effect is consistently larger than in the normal state, $L_{12} \gtrsim 10 \ldots 100 L_{12}^N$,

(ii) the measured potentials oscillate Φ_0-periodically in the flux Φ, with either odd $\sin\phi$ [Fig. (2.13)b] or even $\cos\phi$ symmetry [Fig. (2.13)c], depending on the geometry, [95–99]

(iii) in some of the experiments, a sample- and temperature-dependent "offset" potential difference was observed between the normal and superconducting parts, [100] and

(iv) the coefficient L_{12} has complicated, non-monotonous temperature dependence. [97, 100]

The characteristics (ii) and (iv) are similar to the modulation the proximity effect causes for conductance, except that conductance is always a symmetric function of the flux.

Moreover, it is important to note that in the interferometer in Fig. 2.13, one can define two thermoelectric Seebeck coefficients,

$$S_{NS} \equiv \left.\frac{\mathrm{d}(V_1+V_2)}{2\,\mathrm{d}(T_1-T_2)}\right|_{I_c^1=I_c^2=0}, \qquad S_{NN} \equiv \left.\frac{\mathrm{d}(V_1-V_2)}{\mathrm{d}(T_1-T_2)}\right|_{I_c^1=I_c^2=0}, \tag{2.59}$$

which give the proportionality of the potentials V_1 and V_2 induced in the floating normal terminals N_1 and N_2, when there is a temperature difference T_1-T_2 between them. The potential of the superconductors is chosen as zero, since this is a stationary effect. Of the above experiments, [95–99, 101] probed S_{NN}, and [100, 101] and **IV** probed S_{NS}. Symmetric oscillations have been observed only in S_{NN}.

Some of the above effects can be qualitatively explained based on the quasiclassical theory in [102–104], **I**, and **II**, although these works leave certain basic questions unanswered. Recently, another step towards the solution was proposed in [105]. These works are discussed below.

2.4.1 Quasiclassical thermoelectricity

The superconducting proximity effect couples charge and temperature together and can give rise to thermoelectric effects (see **I**, [102]). This can be seen with a simple argument. The equilibrium supercurrent $I_S(T)$ depends on the temperature T, and when temperature is position dependent, also the supercurrent must vary. However, since electric charge must be conserved, this variation is compensated by normal dissipative current. Hence, the thermoelectric coefficient L_{12} relating the quasiparticle charge current I_c to temperature difference ΔT must be nonzero, and it must, at least in some limits, be related to the supercurrent.

It is important to note that this mechanism of thermoelectric coupling is rather different compared to what gives rise to thermoelectricity in the normal state, Eq. (2.58). In fact, the normal-state thermoelectricity is completely neglected in the quasiclassical approximation (2.21) where all information on ξ dependence is lost. However, this also means that the magnitude of any of the effects is not related to that of L_{12}^N. Rather, these proximity thermoelectric effects are closer to a charge imbalance generation mechanism in superconductors described in Refs. [120–123].

It was found in **I** that the dominating part of the proximity thermoelectric effect at low temperatures can in the structure depicted in Fig. 2.13 be directly related to the supercurrent. This result can be found by solving the kinetic equations (2.50) approximatively, which gives the result

$$S_{NS} \equiv \left.\frac{\mathrm{d}(V_1+V_2)}{2\,\mathrm{d}(T_1-T_2)}\right|_{I_{c,1}=I_{c,2}=0} \approx \frac{4R_3R_4R_5+R_5^2(R_3+R_4)}{4(R_1+R_2+R_5)R_{SNS}}\,\frac{\mathrm{d}I_S(T)}{\mathrm{d}T}, \tag{2.60a}$$

$$S_{NN} \equiv \left.\frac{\mathrm{d}(V_1-V_2)}{\mathrm{d}(T_1-T_2)}\right|_{I_{c,1}=I_{c,2}=0} \approx \frac{(R_3-R_4)R_5^2}{2(R_1+R_2+R_5)R_{SNS}}\,\frac{\mathrm{d}I_S(T)}{\mathrm{d}T}, \tag{2.60b}$$

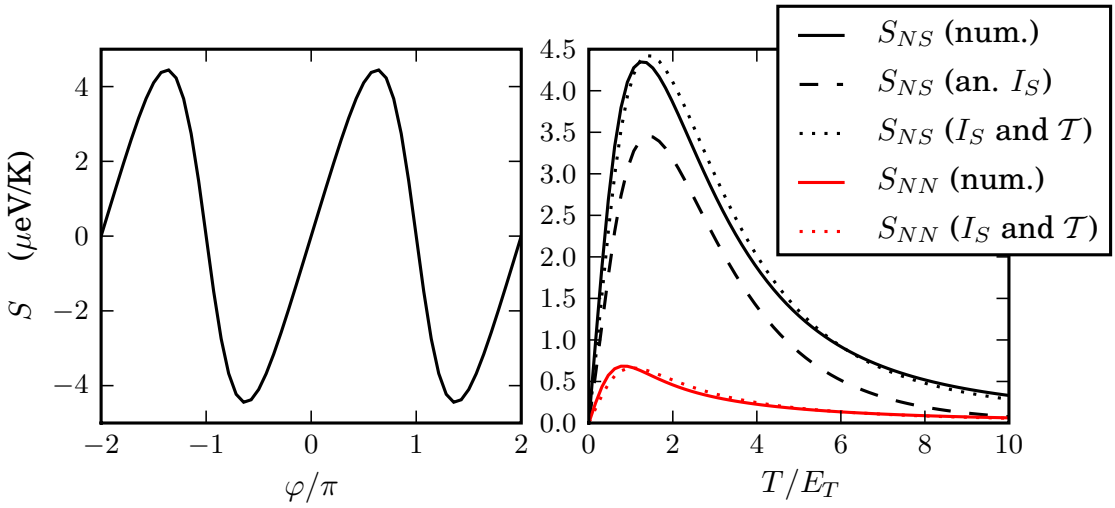

Figure 2.14: Left: Computed thermopower oscillations of maximum thermopower with magnetic flux, in the structure of Fig. 2.13a, using same parameters as in **VI**. Right: Computed temperature dependence, compared with approximations including only I_S (2.60a), and I_S and $\mathcal{T}$ (cf. **VI**).

where R_j are the resistances of the wires in Fig. 2.13, and $R_{SNS} = R_3 + R_4 + R_5$. The above approximation takes only the supercurrent into account. Details are presented in **I** and **II**, and we also compared these results to numerical solutions of the kinetic equations. Several conclusions follow: this effect is large, $S \sim 1\,^{\mu\mathrm{V}}/_{\mathrm{K}}$ and the magnitude is comparable to what is observed in the experiments, as noted also in [102] for S_{NS}. The temperature dependence of S follows that of the derivative of the supercurrent–temperature relation, qualitatively matching experimental observations. The results in **I** show that the expected S_{NS} and S_{NN} are also sensitive to the symmetry of the structure, especially so for the N-N potential difference. Moreover, as shown in **I**, part of this asymmetry can come from the temperature-dependence of the resistances of arms 1 and 2, caused by the proximity effect. Finally, the flux dependence follows that of the supercurrent. The flux and temperature dependence of S_{NN} and S_{NS} and the magnitude of the supercurrent contribution are illustrated in Fig. 2.14.

The supercurrent $I_S(T)$ decays exponentially when the temperature increases. At higher temperatures, $T \gg E_T$, long-range nonequilibrium features of the effect start to appear, and the main contributions come from two different sources not related to the supercurrent: (i) the cross-coupling coefficient $\mathcal{T}$ in the kinetic equations (see **I**, **II**), and (ii) for $T \gtrsim |\Delta|/2$, above-gap contributions start to play a role (see **II** and [103, 104]). The latter contribution, however, may be sensitive to the charge imbalance inside the superconducting contacts (see eg. **VI**).

Additionally, one finds (see **II**) that in the structure in Fig. 2.13c where supercurrent

and temperature gradient do not coexist anywhere, $\boldsymbol{j}_S \cdot \nabla T = 0$, the $\mathcal{T}$ coefficient leaking to arms 1 and 2 can still give rise to a finite thermoelectric voltage. However, due to the symmetry properties of this coefficient, this occurs only if $R_3 \neq R_4$, as was also later noted in [105]. It is possible that the antisymmetric oscillations in the asymmetric "house"-type structure in [100] originate from this. Competition between the effects mentioned above can also result to sign changes in S as a function of the temperature, as discussed in **II**, or this can originate from the above-gap part (cf. [103], **II**). A sign change was also observed in the experiment of Ref. [100].

The main failure of the above theory in describing the experiments is the flux symmetry of the oscillations. This follows from the electron–hole symmetry of the theory, as noted in **II**: electron $\xi > \xi_f$ and hole $\xi < \xi_f$ excitations are in all respects identical, except for their charge and group velocity. Hence, all equations retain their forms under the transformation $V \mapsto -V$, $\Phi \mapsto -\Phi$, $I_c \mapsto -I_c$. This implies that the thermopower predicted by the theory always has the flux symmetry $S(-\Phi) = -S(\Phi)$, irrespective of geometry. This is an exact relation, valid within the quasiclassical theory, but it is not in agreement with the experiments of Ref. [97].

This leads to a dilemma: the normal-state contribution to thermoelectricity is expected to be small in the experimental situation, [97, 100] the same applies for the contribution modified by superconductivity [117] or the proximity effect [126, 127], and as discussed above, the charge imbalance contribution cannot explain all of the experimental data. Other causes for thermoelectric effects and their interplay with the proximity effect are not well understood. How can one then explain the large symmetric oscillations in the thermoelectric coefficient and the large offset potentials?

Recently, a suggestion was put forward in Ref. [105] to explain the symmetric thermopower oscillations. The gist of this article is that the flux-symmetric factor $\mathcal{D}_T$ in arms 1 and 2, when combined with a temperature gradient, can amplify a small potential difference μ between N and S to a large potential difference between N_1 and N_2. The enhancement factor is certainly a promising finding. However, one issue with the model in [105] is that the small potential μ is inserted by hand, breaking charge conservation. Constructing models where the potential μ appears naturally could therefore be useful.

It is quite possible that most of the complete explanation for the proximity thermoelectric effects [95–98, 100, 101], which were first observed over ten years ago, is in place today. However, as we found out in **IV** where the oscillation symmetry was not a problem, making quantitative comparisons to the above theory is challenging as there can be many factors bringing uncertainties: sample characterization, effects neglected in the theory such as inelastic scattering, to name a few. In fact, satisfactory agreement has not been found so far, and more work is certainly still needed. But even if this question can be closed, new ones are opened: for example, what is the exact source of the electron-hole asymmetry required for symmetric oscillations? Solving these issues may require turning back to other aspects of the thermoelectric effects in superconductors.

2.4.2 Peltier effect

The two thermoelectric coefficients L_{12} and L_{21} are not independent, but coupled together by an Onsager relation [85, 129, 130]

$$L_{12} = L_{21}|_{\mathrm{TR}} \ , \tag{2.61}$$

which relates the two off-diagonal transport coefficients. Onsager relations follow quite generally already from thermodynamics for many different systems; the one associated with thermoelectric coefficients is usually known as the Kelvin relation. Above, the notation TR indicates that the coefficient on the right-hand side should be computed for a time-reversed system, whose microscopic equations of motion propagate time to the negative direction.

How the time reversal operation affects a superconducting proximity structure can be seen from basic considerations. The simplest underlying Hamiltonian for studying the proximity effect was

$$H = \int \mathrm{d}^3\boldsymbol{r} \left[\psi_\alpha^\dagger(\boldsymbol{r}) \frac{(\nabla - i\boldsymbol{A})^2}{2m} \psi_\alpha(\boldsymbol{r}) + \frac{g}{2} \psi_\alpha^\dagger(\boldsymbol{r}) \psi_\beta^\dagger(\boldsymbol{r}) \psi_\beta(\boldsymbol{r}) \psi_\alpha(\boldsymbol{r}) \right] . \tag{2.62}$$

Time-reversed, it reads

$$H|_{\mathrm{TR}} = THT^{-1} = \int \mathrm{d}^3\boldsymbol{r} \left[\psi_\alpha^\dagger(\boldsymbol{r}) \frac{(\nabla + i\boldsymbol{A})^2}{2m} \psi_\alpha(\boldsymbol{r}) + \frac{g}{2} \psi_\alpha^\dagger(\boldsymbol{r}) \psi_\beta^\dagger(\boldsymbol{r}) \psi_\beta(\boldsymbol{r}) \psi_\alpha(\boldsymbol{r}) \right] . \tag{2.63}$$

Time-reversal also complex conjugates the order parameter, and hence, in this model time reversal amounts to changing the sign of the magnetic field and the superconducting phases, $\boldsymbol{B} \mapsto -\boldsymbol{B}$, $\phi \mapsto -\phi$. One would then expect the Kelvin relation (2.61) to apply in this sense for proximity structures.

Nevertheless, it is still useful to study the coefficient L_{21} separately in proximity structures, to answer question such as: i) what are the mathematical implications to the kinetic equations (2.50), and ii) is the effect in practice large enough to be measured. This is what was done in **V**. Earlier, the coefficient L_{21} had been computed from a tight-binding model in [106], but only for small structures with significant finite-size effects.

Mathematically, what the time reversal symmetry amounts to in the kinetic equations (2.50) is that there is a conserved flux, (see **V**)

$$J = \rho^\dagger j[\psi] - \psi^\dagger j[\rho] - j_S \rho^\dagger \hat{\tau}_1 \psi \tag{2.64}$$

where $\rho = (f_L, f_T)$ is any solution to the kinetic equations, ψ a solution to the time-reversed equations, and $J = (j_L, j_T)$ contains the corresponding spectral currents. That the above quantity is conserved for any choice of boundary conditions can then

be used to derive the relation

$$\tilde{L}^{ij}_{\alpha\beta}(E) = \tilde{L}^{ji}_{\beta\alpha}(E)|_{\mathrm{TR}}\,, \tag{2.65}$$

between elements of the spectral thermoelectric matrix (2.56). Note that also the terminal indices i and j are exchanged in this relation, and that it applies at each energy E separately. The above relation is also valid only when i and j correspond to normal terminals. The Kelvin relation (2.61) appears as a direct consequence of (2.65).

That the conservation $\nabla \cdot J = 0$ applies also inside superconductors can be used for deriving effective boundary conditions for NS interfaces in some limiting cases, as noted in **VI**. These are needed when one wants to avoid solving differential equations inside the terminals, but still model the fact that superconducting terminals do not necessarily stay at equilibrium.

Typically, when one studies controlling heat current with charge current, the magnitude of the effect is quantified with the Peltier coefficient

$$\Pi = \frac{\mathrm{d}I_Q}{\mathrm{d}I_c}\,. \tag{2.66}$$

As for the Seebeck coefficient S, in the geometry of Fig. 2.13a there are two possible ways for defining a Peltier coefficient:

$$\Pi_{NS} \equiv \left.\frac{\mathrm{d}I^1_Q}{\mathrm{d}I_c}\right|_{I^1_c = I^2_c = I_c/2}\,, \qquad\qquad \Pi_{NN} \equiv \left.\frac{\mathrm{d}I^1_Q}{\mathrm{d}I_c}\right|_{I^1_c = -I^2_c = I_c}\,. \tag{2.67}$$

These correspond to different ways to drive the current I_c in the structure, illustrated in Fig. 2.15a. Similar calculation as made in the preceding section for the Seebeck coefficients S results now to (see **V**, **VI**)

$$\Pi_{NS} = TS_{NS}\,, \qquad\qquad \Pi_{NN} = TS_{NN}\,, \tag{2.68}$$

ie., the two Peltier coefficients are directly related to the Seebeck coefficients (2.60a) by the Kelvin relation discussed above. From the estimates given above, one finds "typical" magnitudes $\Pi_{NS} \sim 1\,\mu\mathrm{V}$ at temperatures close to $T = 400\,\mathrm{mK}$.

The ability of a Peltier element to induce cooling can be measured with the dimensionless figure of merit

$$ZT = \frac{\Pi^2 G}{T G_{\mathrm{th}}}\,. \tag{2.69}$$

Where this expression comes from can be understood by studying the structure in Fig. 2.15, where terminal 1 is assumed to be thermally isolated, apart from the heat contact via the proximity structure. Its temperature is then determined from the

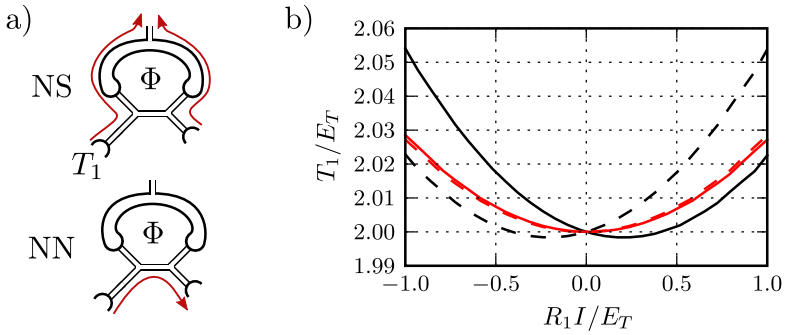

Figure 2.15: a) Peltier current flow configurations. b) Predicted temperature oscillations, when terminal T_1 is thermally isolated, apart from the contact to the circuit. Current is driven in the "NS" configuration (black) or "NN" (gray) configurations, with $\varphi = \pm\pi/2$ (solid/dashed). Parameters are chosen as in **V**. Temperature oscillations are numerically computed by varying V_1 and V_2, solving I_c^1 and I_c^2 with δT_1 determined so that $I_Q^1 = 0$, and finally interpolating to find δT_1 under the correct current configuration.

heat balance

$$I_Q^1 = -G_{\rm th}\delta T_1 + \Pi I_c^1 + [I_c^1]^2/G = 0\,, \tag{2.70}$$

and the maximum relative cooling obtainable is

$$\delta T_1/T = -\frac{1}{4}ZT\,. \tag{2.71}$$

For best Peltier coolers near room temperatures, $ZT \sim 1$, and the number scales as T^α with $\alpha \gtrsim 1$ to low temperatures. For the proximity-induced effect here, $ZT \sim 10^{-4}$. It follows that building a thermoelectric cooler based on the proximity effect is not very practical, especially as better alternatives that work in the same size and temperature range exist [6]. The small value of ZT is problematic also for the detection of this cooling effect. However, the amplitude of proximity-modulated oscillations in δT_1 is proportional to the current I_c and can be larger than the maximum cooling, see Fig. 2.15. For practical parameters it is expected to be in the millikelvin range. Moreover, the oscillation is expected to be antisymmetric in the magnetic flux, and can so be distinguished from the symmetric oscillations of proximity-modified heat conductivity. While temperature changes this small are challenging to measure, sufficient resolution has already been experimentally demonstrated [131].

Existence of Peltier cooling that appears essentially because of supercurrent at first sight seems to contradict the fact that supercurrent does not carry entropy. [28] However, presence of the normal current allows this to occur in this nonequilibrium effect. Indeed, to change the temperature, a nonequilibrium process must take place.

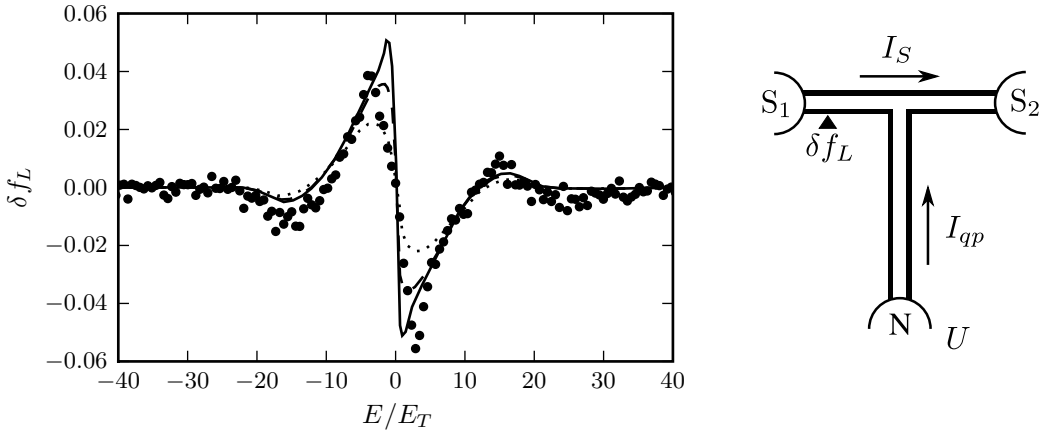

Figure 2.16: Left: Computed change δf_L in the distribution function, with spin-flip rates $\Gamma_{sf} = 0$ (solid), $0.65E_T$ (dashed), and $2.5E_T$ (dotted). Experimental data from **III** corresponding to potential $U = 63\,\mu$eV is shown as dots. Fitted $E_T = 3.47\,\mu$eV is assumed; it mostly affects the scaling of the x-axis. Right: schematic structure.

2.5 Tuning the electron distribution

In addition to studying how the proximity effect changes energy-integrated quantities such as the charge and heat currents, one can also consider spectral quantities such as the electron distribution function $f(E)$. It is, however, not a directly observable quantity, and can only be inferred indirectly. Two situations in which changes in it are expected to be visible are discussed below.

2.5.1 Nonequilibrium Peltier-like effect

A distinct signature of the proximity effect appearing in the distribution function was predicted in [132], and measured by N. Birge's group in **III**, using tunnel junction spectroscopy [133]. A low-energy change $\delta f_L(E) = f_L(E;U) - f_L(E,U=0)$ (cf. Fig. 2.16) arises in a part of the structure, when a voltage bias U drives normal current alongside the same path as the supercurrent flows. In a sense, this is similar to the Peltier effect discussed above, as the nonequilibrium feature in the distribution function corresponds to changes in the effective temperature in different parts of the structure [66]. However, it occurs far from equilibrium, and in the configuration of [132] changes in temperatures of reservoirs cannot be obtained.

To find a quantitative match between Ref. [132] and the experiment, we made a detailed comparison between the experimental results and the model, and I investigated some additional effects left out in [132]: breaking of the "rigidity" approxima-

tion of the superconducting terminals (cf. Section 2.1.6), self-consistent computation of Δ (cf. Eq. (2.17)), and the effect of spin-flip scattering $\check{\Sigma}_{\mathrm{sf}} = \frac{1}{\tau_{\mathrm{sf}}}\hat{\tau}_3\check{G}\hat{\tau}_3$ from the small applied magnetic field (see Section 2.2.3 and Fig. 2.16). Note that the deconvolution of δf_L was performed independently and prior to this analysis, and is explained in detail in Ref. [134].

The main result obtained in the analysis is that the feature δf_L in the electron distribution function is robust with variations of the model parameters, such as the size of the superconducting terminals or whether the energy gap Δ is assumed rigid or whether it is self-consistent. The main effect from taking into account what occurs inside the superconductors is an effective lengthening [62] of the normal wire, by $2\xi_0 = 2\sqrt{\hbar D/2|\Delta|}$. The behavior of δf can be contrasted to the proximity-modified density of states. Understanding the experimentally observed DOS required taking the finite size of the superconducting terminals into account, as we discuss in **III** and **VIII**. Such behavior of the density of states is in agreement with the findings of Refs. [79, 135].

2.5.2 Stable phase states

Driving the electron distribution function far from equilibrium has direct and indirect consequences. A direct consequence is that a change in f can, in addition to changing the dissipative charge current, alter also the non-dissipative supercurrent component. [136–138] This is directly visible in Eqs. (2.50): the supercurrent component is

$$I_S(\varphi) = -\frac{A\sigma}{2e}\int_{-\infty}^{\infty} \mathrm{d}E\, j_S(E,\varphi) f_L(E)\,, \tag{2.72}$$

and as visible in Fig. 2.5, this part is sensitive to changes in the low-energy part of f_L. By adjusting the distribution function, one can also make the supercurrent contribution change its sign. [65, 82, 136, 139] A sign change in the current–phase relation $I(\varphi)$ changes the stable value of φ satisfying the stationarity condition $I(\phi) = 0$. This is seen in the RCSJ washboard potential [23]

$$U(\varphi) = \frac{\hbar}{2e}\int_0^{\varphi} \mathrm{d}\varphi'\, I_S(\varphi') \sim (1-\cos\varphi)E_J\,, \tag{2.73}$$

as a change of minimum from $\varphi = 0$ to $\varphi = \pi$. Such a π-state originating from nonequilibrium has been experimentally realized, [140–142] and π-states have also been created for example using ferromagnetic materials [22].

The π state is one of the effects that appears in proximity circuits when the superconducting phases ϕ at the terminals can adjust freely, ie., the structure is not phase-biased (see Section 2.2.1). Another effect of this type was examined in [83, 134], where one superconducting terminal floated, and its phase was determined from the

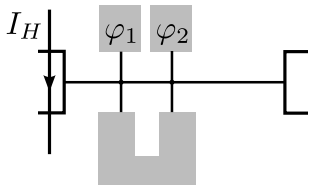

Figure 2.17: The modelled structure: four superconducting terminals, two of them forming a loop, connected by normal wires. Phase differences across the two vertical SNS junctions are marked. It is assumed that on the left, the current I_H creates a nonequilibrium electron distribution $f_q(E)$, which spreads along the horizontal wire. The transconductance $G = dI/dV$ discussed in the text corresponds to voltage induced in the right terminal when current is injected from the right terminal to the superconductors.

condition

$$I = I_s(\phi) + I_n = 0\,, \tag{2.74}$$

ie., that the supercurrent entering the terminal cancels the normal current.

From the theoretical point of view, article **VII** was concerned with an effect between the two types discussed above. The studied schematics is shown in Fig. 2.17. All of the superconducting arms are floating, and current I_H is injected in a part of the circuit. What is observed in the corresponding experiment is that the N-S transconductance G undergoes two rapid changes as the current I_H is increased. We offered one possible qualitative explanation for this in **VII**: with increasing I_H, first the SNS junction on the left switches to π-state, and after it the one on the right. These transitions show up in the magnetoconductance.

The theoretical picture is as follows. The first question is what determines the phase state in this type of a multiterminal structure when out of equilibrium. For finding the transitions, we used in **VII** an extended RCSJ model,

$$\frac{\hbar}{2e}\mathbf{C}\ddot{\boldsymbol{\phi}} = \boldsymbol{I}[\boldsymbol{\phi}] = \boldsymbol{I}_S(\boldsymbol{\phi}) + \frac{\hbar}{2e}\mathbf{G}[\boldsymbol{\phi}]\dot{\boldsymbol{\phi}}\,, \tag{2.75}$$

where $\boldsymbol{\phi} = (\phi_1, \ldots, \phi_N)$ contains the phases of the terminals, $\boldsymbol{I} = (I^1, I^2, \ldots, I^N)$ the currents entering the terminals, and the dissipative and the nonequilibrium supercurrent parts of the total current are written separately. This model is gauge-invariant (we neglect magnetic field): replacing $\phi_j(t) \mapsto \phi_j(t) + \chi(t)$ with arbitrary $\chi(t)$ retains the form of the equations since row sums of conductance and capacitance matrices $\mathbf{G}$ and $\mathbf{C}$ vanish. Similarly to (2.74), stationary solutions $\dot{\boldsymbol{\phi}} = 0$ are found where $\boldsymbol{I}_S(\boldsymbol{\phi}) = 0$, if no bias currents enter the superconductors, as is the case in Fig. 2.17. Not all of these points are stable, however, similarly as in the simpler π-state problem. The stability is determined by whether the vector field $\boldsymbol{I}_S$ tends to make small deviations from a stationary point to grow or to decrease. These

conclusions do not crucially depend on details of **C** and **G**.

Finding the supercurrent I_S is a problem that can be directly addressed based on the time-independent quasiclassical theory. In fact, reasonable approximations for I_S can be obtained analytically, with the methods discussed in Section (2.2.1) and Appendix (A.2): one can find an accurate closed-form expression for $j_S(E)$ even in this somewhat involved multiterminal circuit. This allows evaluating the supercurrent from Eq. (2.72) also under nonequilibrium conditions, extending the approach of Ref. [65]. From this method, one finds an approximate expression for the washboard potential, (see **VII**)

$$U(\boldsymbol{\phi}) = -\frac{\hbar}{2e}\sum_{mk} I_{mk}(V_H)\cos(\phi_m - \phi_k)\,, \tag{2.76}$$

where I_{mk} are critical currents obtained by the approximation method, in the presence of a potential V_H characterizing the nonequilibrium distribution of electrons. If the finite inductance of the superconducting loop needs to be included, an additional term can be added to this potential to represent the imperfect phase bias. Equation (2.76) can be directly used to pinpoint the stable states.

Once a stable phase configuration is found, the corresponding transconductance can be evaluated numerically, by solving the kinetic equations (2.50), taking into account the measurement current configuration in the boundary conditions. When considering linear response, we used a slightly more convenient way to do this, making use of the thermoelectric matrix (2.55) and writing

$$\mathrm{d}I_c^i = \sum_j L_{11}^{ij}\,\mathrm{d}V_j + \sum_j L_{12}^{ij}\,\mathrm{d}T_j\,/T + \sum_j \left.\frac{\partial I_c^i}{\partial \phi_j}\right|_{\{V\}=0,\{\phi\}} \mathrm{d}\phi_j\ . \tag{2.77}$$

The last term in the above equation needs to be included in principle, since in floating terminals the superconducting phases adjust to cancel any additional quasiparticle currents, similarly as in Eq. (2.74). Note, however, that for currents entering normal terminals, $\partial I_c^i/\partial\phi_j = 0$, so that $\mathrm{d}I_c^i$ and $\mathrm{d}T_j$ determine $\mathrm{d}V_j$ for the normal terminals uniquely (for superconductors $\mathrm{d}V = 0$ due to stationarity). This implies that the transconductances can be computed if $L_{\alpha\beta}^{ij}$ are known, and it is not necessary to compute $\partial I_c^i/\partial\phi_j$. This is a significant help, since the coefficients L can be easily obtained from the matrix $\tilde{L}(E)$ discussed in Section 2.3.3. An example of oscillations computed in this way for the stable phase state is shown in Fig. 2.18. However, away from linear response, the above argument is not valid and the adjustment of the superconducting phases must be fully included.

The above theory produces a qualitative match between the observed and predicted conductance oscillations, and can produce two sudden transitions. However, the agreement between the predicted and observed positions in I_H is not very satisfactory. The model also neglects fluctuations, and effects such as electron-electron interactions that can limit nonequilibrium-induced π-states (cf. **VIII**). Moreover, it assumes as a first step a model form of the electron distribution function f_q on

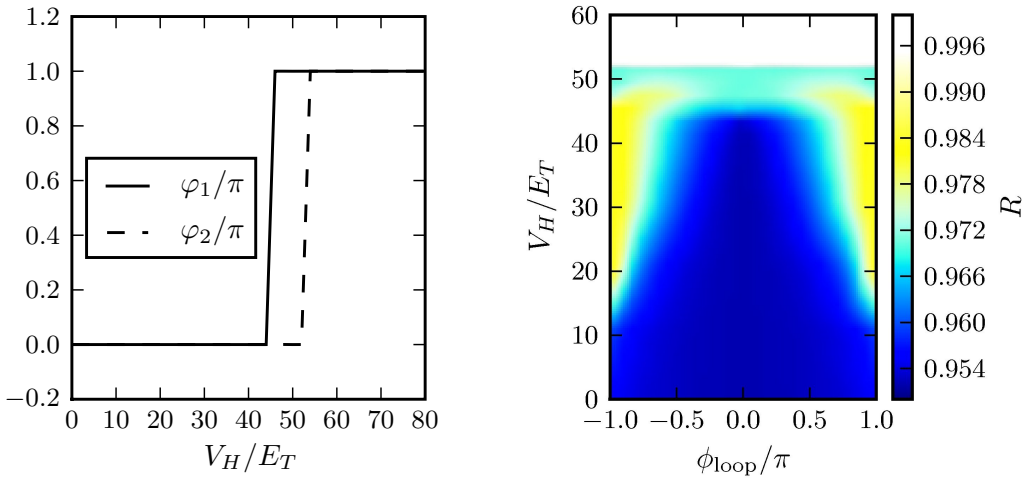

Figure 2.18: Left: Computed phase jumps. Same parameters as in **VII**. Right: Computed resistance oscillations, as V_H (in units of E_T) is increased, as a function of the phase difference $\phi_{\mathrm{loop}} = 2\pi\Phi/\Phi_0$ related to the magnetic flux in the loop of Fig. 2.17. The finite inductance of the loop affects the shape of the low V_H part of the oscillations.

the left, as details of the superconducting injection contacts were neglected. These bring uncertainty to the comparison of the model to the experiment.

An interesting fact following from (2.77) is that (within this model) in a proximity circuit, a N-S transconductance does not depend on which superconducting contact the measurement current injected from the N contact goes to. This occurs because all of the superconducting parts in a circuit are in principle linked together by the proximity effect, no matter how distant they are from each other. If the injected current is smaller than the smallest critical current of any of these links, then it can first be converted to supercurrent in the nearest superconductors, and then travel the rest of the way without dissipation. The measured resistance arises solely from the first step. I am not aware of experiments explicitly probing for this multiterminal effect.

One point that is glossed over in Eq. (2.76) is that, strictly speaking, such a washboard potential cannot be defined out of equilibrium, when there are three or more superconducting contacts. This is because existence of a potential U such that $\boldsymbol{I}_S = -\nabla U$ implies that the vector field $\boldsymbol{I}_S(\boldsymbol{\phi})$ satisfies $\nabla \times \boldsymbol{I}_S(\boldsymbol{\phi}) = 0$. That this is valid at equilibrium follows from the observation that the Usadel equations (2.33) result to

$$\int_{\mathcal{S}_j} \boldsymbol{n} \cdot \frac{\partial j_S}{\partial \phi_k} = \int_{\mathcal{S}_k} \boldsymbol{n} \cdot \frac{\partial j_S}{\partial \phi_j}\,, \tag{2.78}$$

ie., total spectral supercurrents going through terminal interfaces $\mathcal{S}_j$ satisfy a reciprocity relation. This can be shown using similar techniques as used in **V** to show Eq. (2.65). Since at equilibrium $f_L = \tanh(E/2T)$ everywhere, Eq. (2.78) is equivalent to $\partial I_S^i/\partial\phi_j = \partial I_S^j/\partial\phi_i$, ie., $\nabla \times \boldsymbol{I}_S = 0$. Out of equilibrium, however, there does not appear to be a reason why this law could not be broken, and numerical calculations indicate that it breaks. Of course, in structures with only one phase difference (ie. at most two superconductors) defining a 1D potential $U(\varphi)$ is always possible, so observing any effects caused by this requires at least three superconducting probes. In summary, Eq. (2.76) applies only approximatively, and in reality a small non-conservative part of $\boldsymbol{I}_S$ is expected. However, in the structure of Fig. 2.17, we estimated this to be negligible compared to the dissipation.

The non-conservative part of the supercurrent in the structure of Fig. 2.17 attempts to transfer a part of the heat current flowing through the structure to motion of the superconducting phases ϕ. If undamped, this could induce measurable finite potentials in the superconductors. Hence, this effect is also closely related to the discussion in Section 2.4. One can note that a thermoelectric effect in which the normal-state thermopower (2.58) causes an SNS junction to switch to a finite-voltage state because of applied temperature difference has been both predicted [143] and observed [144]. At the moment, it is an open question whether there is a structure in which similar effects can occur because of the proximity effect, or whether dissipation always stabilizes some of the stationary phase states or if fluctuations disturb the effect significantly.

Above, we have shown that driving the electron system out of equilibrium is expected to lead to interesting effects for the phase configuration in multiprobe structures. Moreover, the experiments in **III** demonstrated that effects arising from similar parts of the quasiclassical theory that give rise to thermoelectric effects (j_S and $\mathcal{T}$) can be observed also far from equilibrium.

Several aspects of the proximity effect are discussed in this Section 2. Compensation between supercurrent and normal current leads to thermoelectric effects, and in suitable situations also to observable changes in the distribution function. Interference contributions that are important for these nonequilibrium transport phenomena are also sensitive to breaking of geometrical symmetries. Moreover, non-locality caused by supercurrents flowing in response to applied normal currents must be taken into account when considering these structures. This shows that mesoscopic proximity circuits can support several complex phenomena, even if we consider only stationary situations.

3 Mesoscopic noise

The interest in detailed physics of electrical noise and its statistics is a recent development in mesoscopics. [13] The main idea is that the measured noise reflects internal properties of the conductor, such as the charge of the elementary excitations [145]. This is especially relevant for mesoscopic structures, since many features of their transport properties are not necessarily visible in the average value of the current.

Classical noise in the current is most often characterized with a spectrum of the current-current correlator: [13]

$$S(\omega) = 2\int_{-\infty}^{\infty} \mathrm{d}t\, e^{i\omega t} \left\langle \delta I(t)\delta I(0)\right\rangle \,, \qquad \delta I(t) = I(t) - \left\langle I\right\rangle \,, \tag{3.1}$$

where the brackets $\langle\cdot\rangle$ denote an average over the realizations of all possible fluctuations δI. This does not capture all information about the fluctuations δI, as Eq. (3.1) essentially represents only the standard deviation for the distribution of fluctuations. So, higher-order moments such as

$$M_3(\omega,\omega') = \int_{-\infty}^{\infty} \mathrm{d}t\,\mathrm{d}t'\, e^{i\omega t + i\omega' t'} \left\langle I(t)I(t')I(0)\right\rangle \tag{3.2}$$

$$M_4(\omega,\omega',\omega'') = \int_{-\infty}^{\infty} \mathrm{d}t\,\mathrm{d}t'\,\mathrm{d}t''\, e^{i\omega t + i\omega' t' + i\omega'' t''} \left\langle I(t)I(t')I(t'')I(0)\right\rangle \,, \tag{3.3}$$

can also be studied. A different viewpoint is taken in studies of full counting statistics, where the probabilities $P_N(t)$ for N charges to pass through the conductor in time t are studied instead. Typically this information is there discussed using the generating function of the distribution

$$e^{\mathcal{S}_t(\chi)} = \sum_N e^{i\chi N} P_N(t)\,, \tag{3.4}$$

which contains the full information of the statistics, and from which all moments of the distribution can be computed.

In quantum coherent mesoscopic conductors, generalizations of Eqs. (3.1) and (3.4) are required. Detailed reviews on this can be found in Refs. [13, 36, 146]. The main points are that one can define a quantum analogue of (3.1) as

$$S(\omega) = \int_{-\infty}^{\infty} \mathrm{d}t\, e^{i\omega t} \left\langle \{\delta\hat{I}(t), \delta\hat{I}(0)\}\right\rangle \,, \tag{3.5}$$

in terms of a current operator $\hat{I}$. The symmetrization is necessary for obtaining the classical correspondence, since the operators at different times do not commute. [13] A second point is that generalization of Eq. (3.4) has certain subtleties, part of which also arise from non-commutativity. [14, 36, 146, 147] One can however write

a generating function on the Keldysh contour, [14, 147–149]

$$e^{\mathcal{S}(\chi)} = \left\langle T_c[S_c e^{\int_c \mathrm{d}\tau\, \chi(\tau)\hat{I}(\tau)}] \right\rangle , \tag{3.6}$$

and this quantity can be interpreted similarly as Eq. (3.4), although with certain restrictions [14, 150, 151]. The quantity χ is commonly called the counting field. Studying the counting statistics (3.6) and the higher-order correlations (3.2) in mesoscopic conductors has recently generated significant interest.

Below, I discuss two contributions to the field of mesoscopic noise: a connection between the Green function circuit theory for computing (3.6) and certain semiclassical theories, and then one possible way in which (3.1) and (3.2) could be probed.

3.1 Noise in N-S circuits

A semiclassical theory for computing the zero-frequency noise (3.5) in normal-metal superconductor hybrid circuits was introduced in Refs. [152–154]. Incoherent implies that the Thouless energy E_T is vanishingly small and the proximity effect can be neglected. [7] However, the fact that Andreev reflection blocks energy currents still needs to be taken into account. An equivalent-circuit Green function theory was also formulated under these conditions in [158], based on the general theory of Refs. [148, 149]. Article **X** presented an addition to these results, by showing how the Green function theory connects to the semiclassical one, extending previously demonstrated special cases [152] to a more general statement.

One of the main points of **X** is that expansion of the incoherent Green function in the counting fields,

$$\check{G}_j = \begin{pmatrix} \hat{\tau}_3 & 2\hat{h}_j\hat{\tau}_3 \\ 0 & -\hat{\tau}_3 \end{pmatrix} + \sum_{k\in\mathcal{T}} i\chi_k \begin{pmatrix} -\hat{h}_j\hat{b}_k^j & 4\hat{c}_k^j - \hat{b}_k^j \\ \hat{b}_k^j & \hat{h}_j\hat{b}_k^j \end{pmatrix} + \ldots , \tag{3.7}$$

leads to an interpretation of the components b_k^j as the characteristic potentials, [159] which indicate how the potential in node j depends on the potential in terminal k. These can be understood as probabilities for the particle at node j to eventually end up in terminal k. Dealing with expansion (3.7) becomes impractical already at the third order, but it is manageable in the second order. We showed in **X** how starting from (3.7), the Green function approach of [148, 149] leads to the semiclassical noise formula

$$\tilde{S}_{kl} = \sum_{(i,j)} \int_{-\infty}^{\infty} \mathrm{d}\varepsilon\, (b_k^i - b_k^j)(b_l^i - b_l^j) s_{ij}(\varepsilon) , \tag{3.8}$$

which connects the noise cross-correlations observed between terminals k and l to noise s_{ij} generated in individual circuit elements. The terms s_{ij} coincide with pre-

[7] Changes from the proximity effect were discussed in [155–157].

dictions from the scattering theory: [13] for example the one between nodes reads

$$s_{ij} = \frac{1}{4} g_{ij}[2 - (f_L^i + f_T^i)^2 - (f_L^j + f_T^j)^2 + F_{ij}(f_L^i + f_T^i - f_L^j - f_T^j)^2] \,, \qquad (3.9)$$

where F is the Fano factor [13] and g the conductance of the connector. As in the semiclassical theory, [152–154] the noise $s_{ij}(\varepsilon)$ depends on the distribution of electrons at each energy, and is expected to be sensitive to the nonequilibrium state. Theories of the above kind can be useful in interpreting cross-correlation measurements.

3.2 An on-chip detector for higher moments

Noise is often measured by "classical" means: using electronics that consist of macroscopic components. These function so that they capture the classical signal $I(t)$ and square and band-pass filter it to produce an estimator for example for the power spectral density (3.1). However, accessing the higher moments of the statistics (3.4) this way turns out to require long averaging times, and accessing the very-high-frequency parts of the noise spectra is difficult. [160–162] Hence, there has been interest in designing on-chip detectors: structures fabricated in the vicinity of the studied mesoscopic conductor, for the purpose of transforming the electrical noise of the conductor to a quantity that is experimentally easier to access.

Several different types of on-chip detectors have been proposed and used to detect the noise or higher moments so far: quantum point contacts or single-electron transistors for resolving individual electron tunnelling events [163, 164] and Josephson junction threshold detectors [165–168], to mention a few. The detector proposed in **IX** was also based on a Josephson junction, but in a different limit of device parameters than the threshold detector.

It was noted and explained in [169, 170] that a Coulomb blockaded Josephson junction can detect the asymmetry, ie., the third moment of the noise in its environment. This idea was taken further in **IX** where we constructed a scheme for relating the measured $I(V)$ of the junction to the power spectrum (3.1) and the third moment correlator (3.2). Related work on a somewhat similar type of a detector was also made in [171–174] concerning the power spectrum.

The measurement device studied in **IX** and [169, 170] is an ultra-small Josephson tunnel junction in the Coulomb blockade limit. [175] These devices have a small capacitance, which makes the charging energy $E_C = q^2/2C$ associated with additional charges q on the capacitor so large that electrons and Cooper pairs cannot pass through the junction unless supplied with additional energy $E \sim E_C$. This additional energy can come from electromagnetic fluctuations in the environment of the junction, or from the bias voltage over the device. This mechanism enables the junction to probe for the electromagnetic fluctuations in its vicinity.

The Cooper pair tunnelling current in a SIS Josephson tunnel junction can be com-

puted in the simplest way based on a tunnelling Hamiltonian, [175]

$$H = H_{\text{env}} - \frac{E_J}{2}(e^{-i\phi} + e^{i\phi}) \,, \tag{3.10}$$

which consists of a Hamiltonian for the electromagnetic environment of the junction, and the Cooper pair tunnelling part, where $E_J = \hbar I_c/2e$ is the Josephson energy. Quasiparticle tunnelling is neglected here. The phase operators ϕ represent a macroscopic degree of freedom, the electromagnetic/superconducting phase $\phi(t) = 2\int^t \mathrm{d}t'\, V(t')$ (see [175, 176] for details), which is a conjugate variable to the charge q on one side of the SIS junction.

Applying the standard Golden rule or linear response theory to the above Hamiltonian yields the current: [170, 175]

$$I(V) = \pi E_J^2 (P_\phi(2eV) - P_{-\phi}(-2eV)) \,, \tag{3.11}$$

$$P_{\pm\phi}(E) = \frac{1}{2\pi}\int_{-\infty}^{\infty} \mathrm{d}t\, e^{iEt} \left\langle e^{\pm i\delta\phi(t)} e^{\mp i\delta\phi(0)} \right\rangle \,. \tag{3.12}$$

This current depends now on the fluctuations of the phase $\delta\phi = \phi - \langle\phi\rangle$, which in turn depend on the electromagnetic environment of the junction. If a noise source is coupled to the junction, this will be visible in the current-voltage relation. Moreover, the above expression is not symmetric under the transformation $\phi \mapsto -\phi$, and so the tunnelling current $I(V)$ will in general depend also on the odd moments of ϕ, and consequently, on the odd moments of the voltage fluctuations. In general, the odd moments of noise in mesoscopic conductors can be separated from the even ones by reversing the direction of the current generating the noise: the signal associated with them is antisymmetric.

In the approach taken in **IX**, we made a cumulant expansion for the correlator,

$$\left\langle e^{\pm i\delta\phi(t)} e^{\mp i\delta\phi(0)} \right\rangle = e^{C_2(t) + C_3(t) + \cdots} \,, \tag{3.13a}$$

$$C_2(t) = -\left\langle (\delta\phi(t) - \delta\phi(0))\delta\phi(0) \right\rangle \,, \tag{3.13b}$$

$$C_3(t) = \mp\frac{1}{2}\left\langle \delta\phi(t)(\delta\phi(t) - \delta\phi(0))\delta\phi(0) \right\rangle \,, \ldots \,. \tag{3.13c}$$

This is motivated by the fact that for a "macroscopic" electromagnetic environment, only C_2 is expected to be finite, ie., the fluctuations are Gaussian for that case. [175] However, when a mesoscopic noise source is introduced in the vicinity of the Josephson junction, also the higher cumulants, starting from C_3, are expected to become nonzero.

We also separated the phase correlators into two parts, by subtracting the Gaussian equilibrium fluctuations: $C = C_{\text{eq}} + (C - C_{\text{eq}}) = C_{\text{eq}} + C_{\text{exc}}$. The equilibrium fluctuations are related to the impedance Z of the environment of the junction by

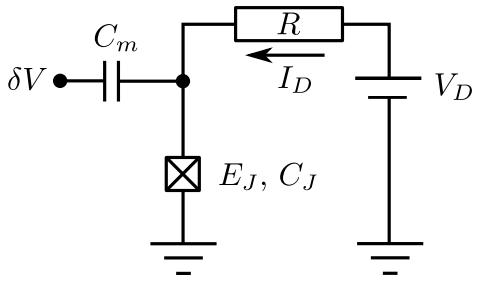

Figure 3.1: Setup for fluctuation measurements. The spectrum of fluctuations, $\langle \delta V(\omega)\delta V(-\omega)\rangle$ and $\langle \delta V(\omega')\delta V(\omega)\delta V(-\omega-\omega')\rangle$ affects the detection current $I_D(V_D)$ relation in the Josephson junction, through the capacitive coupling via $C_m \ll C_J$.

the fluctuation-dissipation theorem in the standard way, [175]

$$C_{2,\mathrm{eq}}(t) = -2\int_0^\infty \mathrm{d}\omega\, \frac{\mathrm{Re}\, Z_t(\omega)}{R_Q}\frac{1}{\omega}\left[\coth\Big(\frac{\beta\hbar\omega}{2}\Big)(\cos(\omega t)-1) - i\sin(\omega t)\right]. \quad (3.14)$$

Moreover, we rewrote the expression for $I_D(V_D)$ so that it involves only the current $I_D^0(V_D)$ with the noise source turned off, and the "excess" cumulants. This way, some of the details of the measurement device itself vanish from the formulation, as $I_D(V_D)$ itself is a measurable quantity.

Relating the excess correlators $C_{j,\mathrm{exc}}$ to the fluctuations of the current in a mesoscopic conductor requires some assumptions made about the measurement setup. In **IX** the schematics of Fig. 3.1 were assumed, and we computed the phase correlators in terms of current correlators of the mesoscopic source, using classical circuit theory — which neglects some quantum effects in the shot noise, see below. We showed that for a small coupling between the detector and the noise source, one finds the simpler formulas reported in **IX** for the symmetric and antisymmetric changes $I_S(V) = I(V) + I(-V)$ and $\delta I_A(V) = I(V) - I(-V) - 2I_D(V)$ in the current, in terms of the current correlators of the noise source:

$$\delta I_A(V_D) = \int_{-\infty}^{\infty}\frac{\mathrm{d}\omega}{2\pi}\mathcal{D}_A(\omega, V_D)S_{2I}(\omega)\,, \quad (3.15)$$

$$\mathcal{D}_A(\omega, V_D) = \left(\frac{\pi R_S C_m}{R_Q C_J}\right)^2 R^2 C_J^2 \frac{I_D^0(V_D+\omega/2) + I_D^0(V_D-\omega/2) - 2I_D^0(V_D)}{1+(\omega R C_J)^2}\,, \quad (3.16)$$

$$I_S(V_D) = \frac{1}{4\pi}\int_{-\infty}^{\infty} I_D^0(V_D - E/2)K_\phi(E)\,, \quad (3.17)$$

and

$$K_\phi(\omega) = \frac{1}{\pi}\int_{-\infty}^{\infty} \mathrm{Im}\, S_{3\phi}(\omega,\omega',-\omega-\omega')\,, \tag{3.18}$$

$$S_{3\phi}(\omega,\omega',\omega'') \simeq \left(\frac{\pi R_S C_m}{R_Q C_J}\right)^3 \frac{(RC_J)^3}{e^3} \frac{S_{3I}(\omega,\omega',\omega'')}{(1-i\omega RC_J)(1-i\omega' RC_J)(1-i\omega'' RC_J)}\,, \tag{3.19}$$

where it is here assumed that the current fluctuations are converted to voltage fluctuations using a macroscopic load resistor, and $C_m \ll C_J$. These results could be used for spectroscopy of noise power and the third cumulant. One point to note is that the RC bandwidth on which the current correlators are accessed in the above expressions can for typical parameters of a Josephson junction be large, $\Delta\omega \sim 100\,\mathrm{GHz}$, which allows for high-frequency measurements.

To my knowledge, the above detection scheme has so far never been used. One experimental challenge is that the weak coupling required to make the response of the detector linear in the excess noise, ensuring the validity of the cumulant expansion and making the results easier to analyze, also makes the signals $\delta I_A(V)$ and $I_S(V)$ small as compared to the unperturbed current $I_D^0(V)$. Some related work for the limit of strong coupling between the detector and noise source can be found in Refs. [170, 177, 178]; however, the relationship between the frequency-dependence of the noise correlators (3.1), (3.2) and the current $I(V)$ appears to be relatively unexplored in this limit.

Above, it is crucial for the result (3.14) that the correlator C_2 is not symmetrized and the difference between emission and absorption [171] in the high-frequency quantum equilibrium noise is taken into account (cf. [13, 175]). An interesting question is if similar quantum effects can be seen also in the shot noise and the higher moments; lack of symmetrization in Eq. (3.13) implies they should be visible. It is known that in mesoscopic structures, different orderings of current operators $\hat{I}$ generally give different results for the noise correlators, [13, 147, 179, 180] and different devices are expected to measure different quantities [179, 181]. To my knowledge, there are currently two experiments that attempted explicitly to comment on this: [161] and [173]. The measurement in [161] claimed to contradict [179] for C_3. However, the current fluctuations were there converted to voltage fluctuations using a macroscopic load resistor, and the voltage fluctuations were measured using conventional electronics, so it is unclear what this implies. The experiment reported in [173] on the other hand confirmed that C_2 should appear as nonsymmetrized in their on-chip detector, also for the excess noise. Recently, more theoretical work addressing this issue has also been published, [182] and the question whether this type of effects can be detected in C_3 is still open.

4 Conclusions

This dissertation concentrates on the physics of mesoscopic superconducting heterostructures. Studying their nonequilibrium response can reveal both their intrinsic properties and characterize their environment. Much of the research in this thesis was motivated by recently published experiments, and part was done alongside them. New predictions are also made. Of these, measuring the Peltier coefficient directly could shed more light on the proximity thermoelectricity, and it might be possible to look for quantum effects in higher-order noise using the Josephson detector.

The relationship between thermoelectricity and the superconducting proximity effect is discussed in Section 2.4. Presence of thermoelectricity is partly due to temperature-dependence of supercurrent and charge conservation. However, in general it arises from several related sources, resulting in a rich variety of predictions. Some of these are sensitive to details. Currently, the theory has not been shown to quantitatively match with the experiments. However, as we have showed, essentially the same theory that gives predictions for the thermoelectric effects matches reasonably well with experimental observations as far as the nonlinear changes in the electron distribution function are concerned. This gives hope for quantitatively bridging the gap between experiments and theory also for thermoelectricity. Indisputably, there are many future challenges left in this, both theoretical and experimental. From the theoretical point of view, one task is to collect the existing results for the charge imbalance contributions discussed here and the normal-state contributions, to produce a coherent single picture. On the experimental side, it should be pointed out that several predicted features in the geometry-dependence of the effect have not yet been systematically investigated. Also, one way forward for testing the predictions could be measuring the Peltier coefficient, which gives an alternative way to access the thermoelectric coupling.

Supercurrent plays a role in thermoelectric and nonlocal effects in proximity structures. We showed a simple scheme for calculating it in metallic proximity circuits, which may prove useful for estimating them in scientific applications. In mesoscopic structures with multiple superconducting parts, supercurrent-phase relations also determine the stable configuration of superconducting phase differences. If such a system is driven out of equilibrium, it may be possible to realize detailed control of the current-phase relations via the electron distribution, beyond single junctions, and conductance measurements could offer a way to probe the phase configuration. Previously, inducing a π-state using Zeeman splitting of energy levels in a magnetic field was suggested. However, as shown in Section 2.2.3, in practice very thin structures are required to avoid the dephasing caused by the magnetic field. This is important to take into account in any future experiments. Our estimates point towards that for observation of this spin-dependent effect, nearly atomic-size materials such as graphene may be required.

Detecting the spectrum of correlators with a Josephson junction is proposed in Sec-

tion 3. The detector has several interesting properties: sensitivity to higher-order correlators, tunable high bandwidth, and possible sensitivity to quantum aspects of the measured correlators. However, the device may be experimentally challenging to realize, and similar power spectrum detectors working in a different regime have already been demonstrated. Still, methods for accessing high-frequency noise are of primary scientific interest. One reason is that in mesoscopic conductors, distinctive features are expected to appear in the noise on the frequency scale of the electron transport time through the conductor. The same is true for the higher-order correlators, and accessing this regime of fluctuations experimentally could aid understanding the dynamics of electron transport.

Superconducting heterostructures already have device applications. Fully realizing their potential is likely to require a detailed understanding of their physics, which can be gained by basic research on their properties. Clearly, there are unanswered questions, and not all of them even in the details. Especially time-dependent effects, which are important for radiation detection, are incompletely understood in proximity structures. The challenge here is in making a connection between the microscopic description and a phenomenological theory useful for engineering. Applications aside, there are also more fundamental questions. For example, what are the limitations on quantum behavior of the phase of the superconducting condensate? Understanding the sources of its decoherence is important for the development of quantum bits. Studying superconductivity and nonequilibrium transport in non-conventional superconductors or in non-metallic systems, such as quantum dots, graphene, or nanotubes, where electron-electron interactions and electronic structure can play a larger role, is also of general interest. Many fruitful opportunities for research are currently available in mesoscopic superconductivity.

References

[1] Y. Nakamura, Y. A. Pashkin, and J. S. Tsai. Nature, **398**, 786 (1999). *(p. 1)*

[2] D. V. Averin. Nature, **398**, 748 (1999). *(p. 1)*

[3] Y. Makhlin, G. Schön, and A. Shnirman. Nature, **398**, 305 (1999). *(p. 1)*

[4] D. Twerenbold. Rep. Prog. Phys, **59**, 349 (1996). *(p. 1)*

[5] K. D. Irwin and G. C. Hilton. Topics Appl. Phys., **99**, 63 (2005). *(p. 1)*

[6] F. Giazotto, T. T. Heikkilä, A. Luukanen, A. Savin, and J. Pekola. Rev. Mod. Phys., **78**, 217 (2006). *(p. 1, 16, 26, 37)*

[7] P. G. de Gennes. Rev. Mod. Phys., **36**, 225 (1964). *(p. 1, 3, 4)*

[8] C. J. Lambert and R. Raimondi. J. Phys.: Condens. Matter, **10**, 901 (1998). *(p. 1, 3, 28)*

[9] B. Pannetier and H. Courtois. J. Low Temp. Phys., **118**, 599 (2000). *(p. 1, 3, 4)*

[10] A. F. Morpurgo, J. Kong, C. M. Marcus, and H. Dai. Science, **286**, 263 (1999). *(p. 1, 3)*

[11] A. Y. Kasumov, et al. Science, **284**, 1508 (1999). *(p. 1, 3)*

[12] H. B. Heersche, P. Jarillo-Herrero, J. B. Oostinga, L. M. K. Vandersypen, and A. F. Morpurgo. Nature, **446**, 56 (2006). *(p. 1, 3)*

[13] Y. A. Blanter and M. Büttiker. Phys. Rep., **336**, 1 (2000). *(p. 1, 44, 46, 49)*

[14] Y. V. Nazarov and M. M. Kindermann. Eur. Phys. J. B, **35**, 413 (2003). *(p. 1, 44, 45)*

[15] P. G. de Gennes. *Superconductivity of metals and alloys*. W. A. Benjamin, New York (1966). *(p. 3, 21, 22)*

[16] H. Meissner. Phys. Rev., **109**, 686 (1958). *(p. 3)*

[17] P. H. Smith, S. Shapiro, J. L. Miles, and J. Nicol. Phys. Rev. Lett., **6**, 686 (1961). *(p. 3)*

[18] J. Clarke. Phys. Rev. B, **4**, 2963 (1971). *(p. 3)*

[19] J. M. Warlaumont, J. C. Brown, T. Foxe, and R. A. Buhrman. Phys. Rev. Lett., **43**, 169 (1979). *(p. 3)*

[20] T. Y. Hsiang and D. K. Finnemore. Phys. Rev. B, **22**, 154 (1980). *(p. 3, 23)*

[21] S. G. den Hartog, C. M. A. Kapteyn, B. J. van Wees, T. M. Klapwijk, and G. Borghs. Phys. Rev. Lett., **77**, 4954 (1996). *(p. 3, 27)*

[22] V. V. Ryazanov, V. A. Oboznov, A. Y. Rusanov, A. V. Veretennikov, A. A. Golubov, and J. Aarts. Phys. Rev. Lett., **86**, 2427 (2001). *(p. 3, 39)*

[23] M. Tinkham. *Introduction to Superconductivity*. McGraw-Hill, New York, 2nd edn. (1996). *(p. 3, 21, 23, 39)*

[24] A. F. Andreev. Sov. Phys. JETP, **19**, 1228 (1964). [Zh. Eksp. Teor. Fiz. 46, 1823 (1964)]. *(p. 3, 11)*

[25] L. P. Gor'kov. Sov. Phys. JETP, **7**, 505 (1958). [Zh. Eksp. Teor. Fiz. 34, 735 (1958)]. *(p. 4, 8, 9)*

[26] A. F. Andreev. Sov. Phys. JETP, **22**, 455 (1966). *(p. 5, 18)*

[27] I. O. Kulik. Sov. Phys. JETP, **30**, 944 (1970). *(p. 5, 18)*

[28] N. W. Ashcroft and N. D. Mermin. *Solid-state physics*. Saunders College Publishing, Philadelphia (1967). *(p. 6, 14, 30, 37)*

[29] J. Rammer and H. Smith. Rev. Mod. Phys., **58**, 323 (1986). *(p. 6, 7, 9, 10, 14, 17)*

[30] N. B. Kopnin. *Theory of nonequilibrium superconductivity*. No. 110 in International series of monographs on physics. Oxford University Press (2001). *(p. 6, 8, 9, 11, 13)*

[31] A. M. Gulian and G. F. Zharkov. *Nonequilibrium electrons and phonons in superconductors*. Selected topics in superconductivity. Kluwer Academic Publishers (2002). *(p. 6)*

[32] J. Rammer. *Quantum Field Theory of Non-Equilibrium States*. Cambridge University Press (2007). *(p. 6, 8, 12)*

[33] H. Haug and A. P. Jauho. *Quantum Kinetics in Transport and Optics of Semiconductors*. Springer, Berlin (1996). *(p. 6, 8)*

[34] W. Belzig, F. K. Wilhelm, C. Bruder, G. Schön, and A. D. Zaikin. Superlatt. Microstruct., **25**, 1251 (1999). *(p. 6, 16, 18, 25, 26)*

[35] L. V. Keldysh. Sov. Phys. JETP, **20**, 1018 (1965). [Zh. Eksp. Teor. Fiz. 47, 1515 (1964)]. *(p. 6)*

[36] M. Kindermann. *Electron counting statistics in nanostructures*. Ph.D. thesis, Leiden University (2003). *(p. 7, 44)*

[37] H. Bruus and K. Flensberg. *Many-body Quantum Theory in Condensed Matter Physics: An Introduction*. Oxford University Press (2004). *(p. 8, 17)*

[38] J. Bardeen, L. N. Cooper, and J. R. Schrieffer. Phys. Rev., **106**, 162 (1957). *(p. 8)*

[39] J. Bardeen, L. N. Cooper, and J. R. Schrieffer. Phys. Rev., **108**, 1175 (1957). *(p. 8)*

[40] L. N. Cooper. Phys. Rev., **104**, 1189 (1956). *(p. 8)*

[41] Y. Nambu. Phys. Rev., **117**, 648 (1960). *(p. 8, 10)*

[42] D. C. Langreth. In *Linear and Nonlinear Electron Transport in Solids*, edited by J. T. Devreese and E. van Doren. Plenum, New York (1976). *(p. 10)*

[43] A. Shelankov. J. Low Temp. Phys., **60**, 29 (1985). *(p. 11, 12, C–1)*

[44] R. E. Prange and L. P. Kadanoff. Phys. Rev., **134**, A566 (1964). *(p. 11)*

[45] G. Eilenberger. Z. Phys, **214**, 195 (1968). *(p. 11, 12)*

[46] A. I. Larkin and Y. N. Ovchinnikov. Sov. Phys. JETP, **28**, 1200 (1969). [Zh. Eksp. Teor. Fiz. 55, 2262 (1968)]. *(p. 11, 12)*

[47] J. W. Serene and D. Rainer. Phys. Rep., **101**, 221 (1983). *(p. 12, 13)*

[48] G. M. Eliashberg. Sov. Phys. JETP, **34**, 668 (1972). [Zh. Eksp. Teor. Fiz. 61, 1254 (1971)]. *(p. 12)*

[49] A. I. Larkin and Y. N. Ovchinnikov. Sov. Phys. JETP, **41**, 960 (1976). [Zh. Eksp. Teor. Fiz. 68, 1915 (1975)]. *(p. 12)*

[50] M. Eschrig. *Mikroskopische Theorie isolierter Wirbel in Hoch-T_c-Supraleitern unter dem Einfluß eines elektromagnetischen Wechselfeldes*. Ph.D. thesis, Universität Bayreuth (1997). *(p. 12, C–1)*

[51] K. D. Usadel. Phys. Rev. Lett., **25**, 507 (1970). *(p. 13)*

[52] Y. Nagato, K. Nagai, and J. Hara. J. Low Temp. Phys., **93**, 33 (1993). *(p. 14)*

[53] N. Schopohl and K. Maki. Phys. Rev. B, **52**, 490 (1995). *(p. 14, 17)*

[54] M. Eschrig. Phys. Rev. B, **61**, 9061 (2000). *(p. 14, 15, 16, 17, C–1)*

[55] A. Schmid and G. Schön. J. Low Temp. Phys., **20**, 207 (1975). *(p. 14, 25)*

[56] A. I. Larkin and Y. N. Ovchinnikov. Sov. Phys. JETP, **46**, 155 (1977). [Zh. Eksp. Teor. Fiz. 73, 299 (1977)]. *(p. 14, 25)*

[57] A. V. Zaitsev. Sov. Phys. JETP, **59**, 1015 (1984). *(p. 15)*

[58] M. Y. Kupriyanov and V. F. Lukichev. Sov. Phys. JETP, **67**, 1163 (1988). *(p. 15, A–2)*

[59] Y. V. Nazarov. Superlatt. Microstruct., **25**, 1221 (1999). *(p. 15, 16, A–1)*

[60] Y. V. Nazarov. Phys. Rev. Lett., **73**, 1420 (1994). *(p. 16, 19, A–1)*

[61] T. T. Heikkilä, J. Särkkä, and F. K. Wilhelm. Phys. Rev. B, **66**, 184513 (2002). *(p. 16, 18)*

[62] K. K. Likharev. Rev. Mod. Phys., **51**, 101 (1979). *(p. 16, 18, 19, 21, 28, 39, A–3)*

[63] T. Matsubara. Prog. Theor. Phys., **14**, 351 (1955). *(p. 17)*

[64] A. A. Golubov, M. Y. Kupriyanov, and E. Il'ichev. Rev. Mod. Phys., **76**, 411 (2004). *(p. 18)*

[65] F. K. Wilhelm, G. Schön, and A. D. Zaikin. Phys. Rev. Lett., **81**, 1682 (1998). *(p. 18, 24, 39, 41)*

[66] T. Heikkilä. *Superconducting proximity effect in mesoscopic metals*. Ph.D. thesis, Helsinki University of Technology (2002). *(p. 18, 21, 38)*

[67] A. D. Zaikin and G. F. Zharkov. Sov. J. Low Temp. Phys., **7**, 184 (1981). [Fiz. Nizk. Temp. 7, 375 (1981)]. *(p. 19, A–3)*

[68] A. A. Golubov, F. K. Wilhelm, and A. D. Zaikin. Phys. Rev. B, **55**, 1123 (1997). *(p. 20, 28, A–1)*

[69] T. H. Stoof and Y. V. Nazarov. Phys. Rev. B, **54**, R772 (1996). *(p. 20, A–1)*

[70] P. Charlat, H. Courtois, Ph. Gandit, D. Mailly, A. F. Volkov, and B. Pannetier. Phys. Rev. Lett., **77**, 4950 (1996). *(p. 20, 22, 27, 28)*

[71] A. V. Zaitsev. Physica B, **203**, 274 (1994). *(p. 20)*

[72] J. C. Hammer, J. C. Cuevas, F. S. Bergeret, and W. Belzig. Phys. Rev. B, **76**, 064514 (2007). *(p. 21)*

[73] J. C. Cuevas and F. S. Bergeret. Phys. Rev. Lett., **99**, 217002 (2007). *(p. 21)*

[74] T. T. Heikkilä, F. K. Wilhelm, and G. Schön. Europhys. Lett., **51**, 434 (2000). *(p. 21, 23, 24)*

[75] S.-K. Yip. Phys. Rev. B, **62**, R6127 (2000). *(p. 21, 23)*

[76] H. Pothier, S. Guéron, D. Esteve, and M. H. Devoret. Phys. Rev. Lett., **73**, 2488 (1994). *(p. 21, 27)*

[77] P. G. N. de Vegvar, T. A. Fulton, W. H. Mallison, and R. E. Miller. Phys. Rev. Lett., **73**, 1416 (1994). *(p. 21, 27)*

[78] V. T. Petrashov, V. N. Antonov, P. Delsing, and T. Claeson. Phys. Rev. Lett., **74**, 5268 (1995). *(p. 21, 27)*

[79] W. Belzig, C. Bruder, and G. Schön. Phys. Rev. B, **54**, 9443 (1996). *(p. 22, 39)*

[80] A. Anthore, H. Pothier, and D. Esteve. Phys. Rev. Lett., **90**, 127001 (2003). *(p. 22)*

[81] E. Scheer, H. v. Löhneysen, A. D. Mirlin, P. Wölfle, and H. Hein. Phys. Rev. Lett., **78**, 3362 (1997). *(p. 23)*

[82] S.-K. Yip. Phys. Rev. B, **58**, 5803 (1998). *(p. 24, 39)*

[83] R. Shaikhaidarov, A. F. Volkov, H. Takayanagi, V. T. Petrashov, and P. Delsing. Phys. Rev. B, **62**, R14649 (2000). *(p. 25, 39)*

[84] V. Chandrasekhar. In *The Physics of Superconductors*, edited by K. H. Bennemann and J. B. Ketterson, vol. II. Springer, Berlin (2004). *(p. 25)*

[85] H. B. Callen. Phys. Rev., **73**, 1349 (1948). *(p. 26, 35)*

[86] H. Courtois, P. Gandit, D. Mailly, and B. Pannetier. Phys. Rev. Lett., **76**, 130 (1996). *(p. 27)*

[87] W. Belzig, R. Shaikhaidarov, V. V. Petrashov, and Y. V. Nazarov. Phys. Rev. B, **66**, 220505 (2002). *(p. 27)*

[88] Y. V. Nazarov and T. H. Stoof. Phys. Rev. Lett., **76**, 823 (1996). *(p. 28)*

[89] T. H. Stoof and Y. V. Nazarov. Phys. Rev. B, **53**, 14496 (1996). *(p. 28)*

[90] A. F. Volkov and A. V. Zaitsev. Phys. Rev. B, **53**, 9267 (1996). *(p. 28)*

[91] E. Zhao, T. Löfwander, and J. A. Sauls. Phys. Rev. Lett., **91**, 077003 (2003). *(p. 28)*

[92] E. V. Bezuglyi and V. Vinokur. Phys. Rev. Lett., **91**, 137002 (2003). *(p. 28)*

[93] Z. Jiang and V. Chandrasekhar. Phys. Rev. Lett., **94**, 147002 (2005). *(p. 28)*

[94] Z. Jiang and V. Chandrasekhar. Phys. Rev. B, **72**, 020502 (2005). *(p. 28)*

[95] D. A. Dikin, S. Jung, and V. Chandrasekhar. Phys. Rev. B, **65**, 12511 (2002). *(p. 28, 31, 32, 34)*

[96] D. A. Dikin, S. Jung, and V. Chandrasekhar. Europhys. Lett., **57**, 564 (2002). *(p. 28, 31, 32, 34)*

[97] J. Eom, C.-J. Chien, and V. Chandrasekhar. Phys. Rev. Lett., **81**, 437 (1998). *(p. 28, 31, 32, 34)*

[98] Z. Jiang and V. Chandrasekhar. Chinese J. Phys., **43**, 693 (2005). *(p. 28, 31, 32, 34)*

[99] P. Cadden-Zimansky, Z. Jiang, and V. Chandrasekhar. Physica E, **40**, 155 (2007). *(p. 28, 31, 32)*

[100] A. Parsons, I. A. Sosnin, and V. T. Petrashov. Phys. Rev. B, **67**, 140502 (2003). *(p. 28, 31, 32, 34)*

[101] A. Parsons, I. A. Sosnin, and V. T. Petrashov. Physica E, **18**, 316 (2003). *(p. 28, 31, 32, 34)*

[102] R. Seviour and A. F. Volkov. Phys. Rev. B, **62**, 6116 (2000). *(p. 28, 31, 32, 33)*

[103] V. R. Kogan, V. V. Pavlovskii, and A. F. Volkov. Europhys. Lett., **59**, 875 (2002). *(p. 28, 31, 32, 33, 34)*

[104] A. F. Volkov and V. V. Pavlovskii. Phys. Rev. B, **72**, 14529 (2005). *(p. 28, 31, 32, 33)*

[105] M. Titov. Phys. Rev. B, **78**, 224521 (2008). *(p. 28, 31, 32, 34)*

[106] N. R. Claughton and C. J. Lambert. Phys. Rev. B, **53**, 6605 (1996). *(p. 28, 35)*

[107] H. Courtois, P. Charlat, P. Gandit, D. Mailly, and B. Pannetier. J. Low Temp. Phys., **116**, 187 (1999). *(p. 28)*

[108] W. H. Press, S. A. Teukolsky, W. T. Vetterling, and B. P. Flannery. *Numerical recipes in FORTRAN 77*. Cambridge University Press, 2nd edn. (1992). *(p. 30)*

[109] J. Cash and M. H. Wright. "TWPBVP" (1995). A numerical solver for boundary value problems. *(p. 30)*

[110] G. Bader and U. Ascher. SIAM J. Scient. Stat. Comput., **8**, 483 (1987). *(p. 30)*

[111] J. R. Cash and M. H. Wright. Computing, **45**, 17 (1990). *(p. 30)*

[112] M. Cutler and N. F. Mott. Phys. Rev., **181**, 1336 (1969). *(p. 30)*

[113] U. Sivan and Y. Imry. Phys. Rev. B, **33**, 551 (1986). *(p. 30)*

[114] W. Meissner. Zeits. f. d. ges. Kalte Ind., **34**, 197 (1927). *(p. 30)*

[115] V. L. Ginzburg. Rev. Mod. Phys., **76**, 981 (2004). *(p. 30)*

[116] D. J. van Harlingen. Physica B+C, **109-110**, 1710 (1982). *(p. 30)*

[117] U. M. Galperin, V. L. Gurevich, and V. Kozub. Sov. Phys. JETP, **39**, 680 (1974). *(p. 30, 34)*

[118] S. N. Artemenko and A. F. Volkov. Sov. Phys. JETP, **43**, 548 (1976). [Zh. Eksp. Teor. Fiz. 70, 1051 (1976)]. *(p. 30)*

[119] J. Kolacek and P. Lipavsky. Phys. Rev. B, **71**, 092503 (2005). *(p. 30, 31)*

[120] A. Schmid and G. Schön. Phys. Rev. Lett., **43**, 793 (1979). *(p. 31, 32)*

[121] C. J. Pethick and H. Smith. Phys. Rev. Lett., **43**, 640 (1979). *(p. 31, 32)*

[122] J. Clarke, B. R. Fjordbøge, and P. E. Lindelof. Phys. Rev. Lett., **43**, 642 (1979). *(p. 31, 32)*

[123] J. Clarke and M. Tinkham. Phys. Rev. Lett., **44**, 106 (1980). *(p. 31, 32)*

[124] Y. M. Galperin, V. L. Gurevich, V. I. Kozub, and A. L. Shelankov. Phys. Rev. B, **65**, 64531 (2002). *(p. 31)*

[125] V. L. Gurevich, V. I. Kozub, and A. L. Shelankov. Eur. Phys. J. B, **51**, 285 (2006). *(p. 31)*

[126] F. K. Wilhelm. *Ladungstransport in supraleitenden Nanostrukturen*. Ph.D. thesis, University of Karlsruhe, Germany (1999). *(p. 31, 34)*

[127] B. Meyer. *Thermoelektrische Effekte in mesoskopischen Normal-/Supraleiter Heterostrukturen*. Master's thesis, University of Karlsruhe (1999). *(p. 31, 34)*

[128] T. T. Heikkilä, M. P. Stenberg, M. M. Salomaa, and C. J. Lambert. Physica B, **284-288**, 1862 (2000). *(p. 31)*

[129] L. Onsager. Phys. Rev., **37**, 405 (1931). *(p. 35)*

[130] H. B. G. Casimir. Rev. Mod. Phys., **17**, 343 (1945). *(p. 35)*

[131] M. Meschke, W. Guichard, and J. Pekola. Nature, **444**, 187 (2006). *(p. 37)*

[132] T. T. Heikkilä, T. Vänskä, and F. K. Wilhelm. Phys. Rev. B, **67**, 100502(R) (2003). *(p. 38)*

[133] H. Pothier, S. Guéron, N. O. Birge, D. Esteve, and M. H. Devoret. Phys. Rev. Lett., **79**, 3490 (1997). *(p. 38)*

[134] M. Crosser. *Experiments on Non-equilibrium Superconductor-Normal Metal-Superconductor Josephson junctions*. Ph.D. thesis, Michigan State University (2005). *(p. 39)*

[135] S. Guéron, H. Pothier, N. O. Birge, D. Esteve, and M. H. Devoret. Phys. Rev. Lett., **77**, 3025 (1996). *(p. 39)*

[136] A. F. Volkov. Phys. Rev. Lett., **74**, 4730 (1995). *(p. 39)*

[137] T. Schäpers, et al. Appl. Phys. Lett., **73**, 2348 (1998). *(p. 39)*

[138] J. Kutchinsky, R. Taboryski, C. B. Sorensen, J. Bindslev Hansen, and P. E. Lindelöf. Phys. Rev. Lett., **83**, 4856 (1999). *(p. 39)*

[139] B. J. van Wees, K.-M. H. Lenssen, and C. J. P. M. Harmans. Phys. Rev. B, **44**, 470 (1991). *(p. 39)*

[140] J. J. A. Baselmans, A. F. Morpurgo, B. J. van Wees, and T. M. Klapwijk. Nature, **397**, 43 (1999). *(p. 39)*

[141] J. J. A. Baselmans, B. J. van Wees, and T. M. Klapwijk. Phys. Rev. B, **63**, 094504 (2001). *(p. 39)*

[142] J. Huang, F. Pierre, T. T. Heikkilä, F. K. Wilhelm, and N. O. Birge. Phys. Rev. B, **66**, 020507 (2002). *(p. 39)*

[143] A. G. Aronov and Y. M. Gal'perin. JETP Lett., **19**, 165 (1974). *(p. 43)*

[144] V. V. Ryazanov and V. V. Schmidt. Solid State Commun., **40**, 1055 (1981). *(p. 43)*

[145] M. Reznikov, R. de Picciotto, T. G. Griffiths, M. Heiblum, and V. Umansky. Nature, **399**, 238 (1999). *(p. 44)*

[146] L. S. Levitov. In *Quantum Noise in Mesoscopic Systems*, edited by Y. V. Nazarov. Kluwer (2003). *(p. 44)*

[147] L. S. Levitov, H. Lee, and G. B. Lesovik. J. Math. Phys., **37**, 4845 (1996). *(p. 44, 45, 49)*

[148] Y. V. Nazarov. Ann. Phys. (Leipzig), **8 SI-193**, 507 (1999). *(p. 45)*

[149] Y. V. Nazarov and D. A. Bagrets. Phys. Rev. Lett., **88**, 196801 (2002). *(p. 45)*

[150] A. Shelankov and J. Rammer. Europhys. Lett., **63**, 485 (2003). *(p. 45)*

[151] A. Bednorz and W. Belzig. Phys. Rev. Lett., **101**, 206803 (2008). *(p. 45)*

[152] P. Samuelsson and M. Büttiker. Phys. Rev. B, **66**, 201306(R) (2002). *(p. 45, 46)*

[153] K. E. Nagaev and M. Büttiker. Phys. Rev. B, **63**, 081301(R) (2001). *(p. 45, 46)*

[154] K. E. Nagaev. Phys. Rev. B, **64**, 081304(R) (2001). *(p. 45, 46)*

[155] W. Belzig and Yu. V. Nazarov. Phys. Rev. Lett., **87**, 67006 (2001). *(p. 45)*

[156] M. Houzet and F. Pistolesi. Phys. Rev. Lett., **92**, 107004 (2004). *(p. 45)*

[157] M. Stenberg, P. Virtanen, and T. Heikkilä. Phys. Rev. B, **76**, 144504 (2007). *(p. 45)*

[158] W. Belzig and P. Samuelsson. Europhys. Lett., **64**, 253 (2003). *(p. 45)*

[159] M. Büttiker. J. Phys.: Condens. Matter, **5**, 9361 (1993). *(p. 45)*

[160] B. Reulet, J. Senzier, and D. E. Prober. Phys. Rev. Lett., **91**, 196601 (2003). *(p. 46)*

[161] Y. Bomze, G. Gershon, D. Shovkun, L. S. Levitov, and M. Reznikov. Phys. Rev. Lett., **95**, 176601 (2005). *(p. 46, 49)*

[162] T. T. Heikkilä and L. Roschier. Phys. Rev. B, **71**, 085316 (2005). *(p. 46)*

[163] J. Bylander, T. Duty, and P. Delsing. Nature, **434**, 361 (2005). *(p. 46)*

[164] S. Gustavsson, et al. Phys. Rev. Lett., **96**, 076605 (2006). *(p. 46)*

[165] J. Tobiska and Yu. V. Nazarov. Phys. Rev. Lett., **93**, 106801 (2004). *(p. 46)*

[166] A. V. Timofeev, M. Meschke, J. T. Peltonen, T. T. Heikkilä, and J. P. Pekola. Phys. Rev. Lett., **98**, 207001 (2007). *(p. 46)*

[167] B. Huard, H. Pothier, N. Birge, D. Esteve, X. Waintal, and J. Ankerhold. Ann. Phys. (Leipzig), **16**, 736 (2007). *(p. 46)*

[168] Q. L. Masne, H. Pothier, N. O. Birge, C. Urbina, and D. Esteve. Phys. Rev. Lett., **102**, 067002 (2009). *(p. 46)*

[169] R. K. Lindell, J. Delahaye, M. A. Sillanpää, T. T. Heikkilä, E. B. Sonin, and P. J. Hakonen. Phys. Rev. Lett., **93**, 197002 (2004). *(p. 46)*

[170] E. B. Sonin. Phys. Rev. B, **70**, 140506 (2004). *(p. 46, 47, 49)*

[171] R. Aguado and L. P. Kouwenhoven. Phys. Rev. Lett., **84**, 1986 (2000). *(p. 46, 49)*

[172] R. Deblock, E. Onac, L. Gurevich, and L. P. Kouwenhoven. Science, **301**, 203 (2003). *(p. 46)*

[173] P.-M. Billangeon, F. Pierre, H. Bouchiat, and R. Deblock. Phys. Rev. Lett., **96**, 136804 (2006). *(p. 46, 49)*

[174] P.-M. Billangeon, F. Pierre, H. Bouchiat, and R. Deblock. Phys. Rev. Lett., **98**, 216802 (2007). *(p. 46)*

[175] G.-L. Ingold and Y. V. Nazarov. In *Single Charge Tunneling*, edited by H. Grabert and M. H. Devoret, vol. 294 of *NATO ASI Series B: Physics*, chap. 2, pp. 21–107. Plenum Press, New York (1992). *(p. 46, 47, 48, 49)*

[176] M. H. Devoret. In *Quantum Fluctuations*, edited by S. Reynaud, E. Giacobino, and J. Linn-Justin, chap. 10, pp. 351–386. Elsevier Science B. V. (1997). *(p. 47)*

[177] E. B. Sonin. Phys. Rev. Lett., **98**, 030601 (2007). *(p. 49)*

[178] E. B. Sonin. J. Low Temp. Phys., **146**, 161 (2007). *(p. 49)*

[179] G. B. Lesovik and N. M. Chtchelkatchev. JETP Lett., **77**, 393 (2003). [Pis'ma Zh. Eksp. Teor. Fiz., 77, 464 (2003)]. *(p. 49)*

[180] J. Salo, F. W. J. Hekking, and J. P. Pekola. Phys. Rev. B, **74**, 125427 (2006). *(p. 49)*

[181] T. Ojanen and T. T. Heikkilä. Phys. Rev. B, **73**, 020501 (2006). *(p. 49)*

[182] K. V. Bayandin, A. V. Lebedev, and G. B. Lesovik. JETP Lett., **106**, 117 (2008). [Pis'ma Zh. Eksp. Teor. Fiz., 133, 140 (2008)]. *(p. 49)*

[183] A. F. Volkov and H. Takayanagi. Phys. Rev. B, **56**, 11184 (1997). *(p. A–1)*

Appendix A Usadel equation on a circuit

Consider a general proximity circuit consisting of several normal wires, joined together by contacts with some given interface resistances. In the spirit of circuit theory [59, 60] it is useful to divide the structure to nodes, terminals, and connectors (diffusive wires, tunnel junctions, etc.) between them, cf. Fig. 2.6. What are the equations modelling such a structure?

In general, the problem can be formulated in terms of Kirchoff-type conservation equations for the matrix currents $\check{I}[\check{G}_i, \check{G}_j]$ flowing from one node to another, which depend on the Green's functions on the nodes. [59, 60] For short connectors, the matrix current can be expressed in terms of a distribution of transmission eigenvalues T_n, [59]

$$\check{I}[\check{G}_i, \check{G}_j] = \sum_n \frac{2T_n[\check{G}_1, \check{G}_2]}{4 - T_n(\{\check{G}_1, \check{G}_2\} - 2)} \,. \tag{A.1}$$

This is valid for structures through which electrons travel fast compared to the time scales given by superconductivity, temperature, etc., $\hbar/\Delta, \hbar/T, \ldots$ The above result also makes the assumption that nodes are sufficiently much larger than the elastic scattering length, so that electron trajectories inside them are randomized.

For larger connectors where the electron spends more time, decay of the superconducting coherence should be taken into account. One way to do this is to model it with "parasitic" connectors [59] that leak coherence. For diffusive wires, one can however also solve the Usadel equation (2.23) to find the Green function $\check{G}$ and the corresponding matrix current density $\check{j} = \sigma\check{G}\hat{\nabla}\check{G}$. This yields a relation $\check{I}[\check{G}_1, \check{G}_2]$ for the matrix current and the Green functions $\check{G}_1$, $\check{G}_2$ at the edges of the connector, and it can be at least numerically evaluated.

In large connectors, the effect of magnetic field may also need to be taken into account. This is simple to do if the field penetrating the connector can be neglected, as is the case for sufficiently thin wires. Then, one can gauge the field away from inside the connector with a transformation $\check{G}(\boldsymbol{R}) \mapsto e^{i\varphi(\boldsymbol{R})\hat{\tau}_3/2}\check{G}(\boldsymbol{R})e^{-i\varphi(\boldsymbol{R})\hat{\tau}_3/2}$ where $\varphi(\boldsymbol{R}) = 2\int_{\boldsymbol{R}_0}^{\boldsymbol{R}} \mathrm{d}\boldsymbol{l}\cdot\boldsymbol{A}$ is a magnetic phase, which is well defined if $\nabla \times \boldsymbol{A}$ is assumed negligible. (Cf. [68, 69, 183].) However, as a consequence, the matrix currents acquire the additional phase factors $\phi(\boldsymbol{R}_2) - \phi(\boldsymbol{R}_1)$, which affect the properties of the circuit unless it is simply connected, ie., contains no loops.

Below, we discuss a systematic approximation for computing the supercurrent in this type of circuits, based on the above approach.

A.1 Linearized spectral equation

One configuration where the proximity circuit problem is analytically tractable is when the superconducting coherence in the structure is weak, and all equations can be linearized in the coherence parameters γ. This can be the case for example due to strong tunnel barriers or large pieces of normal metal between superconductors and the part of the structure under study. This approximation is commonly used in the literature.

The linearized equations need to be coupled to the more strongly coherent parts of the circuits by matching conditions. When we are interested only in γ, it is necessary to consider only the parts $I_\gamma = \frac{1}{2}N^{-1}[P_+ I^R P_-]_{12}\tilde{N}^{-1}$ and $I_{\tilde{\gamma}} = \frac{1}{2}\tilde{N}^{-1}[P_- I^R P_+]_{21}N^{-1}$ of the matrix current (see Appendix C). The latter can also be usually related to the former by exchanging tildes on all quantities, so we need only to consider I_γ. Note that gauging away the magnetic field results in an additional phase factor of $e^{i\phi_{ij}}$ in $I_{\gamma,ij}$ where ϕ_{ij} is the magnetic phase difference across the junction.

In the case where the coupling connectors are short junctions of large resistance, Eq. (A.1) can be used. For tunnel junctions it then reduces to Kupriyanov-Lukichev boundary conditions; [58] for an SN contact this reads after linearization

$$I_\gamma = -R_B^{-1}\frac{\gamma_S - (1-\gamma_S\tilde{\gamma}_S)\gamma}{1+\gamma_S\tilde{\gamma}_S} + \mathcal{O}(\gamma^2)\,, \tag{A.2}$$

where $\gamma_S = \tanh(\theta_0/2)$, $\theta_0 = \operatorname{artanh}(|\Delta|/E)$ is the coherence parameter inside the superconductor, and R_B the interface resistance.

Another simple case occurs when the weak-proximity part is coupled to a superconductor via a long quasi-1D diffusive wire, assumed to be of length L. The corresponding matrix current can be solved when the phase χ (in θ-parameterization) does not change appreciably inside this wire; this approximation can be justified by the fact that typically the largest changes in χ occur where $|\theta|$ is the smallest. If so, the Usadel equation in the θ parameterization reads simply

$$\partial_x^2\theta = k^2\sinh\theta\,, \tag{A.3}$$

where $k = \sqrt{-2iE}$. Assuming a superconductor at $x = 0$ and a weak-proximity structure at $x = L$, this has the solution

$$\int_{\theta_0/2}^{\theta(L)/2}\frac{\mathrm{d}q}{\sqrt{\sinh^2 q - A}} = -kL\,. \tag{A.4}$$

The integration constant is $A = -(2k)^{-2}(\partial_x\theta)^2 + \sinh^2(\theta/2)$. Now, one can expand

the above integral in $\theta(L)$, in terms of a formal small parameter λ:

$$\int_{\theta_0/2}^{\lambda\theta(L)/2} \frac{\mathrm{d}q}{\sqrt{\sinh^2 q - \lambda^2 A}} = \ln\left[\left(q + \sqrt{q^2 - \lambda^2 A}\right) q^{-1} \tanh\frac{q}{2}\right]\Bigg|_{q=\theta_0/2}^{q=\lambda\theta(L)/2} + \mathcal{O}(\lambda^2 \ln\lambda)\,. \tag{A.5}$$

Solving A from (A.4) and (A.5) in leading order in e^{-kL} and $\theta(L)$ results into

$$A = \theta_1(\theta(L) - \theta_1)\,, \qquad \theta_1 = 4e^{-kL}\tanh\frac{\theta_0}{4}\,. \tag{A.6}$$

Expanding the expression of A to the same accuracy, one finds the associated matrix current at the edge of the weak-proximity region:

$$I_\gamma = -k(\theta_1 e^{i\phi} - \gamma)\,, \tag{A.7}$$

using the equality that $\gamma \approx \theta e^{i\chi}/2$ for $|\gamma| \ll 1$. Here, ϕ is the superconducting phase of the superconductor at the other end of the diffusive wire. The result (A.7) is an extension of the approximation derived in [62, 67] to multiterminal circuits.

Finally, interconnector currents are given in the weak-proximity regime for diffusive wires by

$$I_{\gamma,ij} = -A_{ij}\sigma_{ij}k\coth(kL)(\mathrm{sech}(kL)\gamma_j - \gamma_i) \simeq -A_{ij}\sigma_{ij}k(2e^{-kL}\gamma_j - \gamma_i)\,, \tag{A.8}$$

where the latter approximation is valid for $kL \gg 1$. For tunnel junctions a similar equation reads

$$I_{\gamma,ij} = -R_B^{-1}(\gamma_j - \gamma_i)\,. \tag{A.9}$$

These follow from the solution of the linearized ($|\gamma| \ll 1$) time-independent Usadel equation

$$\nabla^2\gamma = k^2\gamma\,, \tag{A.10}$$

and linearization of the Kupriyanov-Lukichev boundary condition (eg. linearizing Eq. (A.2) in $\gamma_j = \gamma_S$).

A.2 Supercurrent

There is an illustrative way to find the supercurrent in weak-proximity circuits. First, notice that the currents (A.2, A.7, A.8, A.9) can be written in the form

$$I_{\gamma,ij} = a_{ij}\gamma_j - b_{ij}\gamma_i \tag{A.11}$$

for suitably defined a_{ij} and b_{ij}. These are summarized in Table. 2.1. The conservation equations for the matrix currents then take the form

$$\sum_{j\in N} a_{ij}\gamma_j - \underbrace{\sum_{j\in N} b_{ij}}_{=b_i}\gamma_i = -\sum_{j\in T} a_{ij}\gamma_j \Leftrightarrow (\mathbf{A}-\mathbf{B})\boldsymbol{\gamma} = -\mathbf{A}'\boldsymbol{\gamma}_0\,, \tag{A.12}$$

decomposed to sums over nodes N and terminals T. The solution to this problem can be written as a Neumann series

$$\boldsymbol{\gamma} = \mathbf{B}^{-1}\sum_{n=0}^{\infty}(\mathbf{A}\mathbf{B}^{-1})^n\mathbf{A}'\boldsymbol{\gamma}_0\,. \tag{A.13}$$

Note that $\mathbf{B}$ is diagonal. Consider the value of γ in node i_0 and write the matrix products explicitly:

$$\gamma_{i_0} = \sum_{k\in T}\sum_{n=0}^{\infty}\sum_{i_1,\ldots,i_n\in N}\frac{a_{i_0,i_1}\cdots a_{i_{n-1},i_n}a_{i_n,k}}{b_{i_0}\cdots b_{i_n}}\gamma_k \qquad = \sum_{k\in T}\underbrace{\sum_{\mathfrak{P}:k\mapsto i_0} C_{\mathfrak{P}}\gamma_k}_{=Q_{i_0,k}} \tag{A.14}$$

The two inner sums are in fact nothing but a sum over all paths $\mathfrak{P}$ connecting k to i_0 in the circuit, weighed by amplitudes $C_{\mathfrak{P}}$. We can now write down the spectral supercurrent flowing from node i to terminal j,

$$j_E|_{ij} = 2i[\tilde{\gamma}\partial_x\gamma - \gamma\partial_x\tilde{\gamma}]|_{ij} = 2i\sum_{k\in T}\left[\tilde{\gamma}_k\tilde{Q}_{i,k}\left(a_{ij}\gamma_j - b_i\sum_{p\in T}Q_{i,p}\gamma_p\right) - \text{tildes exch.}\right]. \tag{A.15}$$

The total supercurrent entering terminal j then becomes

$$j_{E,j} = 4\sum_{k\in T}\sum_{\mathfrak{P}:k\mapsto j}\bar{C}_{\mathfrak{P}}\bar{\gamma}_k\bar{\gamma}_j\sin\left(\varphi_j - \varphi_k - \frac{2e}{\hbar}\int_{\mathfrak{P}}\mathrm{d}\boldsymbol{l}\cdot\boldsymbol{A}\right), \tag{A.16}$$

where we have extracted the magnetic phase factors from $a_{ij} = \bar{a}_{ij}e^{i\phi_{ij}}$, $\tilde{a}_{ij} = \bar{a}_{ij}e^{-i\phi_{ij}}$, $C_{\mathfrak{P}} = \bar{C}_{\mathfrak{P}}\exp(i\sum_{(i,j)\in\mathfrak{P}}\phi_{ij})$ and $\gamma_j = \bar{\gamma}_j e^{i\varphi_j}$, $\tilde{\gamma}_j = -\bar{\gamma}_j e^{-i\varphi_j}$, noting that $\tilde{b}_j = b_j$. The argument inside sin is the gauge-invariant phase difference along the path $\mathfrak{P}$. Note also that $C_{\mathfrak{P}} \sim e^{-kL}R_B^{-m}$ where L is the length of the path in diffusive conductors and m the number of tunnel barriers it traverses through. Since the amplitude often is large only for a small number of paths, Eq. (A.16) is a useful representation for quick estimates of supercurrent in hybrid structures. Examples and more detailed discussion on its use can be found in Section 2.2.2.

Appendix B Fourier representations

The following representations of two-time correlation functions are commonly used:

$$A(E,T) = \int_{-\infty}^{\infty} \mathrm{d}t\, e^{iEt} A(T+\frac{t}{2}, T-\frac{t}{2})\,, \tag{B.1}$$

$$A(\omega_1,\omega_2) = \int_{-\infty}^{\infty} \mathrm{d}t_1 \int_{-\infty}^{\infty} \mathrm{d}t_2\, e^{i\omega_1 t_1} e^{-i\omega_2 t_2} A(t_1,t_2)\,, \tag{B.2}$$

$$A(E,\omega) = \int_{-\infty}^{\infty} \mathrm{d}t \int_{-\infty}^{\infty} \mathrm{d}T\, e^{iEt} e^{i\omega T} A(T+\frac{t}{2}, T-\frac{t}{2})\,, \tag{B.3}$$

involving the "relative" and "center-of-mass" (CM) times $t = t_1 - t_2$ and $T = (t_1 + t_2)/2$, and the relative and CM energies $\omega = \omega_1 - \omega_2$ and $E = (\omega_1 + \omega_2)/2$. It is useful to remember the relations

$$\partial_T = \partial_{t_1} + \partial_{t_2}\,, \qquad \partial_t = \frac{1}{2}(\partial_{t_1} - \partial_{t_2})\,, \tag{B.4}$$

$$\partial_{t_1} = \partial_t + \frac{1}{2}\partial_T\,, \qquad \partial_{t_2} = -\partial_t + \frac{1}{2}\partial_T\,. \tag{B.5}$$

and the correspondences

$$\partial_T \leftrightarrow -i\omega\,, \qquad \partial_t \leftrightarrow -2iE\,. \tag{B.6}$$

With respect to the above representations, time convolutions take the forms

$$(A\circ B)(E,T) = e^{\frac{i}{2}(\partial_{E_1}\partial_{T_2} - \partial_{E_2}\partial_{T_1})} A(E_1,T_1)B(E_2,T_2)\Big|_{E_1=E_2=E,\, T_1=T_2=T}\,, \tag{B.7}$$

$$(A\circ B)(\omega_1,\omega_2) = \int_{-\infty}^{\infty} \frac{\mathrm{d}\omega_3}{2\pi} A(\omega_1,\omega_3)B(\omega_3,\omega_2)\,. \tag{B.8}$$

It is useful to note that time convolution in the (E,T) representation has the property

$$A(E,T)\circ e^{i\omega T} = e^{i\omega T} A(E+\frac{\omega_0}{2},T)\,, \quad e^{i\omega T}\circ A(E,T) \;\; = e^{i\omega T} A(E-\frac{\omega_0}{2},T)\,, \tag{B.9}$$

i.e., periodic perturbations only generate energy shifts.

Similar formulas as above hold for the spatial coordinates $\boldsymbol{r}_1$, $\boldsymbol{r}_2$, relative and CM coordinates $\boldsymbol{r} = \boldsymbol{r}_1 - \boldsymbol{r}_2$, $\boldsymbol{R} = (\boldsymbol{r}_1 + \boldsymbol{r}_2)/2$, and the relative and CM momentum $\boldsymbol{p}$ and $\boldsymbol{P}$.

Appendix C Consequences of the normalization

The normalization condition $\check{G}^2 = 1$ has some interesting mathematical consequences. These are most useful for time-dependent problems where the $\circ$ products are non-commutative, but also simplify some issues for time-independent problems. First, the normalization implies that eigenvalues of $\check{G}$ are only $+1$ and -1, so that $\check{G}$ can be written in the spectral representation $\check{G} = P_+ - P_-$ where $P_\pm$ are projectors onto the positive and negative subspaces of $\check{G}$. These projection operators are also known as the Shelankov projectors, [43]

$$\check{P}_\pm = \frac{1}{2}(1 \pm \check{G}) \,, \tag{C.1}$$

and they come useful when dealing with the Riccati parameterization (cf. eg. [54]). Another consequence of normalization is that the equation $[\check{G}, \check{\sigma}] = 0$ which for example determines the bulk Green functions, is solved by $\check{G} = \operatorname{sgn} \check{\sigma}$, by properties of the matrix sign function.

Equations of motion for the γ parameters are conveniently derived by taking Shelankov projections and extracting the Nambu elements,

$$N^{-1}[P_+^R(\ldots)P_-^R]_{12}\tilde{N}^{-1} \,, \qquad\qquad \tilde{N}^{-1}[P_-^R(\ldots)P_+^R]_{12}N^{-1} \tag{C.2}$$

of for example the Usadel equations written for the Green functions. The point in this is that the projectors, when written in terms of Riccati parameters are (cf. eg. [50])

$$P_+ = \begin{pmatrix} N & N\gamma \\ \tilde{\gamma}N & \tilde{\gamma}N\gamma \end{pmatrix} \,, \qquad\qquad P_- = \begin{pmatrix} \gamma\tilde{N}\tilde{\gamma} & -\gamma\tilde{N} \\ -\tilde{N}\tilde{\gamma} & \tilde{N} \end{pmatrix} \,, \tag{C.3}$$

and they have the property

$$\nabla P_\pm = \pm P_+[\nabla U]P_- \pm P_-[\nabla \tilde{U}]P_+ \,, \quad U = \begin{pmatrix} 0 & \gamma \\ 0 & 0 \end{pmatrix} \,, \quad \tilde{U} = \begin{pmatrix} 0 & 0 \\ \tilde{\gamma} & 0 \end{pmatrix} \,, \tag{C.4}$$

which helps in unravelling the gradient terms. For example, one can directly see that $N^{-1}[P_+(G^R\nabla G^R)P_-]_{12}\tilde{N}^{-1} = 2\nabla\gamma$.

Appendix D Summary of equations

The set of γ–f parameterized stationary Usadel equations are collected in this Appendix, for convenience and completeness.

The Green function is parameterized as [(2.26), (2.28)]

$$\hat{g}^R = \frac{1}{1+\gamma\tilde{\gamma}} \begin{pmatrix} 1-\gamma\tilde{\gamma} & 2\gamma \\ 2\tilde{\gamma} & -1+\tilde{\gamma}\gamma \end{pmatrix}, \qquad \hat{g}^A = -\hat{\tau}_3(\hat{g}^R)^\dagger\hat{\tau}_3 \tag{D.1}$$

$$\hat{g}^K = \hat{g}^R \begin{pmatrix} f_L+f_T & 0 \\ 0 & f_L-f_T \end{pmatrix} - \begin{pmatrix} f_L+f_T & 0 \\ 0 & f_L-f_T \end{pmatrix} \hat{g}^A . \tag{D.2}$$

The Usadel equations governing the coherence parameters γ, $\tilde{\gamma}$ read [(2.33)]

$$D(\nabla - 2i\boldsymbol{A})^2\gamma - \frac{2\tilde{\gamma}[(\nabla-2i\boldsymbol{A})\gamma]^2}{1+\gamma\tilde{\gamma}} = -2iE\gamma + i\Delta^*\gamma^2 + i\Delta\,, \tag{D.3a}$$

$$D(\nabla + 2i\boldsymbol{A})^2\tilde{\gamma} - \frac{2\gamma[(\nabla+2i\boldsymbol{A})\tilde{\gamma}]^2}{1+\gamma\tilde{\gamma}} = -2iE\tilde{\gamma} + i\Delta\tilde{\gamma}^2 + i\Delta^*\,. \tag{D.3b}$$

The kinetic equations governing the distribution functions f_L, f_T read [(2.50)]

$$D\nabla\cdot\boldsymbol{j}_L = 0, \qquad \boldsymbol{j}_L \equiv \mathcal{D}_L\nabla f_L - \mathcal{T}\nabla f_T + j_S f_T\,, \tag{D.4a}$$

$$D\nabla\cdot\boldsymbol{j}_T = (\nabla\cdot j_S)f_L + 2|\Delta|\mathcal{R}f_T, \qquad \boldsymbol{j}_T \equiv \mathcal{D}_T\nabla f_T + \mathcal{T}\nabla f_L + j_S f_L\,, \tag{D.4b}$$

with the coefficients [(2.51)]

$$\mathcal{D}_L = |N|^2(|\gamma|^2-1)(|\tilde{\gamma}|^2-1)\,, \qquad \mathcal{D}_T = |N|^2(|\gamma|^2+1)(|\tilde{\gamma}|^2+1)\,, \tag{D.5a}$$

$$\mathcal{T} = |N|^2(|\tilde{\gamma}|^2-|\gamma|^2)\,, \qquad j_S = \mathrm{Re}\,2N^2[\gamma(\nabla+2i\boldsymbol{A})\tilde{\gamma} - \tilde{\gamma}(\nabla-2i\boldsymbol{A})\gamma]\,, \tag{D.5b}$$

$$\mathcal{R} = 2|N|^2\,\mathrm{Re}[(1+|\tilde{\gamma}|^2)e^{-i\phi}\gamma - (1+|\gamma|^2)e^{i\phi}\tilde{\gamma}]\,, \qquad N \equiv \frac{1}{1+\gamma\tilde{\gamma}}\,. \tag{D.5c}$$

where the order parameter is $\Delta = |\Delta|e^{i\phi}$.

The observable charge and heat currents are [(2.52)]

$$\boldsymbol{j}_c = -\frac{\sigma_N}{2e}\int_{-\infty}^{\infty}\mathrm{d}E\,\boldsymbol{j}_T\,, \quad \boldsymbol{j}_Q = \frac{\sigma_N}{2e^2}\int_{-\infty}^{\infty}\mathrm{d}E(E-\mu)\,\boldsymbol{j}_L\,. \tag{D.6}$$

Boundary conditions at a circuit node read [(2.32)]

$$\sum_j A_j\sigma_j\partial_x\gamma_j = \sum_j A_j\sigma_j\partial_x\tilde{\gamma}_j = \sum_j A_j\sigma_j\partial_x j_{T,j} = \sum_j A_j\sigma_j\partial_x j_{L,j} = 0\,. \tag{D.7}$$

Currents sum to zero, and, in addition, γ, $\tilde{\gamma}$, f_L, and f_T are continuous.

Boundary conditions at clean contacts to normal terminals are

$$\gamma = \tilde{\gamma} = 0\,, \quad f_L = f_L^0 = f^0(\mu_N - E) - f^0(\mu_N + E)\,, \tag{D.8}$$

$$f_T = f_T^0 = 1 - f^0(\mu_N - E) - f^0(\mu_N + E)\,, \tag{D.9}$$

where $f^0(E) = 1/(e^{E/T} + 1)$ is the Fermi function and μ and T terminal potential and temperature. At superconducting terminals,

$$\gamma^R = -\frac{\Delta}{E + i\sqrt{|\Delta|^2 - (E + i0^+)^2}}\,, \quad \tilde{\gamma}^R = +\frac{\Delta^*}{E + i\sqrt{|\Delta|^2 - (E + i0^+)^2}}\,, \tag{D.10}$$

$$\hat{\boldsymbol{n}} \cdot \nabla f_L = 0\,, \quad f_T = 0\,, \quad \text{for } |E| < |\Delta|\,, \tag{D.11}$$

$$f_L = f_L^0\,, \quad f_T = f_T^0\,, \qquad \text{for } |E| > |\Delta|\,. \tag{D.12}$$

Potential of superconducting terminals is chosen as $\mu_S = 0$, and charge imbalance in superconductors is neglected.

ISBN 978-952-248-085-9
ISBN 978-952-248-086-6 (PDF)
ISSN 1795-2239
ISSN 1795-4584 (PDF)